Université de Montréal

Développement de peptidomimétiques antagonistes du récepteur de l'interleukine-1β

Par

Kim Beauregard

Département de chimie

Faculté des arts et des sciences

Mémoire présenté à la Faculté des Études Supérieures

En vue de l'obtention du grade de

Maîtrise ès science (M. Sc.)

En chimie

Janvier 2012

Université de Montréal

Faculté des Études Supérieures

Ce mémoire intitulé :

Développement de peptidomimétiques antagonistes du récepteur de l'interleukine-1β

Présenté par :

Kim Beauregard

A été évalué par un jury composé des personnes suivantes :

Pierre Thibault, *Ph.D.*
président-rapporteur

William D. Lubell, *Ph.D.*
directeur de recherche

Sylvain Chemtob, *M.D., Ph.D.*
co-directeur de recherche

Stephen Hanessian, *Ph.D.*
membre du jury

Accepté le :

17 mai 2012

À ma famille, Jade, Lise et Christian,
Et à mon conjoint, Sylvain

RÉSUMÉ

Dans ce mémoire, je présente mes études sur la synthèse, la caractérisation et l'évaluation biologique de différentes séries d'analogues du D-heptapeptide appelé 101.10, un modulateur négatif allostérique du récepteur de l'interleukine-1β (IL-1β). Sachant que les peptides ont généralement de faibles propriétés pharmacologiques, le but de ce projet portait sur l'examen des structures nécessaires à la bioactivité, la conformation tridimensionnelle de ces derniers afin d'améliorer la droguabilité du peptide parent.

Les stratégies d'optimisation du 101.10 utilisées furent : la coupure *N*- et *C*-terminale; la substitution par la proline, α-amino-γ-lactame (Agl), β-amino-γ-lactame (Bgl) et α-amino-β-hydroxy-γ-lactame (Hgl); et la rigidification du squelette à l'aide d'un bicycle, l'indolozidin-2-one (I^2aa). Afin de clarifier certaines relations de structure-activité, quelques modifications furent apportées au peptide, incluant l'échange de la thréonine pour la valine, la permutation de la stéréochimie de certains résidus clés ainsi que le remplacement de certaines chaînes latérales par un méthyle. Pour pallier aux difficultés de reproductibilité des résultats avec des échantillons provenant de différentes sources, des études sur l'identité du contre-anion et la pureté du peptide furent conduites.

Afin d'évaluer l'effet des modifications sur la conformation aqueuse et l'activité biologique du peptide, des analyses de dichroïsme circulaire et des tests *in vitro* mesurant l'inhibition de certains effets de l'IL-1β furent effectués. Ces essais cellulaires comportaient l'inhibition de la prolifération de cellules immunes et de l'activation des voies de signalisation inflammatoires du facteur nucléaire κB (NF-κB) et de la protéine kinase activée par mitogène (MAPK), toutes deux stimulées par l'IL-1β. La compilation de ces données a permis de déceler certaines tendances entre la structure, la conformation et l'activité anti-IL-1β des peptidomimétiques.

MOTS CLÉS

Inflammation, interleukine-1β, mime peptidique, amino-gamma-lactame, indolizidinone, structure secondaire de peptide, repliement bêta, prolifération de thymocytes, activation du facteur nucléaire kappaB et de la protéine kinase activée par mitogène, contre-anion.

ABSTRACT

In this thesis, I present my studies toward the synthesis, characterisation and biological evaluation of different series of analogues of the D-heptapeptide called 101.10, a negative allosteric modulator of the interleukin-1β (IL-1β) receptor. Considering that peptides generally exhibit poor pharmacological properties, the objective of this project consisted in: the examination of the peptidic structures essential to elicit bioactivity; the investigation of the three-dimensional arrangement of these moieties; and the improvement of the "drug-like" properties of the parent peptide.

The optimisation strategies that were used include: *N*- and *C*-terminal truncation; positional scanning using monocycles such as proline, α-amino-γ-lactam (Agl), β-amino-γ-lactam (Bgl) and α-amino-β-hydroxy-γ-lactam (Hgl); and backbone rigidification with indolizidin-2-one (I^2aa). Moreover, in order to validate certain structure-activity relationships, further modifications were performed on the peptide: substitution of threonine for valine, exchange of stereochemistry, and substitution of certain side-chain for a methyl group. Lastly, due to divergent behaviour between peptide samples obtained from different sources, studies on the identity of the counter-anion and on the sample purity were conducted.

In order to evaluate the influence of these modifications on the aqueous conformation and on the biological activity of the peptide, circular dichroism analyses and *in vitro* tests measuring the inhibition of certain IL-1β-mediated effects were performed. These cellular assays comprised the inhibition of IL-1β-stimulated proliferation of immune cells, as well as activation of the inflammatory pathways of nuclear factor κB (NF-κB) and mitogen-activated protein kinase (MAPK) pathways. Compiling these data revealed certain trends existing between the structure, conformation and anti-IL-1β activity of the peptidomimetics.

KEY WORDS

Inflammation, interleukin-1β, peptide mimic, amino-gamma-lactam, indolizidinone, peptidic secondary structure, bêta turn, thymocyte proliferation, nuclear factor kappaB and mitogen-activated protein kinase activation, counter-anion.

TABLE OF CONTENTS

CHAPTER 3

CHAPTER 4

CHAPTER 5

CHAPTER 6

LIST OF FIGURES

CHAPTER 1

CHAPTER 2

CHAPTER 3

CHAPTER 4

CHAPTER 5

LIST OF SCHEMES

CHAPTER 2

CHAPTER 4

LIST OF TABLES

CHAPTER 2

CHAPTER 3

CHAPTER 4

CHAPTER 5

LIST OF ABBREVIATIONS AND SYMBOLS

[α]	specific rotation
[θ]	mean residue ellipticity
β_2AR	β_2-adrenergic receptor
θ	degree of ellipticity (in mdeg)
ε	molar absorption coefficient (in $L \cdot mol^{-1} \cdot cm^{-1}$)
Δ	deletion
A	absorbance (in a.u.)
Ac	acetyl
Acnc	1-aminocycloalkane-1-carboxylic acid
AcOH	acetic acid
Ac_2O	acetic anhydride
ADMET	pharmacokinetic properties, i.e. administration-distribution-metabolism-excretion-toxicity
Agl	α-amino-γ-lactam
Aib	amino *iso*-butyric acid
AP-1	activator protein-1
AUC	area under the curve
BGE	background electrolyte
Bgl	β-amino-γ-lactam
Boc	*tert*-butyloxycarbonyl
t-Bu	*tert*-butyl
c	concentration
C18	octadecyl packing
cAMP	cyclic adenosine monophosphate
CAPS	cryopyrin-associated periodic syndrome
Cbz	carboxybenzyl
CD	circular dichroism
CGRP	calcitonin gene-related peptide
COPD	chronic obstructive pulmonary disease

COX-2	cyclooxygenase-2
CTAB	cetyltrimethylammonium bromide
CyQUANT NF	cyanine-based intercalating dye
CZE	capillary zone electrophoresis
DAMPS	danger-associated molecular patterns
DBU	1,8-diazabicyclo[5.4.0]undec-7-ene
DCM	dichloromethane
Deg	α,α-diethylglycine
DIEA	*N*,*N*-di-*iso*-propylethylamine
DMEM	Dulbecco's modified Eagle medium
DMF	dimethylformamide
DMSO	dimethylsulfoxide
DNA	deoxyribonucleic acid
Dnp	*N*-2,4-dinitrophenyl
DoF	degree of freedom
DVB	divinylbenzene
E_{max}	maximal effect of a ligand
EOF	electroosmotic flow
ERK	extracellular signal‑regulated kinase
EtOAc	ethylacetate
Et_2O	diethyl ether
f	bioavailability
FA	formic acid
FBS	fetal bovine serum
Fc	crystallisable fragment of an antibody
FCAS	familial cold auto-inflammatory syndrome
FDA	Food and Drug Administration of the U.S.A.
FITC	fluorescein *iso*thiocyanate filter
FMF	family mediterranean fever
Fmoc	fluorenylmethyloxycarbonyl
FXa	blood coagulation factor Xa

GM-CSF	granulocyte macrophage colony-stimulating factor
GMP	good manufacturing practices
[^{3}H]	tritium isotope
HBTU	*O*-Benzotriazole-*N*,*N*,*N'*,*N'*-tetramethyluronium hexafluorophosphate
HEK	human embryonic kidney cells
hGH	human growth hormone
Hgl	α-amino-β-hydroxy-γ-lactam
HIV-1	human immunodeficiency virus-1
HPLC	high performance liquid chromatography
HRMS	high resolution mass spectrometry
hTS	human thymidylate synthase
HTS	high-throughput screening
I^2aa	indolizidin-2-one amino acid
I^9aa	indolizidin-9-one amino acid
IBD	inflammatory bowel disease
IBTM	2-amino-3-oxohexahydroindolizino[8,7-b]indole-5-carboxylate
IC_{50}	half maximal inhibitory concentration
ICAM-1	intercellular adhesion molecule-1
ICE	interleukin-1 converting enzyme
I.D.	internal diameter
IgG	immunoglobulin G
IκB	IkappaBα and IkappaBβ complex
IKKβ	IκB kinase β
IL-1β	interleukin-1β
IL-33	interleukin-33
IL-1Ra	IL-1 receptor antagonist
IL-1RAcP	IL-1 receptor accessory protein
IL-1RI	IL-1 receptor type I
IL-1RII	IL-1 receptor type II
IL-1RL1	IL-1 receptor-like 1
IRAK-1	IL-1 receptor-associated kinase 1

JNK	c-Jun *N*-terminal kinase
kDa	kilodaltons
l	pathlength (in cm)
LC-MS	tandem liquid chromatography-mass spectrometry
LH-RH	luteinizing hormone-releasing hormone
log D	pH-dependent partition coefficient
m/z	mass over charge ratio
mAb	monoclonal antibody
MAPK	mitogen-activated protein kinase
MAS	minimal active sequence
MBHA	4-methylbenzhydrylamine resin
MCX	mixed-mode cation exchange
MeCN	acetonitrile
MeOH	methanol
MIC	minimal inhibitory concentration
MMP-1	metalloproteinase-1
MRW	mean residue weight (in $g \cdot dmol^{-1} \cdot residue^{-1}$)
MS	multiple sclerosis or molecular sieves
MWS	Muckle-Wells syndrome
MyD88	myeloid differentiation primary response gene 88
NAM	negative allosteric modulator
NF-κB	nuclear factor kappaB
NH_4	ammonium
NMR	nuclear magnetic resonance
NO	nitric oxide
NOESY	nuclear Overhauser effect spectroscopy
OA	osteoarthritis
OAc	acetate
OD	optical density
O.D.	outer diameter
P^2aa	pyrroloazepin-2-one amino acid

PAI-1	plasminogen activator inhibitor-1
PAM	positive allosteric modulator
PAMPA	parallel artificial membrane permeability assay
PAMPS	pathogen-associated molecular patterns
PBS	phosphate buffered saline
PDB	protein data bank
PGE_2	prostaglandin E_2
PGF2α	prostaglandin F2α
PMA	phorbol myristate acetate
PPI	polyproline type I helix
PPII	polyproline type II helix
^{i}PrOH	*iso*-propanol
$^{i}Pr_2O$	di-*iso*-propyl ether
PS	polystyrene
Q^2aa	quinolizidin-2-one amino acid
RA	rheumatoid arthritis
ROA	Raman optical activity
RPMI	Roswell Park Memorial Institute medium
r.t.	room temperature
SAR	structure-activity relationship
SEAP	secreted embryonic alkaline phosphatase
SEM	standard error of the mean
SIGIRR	single immunoglobulin IL-1R-related molecule
SMM	smoldering multiple myeloma
SoJIA	systemic-onset juvenile idiopathic arthritis
SPE	solid-phase extraction
SPPS	solid-phase peptide synthesis
SPR	surface plasmon resonance
$t_{½}$	half-life
T2D	type 2 diabetes
TAB1	TAK1-binding protein

TAK1	transforming growth factor-β-activated kinase 1
TEA	triethylamine
TES	triethylsilane
TF-1	human thymocyte cell line
TFA	trifluoroacetic acid
TFE	trifluoroethanol
THF	tetrahydrofuran
TIR	Toll‐like/IL-1R domain
TLC	thin layer chromatography
TLR	Toll-like receptor
TMT	trimethyltyrosine
TNBS	trinitrobenzene sulfonic acid
Tollip	Toll-interacting protein
TRH	thyrotrophin-related hormone
TRAF-6	TNF receptor-associated factor 6
TTAB	tetradecyltrimethylammonium bromide
UV-Vis	ultraviolet-visible
μW	microwave
vCD	vibrational circular dichroism
VEGF	vascular endothelial growth factor

REMERCIEMENTS

Tout d'abord, mes plus sincères remerciements au docteur Sylvain Chemtob qui, à l'été 2008, a accepté de m'engager comme stagiaire d'été au sein de son laboratoire de pharmacologie de l'Hôpital Ste-Justine, malgré mon manque d'expérience et mon curriculum centralisé en sciences pures. Cette expérience dynamique m'a permis de franchir mes premiers pas en recherche. Sans son professionnalisme et son don inné pour l'innovation, je n'aurais probablement pas entrepris un parcours d'études graduées en recherche. Pour la profonde compréhension et le support aiguillonnant qu'il m'a manifesté dans les moments les plus fragiles, merci.

Tout aussi chèrement, j'aimerais remercier le professeur William Lubell, qui m'a convaincu d'entrer en chimie plutôt qu'en pharmacologie à l'Université de Montréal, et qui m'a grandement inspiré par son enthousiasme et son dynamisme sans bornes. Pour les qualités indélébiles de chercheur qu'il ma inculqué telles que le jugement critique, l'acharnement et la pondération, ainsi que pour l'aide inestimable et la moralité assidue qu'il ma promulgué dans les périodes plus ardues, merci.

De surcroît, milles mercis à tous les membres, passés et présents du groupe Chemtob : Mélanie Sanchez, Baraa Noueihed, Nicolas Sitaras, Jean-Sébastien Joyal, Mike Sapieha, Éric Lapalme, Houda Tahiri, François Duhamel, Vikrant Bhosle, François Binet, Xin Hou, Tang Zhu, José-Carlos Rivera et Ankush Madaan. Plus particulièrement merci à Christiane Quiniou pour sa passion contagieuse, Isabelle Lahaie pour son inestimable écoute et serviabilité, et David Hamel pour ses précieux conseils et ses persévérants encouragements. Autant de mercis aux membres du groupe Lubell, anciens et actuels : Yésica Garcìa-Ramos, Daniel St-Cyr, Tanya Godina, Teresa Lama, Robert Hopewell, Julien Dufour-Galant, Stéphane Turcotte, Jochen Spiegel, Carine Bourguet, Felix Polyak, Jeff Tshikaba, Tarek Kassem, Aurélie Dörr et Mildred Bien-Aimé. Plus particulièrement merci à Caroline Proulx pour sa franche camaraderie, les fous rires et son professionnalisme, et Nicolas Boutard pour son support moral et sa cordialité.

Également merci à Karine Venne, Marie-Christine Tang, Christophe Camy et Alexandra Fürtos du laboratoire de spectrométrie de masse pour leur vaste contribution tant au niveau scientifique que social. Énorme merci à Fabrice Galaud, Benoît Jolicoeur et Pierre Lavallée du laboratoire de chimie combinatoire pour leur soutien chevronné; ainsi qu'à Cédric Malveau et Minh Tan Phan Viet du laboratoire de résonance magnétique pour leur assistance soutenue. Je remercie également Golfam Ghafourifar et Karen Waldron pour les analyses d'électrophorèse par capillaire et leurs suggestions analytiques.

Finalement, un profond merci à ma frangine adorée, Jade, pour son réconfort hermétique et sa vision éclairée, ainsi qu'à mes remarquables parents, Lise et Christian, pour leurs coriaces encouragements et leur immuable support. Et un merci tout spécial à celui qui m'a épaulé chaque jour durant, pour le meilleur et pour le pire, Sylvain Dubé.

CHAPTER 1

Introduction

1.1 Interleukin-1β

1.1.1 Cytokines

Cytokines are small (generally 5 to 30 kDa; Vilcek, **2006**) signaling molecules that regulate the mammalian immune system. Cytokines are commonly designated as inflammatory "hormones", because they are secreted by a broad variety of cells and possess auto-, endo- and paracrine actions with potency comparable to other peptide hormones. Of the numerous families of cytokines known, the interleukin-1 (IL-1) superfamily is primarily associated with acute and chronic bouts of inflammation (Gabay *et al.*, **2010**; Dinarello, **2011**). Initially, IL-1 was designated by several terms, each one referring to a biological effect observed by a given laboratory (Dinarello, **1994**). Subsequently, two forms of the cytokine were individually cloned in the 1980s (March *et al.*, **1985**), and a more structure-oriented classification of IL-1 was established; however, confusion still arises from the multiple appellations given to the newly discovered family members by different laboratories. In the new millennium, a standardised nomenclature was proposed in which the term IL-FX is used and X corresponds to the form (F) number (Sims *et al.*, **2001**).

1.1.2 IL-1 superfamily

The IL-1 superfamily includes eleven distinct members. The principal members are IL-1α, IL-1β, IL-1Ra, IL-18 and IL-33, which share close genomic and proteomic similarities (Dinarello, **2011**). For example, the encoding regions of IL-1α and IL-1β are located side by side on the human chromosome 2 (Webb *et al.*, **1986**). In spite of having only 27% amino acid sequence homology, IL-1α and IL-1β both adopt a similar tertiary conformation (Priestle *et al.*, **1989**; Graves *et al.*, **1990**) made of twelve β-strands arranged into a single opening six-stranded-barrel, sometimes called a β-trefoil (Figure 1.1). Typical of most IL-1 family members, IL-1α and IL-1β impart similar physiological effects but have different cellular localization patterns as well as distinct mechanisms of maturation and secretion. Both of these IL-1 forms are produced mainly by stimulated monocytes as well as macrophages (Dinarello, **1994**), and to a lesser extent by multiple other cell types, including neutrophils, keratinocytes, epithelial and endothelial cells, lymphocytes, smooth muscle cells, fibroblasts and certain melanomas. Although both cytokines are synthesized as 31 kDa precursor peptides, only the pro-IL-1α has intrinsic activity (Mosley *et al.*, **1987**; Black *et al.*, **1988**). Mature IL-1α is constitutively secreted in primary cells, anchored primarily into the cytosolic membrane and signals through autocrine or juxtacrine mechanisms (Brody *et al.*, **1989**; Weber *et al.*, **2010**). On the other hand, pro-IL-1β is cleaved by an enzyme known as caspase-1 (or IL-1-converting enzyme, ICE) and secreted through unconventional pathways (Gabay *et al.*, **2010**; Weber *et al.*, **2010**). IL-1β is the predominantly secreted form of IL-1.

Figure 1.1. The β-trefoil structure of IL-1β (β-sheets are shown in red, coil in magenta and α-helices in cyan) (PDB ID 2I1B, Priestle *et al.*, **1989**).

1.1.3 IL-1 Receptors

Members of the IL-1 family of receptors contain activators and suppressors of inflammation. The physiological effects of IL-1 are mediated through binding to the IL-1 type I receptor (IL-1RI) (Sims *et al.*, **1988**). The type II receptor (IL-1RII) functions as a decoy receptor, which inhibits triggering of IL-1-related pathways (Colotta *et al.*, **1994**). In spite of minimal amino acid homology, the structure of all IL-1 receptor family members displays either one or three immunoglobulin (Ig)-like folds. For example, IL-1RI contains three such Ig-like extracellular domains as well as a cytoplasmic domain that shares some homology with other members of the IL-1R and Toll-like receptor (TLR) families, the so-called Toll-like/IL-1R (TIR) domain (Dunne *et al.*, **2003**; Subramaniam *et al.*, **2004**). An Ig fold features two β-pleated sheets fixed by intradomain disulfide bonds between conserved cysteine residues (Subramaniam *et al.*, **2004**). Upon binding of IL-1β to IL-1RI, the receptor undergoes a conformational change which allows recruitment of a second receptor chain, called the IL-1 receptor accessory protein (IL-1RAcP) (Greenfeder *et al.*, **1995**). Assembled together, the IL-1β/IL-1RI/IL-1RAcP complex forms the heterodimeric signaling trigger (Figure 1.2). Although most cell types express ubiquitously IL-1RI, expression of IL-1RAcP is not constitutive in some cells (Dinarello, **2009**). By consequence, not all cell types expressing IL-1RI are able to activate the various IL-1-related signaling pathways.

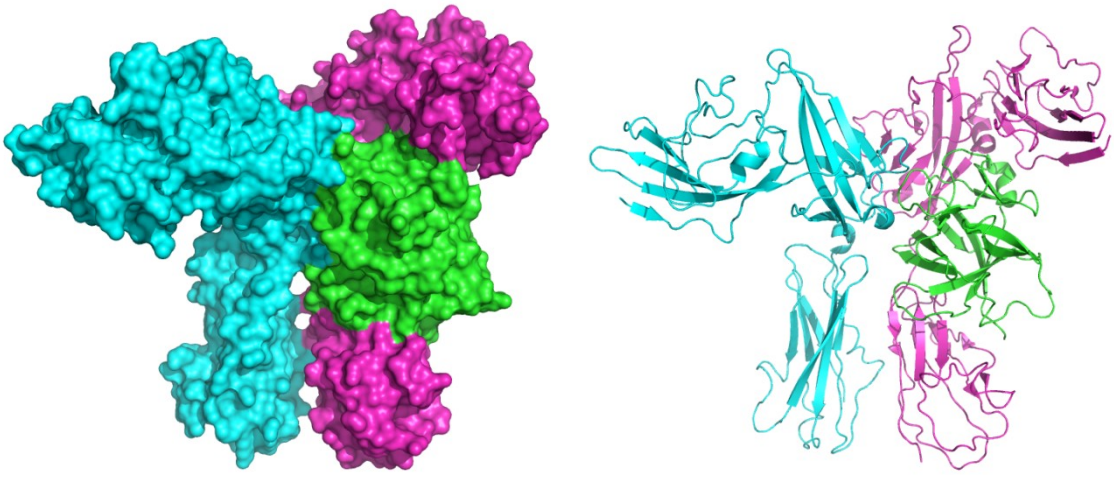

Figure 1.2. Crystal structure of cytosolic IL-1R complex (IL-1RI is shown in magenta, IL-1RAcP in cyan and IL-1β in green; PDB ID 3O4O; Wang *et al.*, **2010**).

1.1.4 IL-1β-mediated signaling pathways

There exist numerous IL-1β-related intracellular signaling pathways (Weber *et al.*, **2010**). Herein, a simplified version of the canonical signaling cascade is described (Figure 1.3). First, in response to the formation of the IL-1β/IL-1RI/IL-1RAcP ternary complex, a mosaic of combinatorial phosphorylation and ubiquitination events are triggered. These ultimately result in the activation of nuclear factor (NF)-κB signaling, as well as initiation of pathways mediated by the extracellular signal‐regulated kinase (ERK), c-Jun *N*-terminal kinase (JNK) and p38 mitogen-activated protein kinase (MAPK). These pathways cooperatively induce the expression of canonical IL-1 target genes (notably IL-6, IL-8, MCP-1, COX-2, IκBα, IL-1α, IL-1β, MKP-1) by transcriptional and posttranscriptional mechanisms. Of note, most intracellular components that partake in the cellular response to IL-1 also mediate responses to other cytokines (IL-18, IL-33 and other IL-1 family members), TLRs and many forms of cytotoxic stresses.

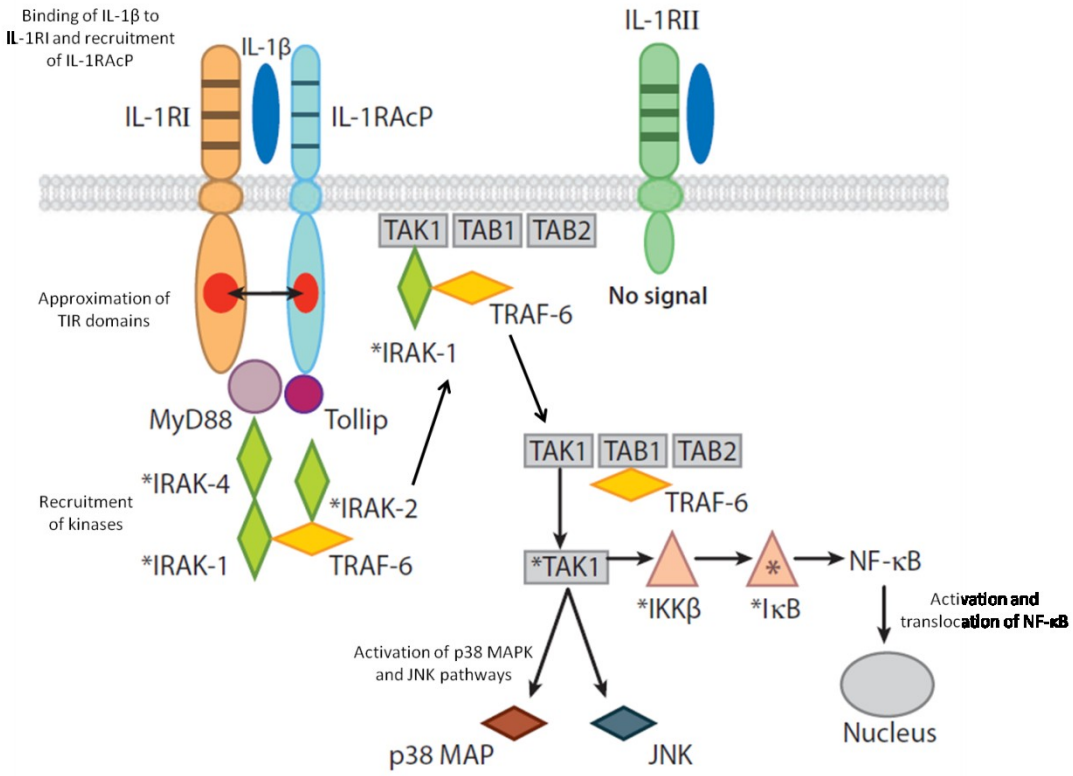

Figure 1.3. Main IL-1β signaling pathways (adapted from Dinarello, **2009**). Common abbreviations: IL-1β, interleukin-1β; IL-1RI, IL-1 receptor type I; IL-1RAcP, IL-1R accessory protein; IL-1RII, IL-1 receptor type II; MyD88, myeloid differentiation primary response gene 88; Tollip, toll-interacting protein; IRAK-1, IL-1 receptor-associated kinase 1; TRAF-6, TNF receptor associated factor 6; TAK1, transforming growth factor-β-activated kinase 1; TAB1, TAK1-binding protein; IκB, IkappaBα and IkappaBβ complex; IKKβ, IκB kinase; NF-κB, nuclear factor kappaB; p38 MAPK, p38 mitogen-activated protein kinase; JNK, c-Jun *N*-terminal kinase. The asterisk (*) denotes phosphorylated proteins.

1.1.5 Physiological roles

The primary function of IL-1-type cytokines is to control proinflammatory reactions in response to detection of pathogen- and danger-associated molecular patterns (PAMPS and DAMPS, respectively) (Weber *et al.*, **2010**). IL-1-type cytokines are therefore considered major mediators of innate immune reactions. In particular, IL-1β is considered as a primary proinflammatory mediator, because it is expressed by many different cellular types and partakes in numerous signaling pathways leading to expression of inflammatory factors. Depending on the cascade activated, IL-1β may stimulate a broad variety of physiological effects (Dinarello, **1997**): metabolic, inflammatory, immunologic, physiologic and hematologic. In brief, IL-1β induces the production of nitric oxide (NO), cyclooxygenase (COX)-2, prostaglandin E_2 (PGE_2), intercellular adhesion molecule-1 (ICAM-1), metalloproteinases (MMP-1), growth factors (GM-CSF, VEGF), cytokines (IL-1β and TNF-α), chemokines and hematopoietic factors (fibrinogen, PAF). The sum of these factors will ultimately lead to hyperthermia, hypotension, tissue destruction, hematopoiesis, triggering of innate and adaptive immune responses and inflammation.

1.1.6 IL-1β-related diseases

By virtue of its various physiologic effects, a slight imbalance in IL-1β frequently leads to pathogenetic conditions. For example, IL-1β plays a major role in a wide range of inflammatory, autoinflammatory and autoimmune diseases. These include, but are not restricted to, rheumatoid arthritis (RA), osteoarthritis (OA), chronic obstructive pulmonary disease (COPD), asthma, inflammatory bowel disease (IBD), atherosclerosis, cryopyrin-associated periodic syndrome (CAPS), family mediterranean fever (FMF), as well as diseases of the central nervous system such as multiple sclerosis (MS), Alzheimer's disease and stroke (Lachmann *et al.*, **2011**; Dinarello, **2011**). In recent years, research has unveiled other potential IL-1β-related indications, such as pericarditis, type 2 diabetes (T2D) and smoldering multiple myeloma (SMM), a hardly curable form of bone cancer (Gabay *et al.*, **2010**). In sum, IL-1β has emerged as an important therapeutic target for an expanding number of systemic and local inflammatory conditions.

1.2 Targeting IL-1β

With greater knowledge of the key physiologic and pathogenetic roles of IL-1β, several endogenous inhibitors have been identified and numerous targeting agents have been developed. The main anti-IL-1β strategies are briefly described below.

1.2.1 Endogenous IL-1β inhibitors

There exist several natural inhibitors of IL-1β, including IL-1Ra, IL-1RII, single immunoglobulin IL-1R-related molecule (SIGIRR), soluble receptors and signaling inhibitors (Figure 1.4) (Gabay *et al.*, **2010**). Several studies have substantiated that the balance between proinflammatory versus anti-inflammatory cytokines affects the severity of inflammatory diseases. Therefore, maintenance of a tight balance between IL-1β and its endogenous regulators is critical to avoid excessive inflammatory responses (Arend, **2002**).

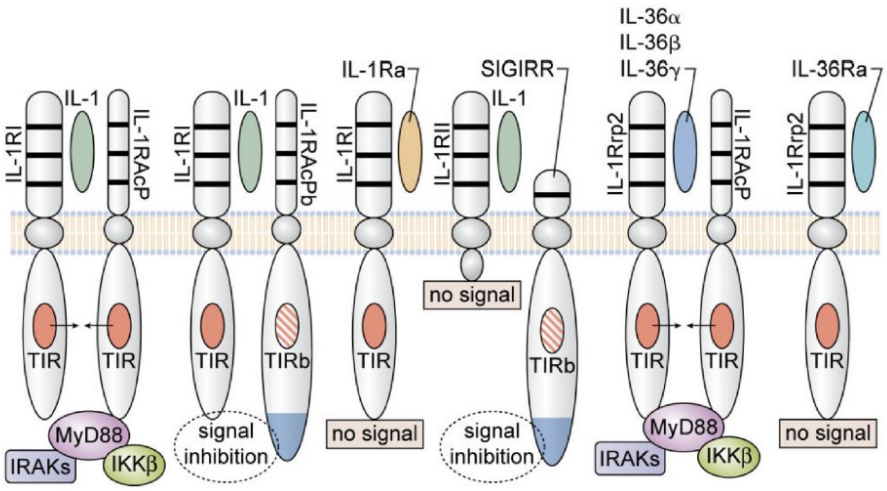

Figure 1.4. Natural inhibitors of IL-1 (Dinarello, **2011**).

IL-1Ra was the first competitive antagonist to a cytokine receptor to be described in the literature (Arend **1985**). The key regulatory role of IL-1Ra was demonstrated using IL-1Ra-knockout mice, which developed excessive inflammatory responses and spontaneous skin and joint inflammation (Ma *et al.*, **1998**; Horai *et al.*, **2000**). Notably, children deficient in IL-1Ra suffer more from autoinflammatory disease (Gabay **2009**). Although IL-1Ra possesses a β-trefoil structure similar to that of IL-1β, it lacks the loop between β-strands 4 and 5, which is essential for agonistic action (Dunn *et al.*, **2003b**). IL-1Ra is therefore a competitive inhibitor of IL1-RI, with near equal affinity as IL-1β. However, a 100- to 1000-fold excess of IL-1Ra is needed to competitively block IL-1 activity both *in vitro* and *in vivo* (Dinarello *et al.*, **1991**).

IL-1RII lacks the cytoplasmic TIR domain necessary for initiating intracellular signaling (Colotta *et al.*, **1994**). By consequence, IL-1RII binding to IL-1β and subsequent recruitment of the accessory protein forms a non-signaling complex which efficiently sequesters IL-1β at the membrane. Moreover, IL-1β binds to IL-1RII with a greater affinity than IL-1α and IL-1Ra (Smith *et al.*, **2003**). Therefore, IL-1RII acts as a dominant negative modulator of the IL-1β-dependent signaling.

SIGIRR belongs to the IL-1R family, but possesses a single extracellular Ig-like domain and an additional 100 amino acid *C*-terminal tail (Qin *et al.*, **2005**; Gabay *et al.*, **2010**). Although no ligands were clearly identified for SIGIRR, its TIR domain is known to inhibit activation of NF-κB, ERKs and JNKs by trapping the signaling molecules TRAF6 and IRAK-1 (Qin *et al.*, **2005**). The extracellular portion of SIGIRR is also suspected to interfere with the heterodimerization of IL-1RI and IL-1RAcP (Qin *et al.*, **2005**).

In addition to their membrane-bound forms, soluble receptors (sIL-1RI, sIL-1RII and sIL-1RAcP) are readily released by cells and bind to IL-1 in this microenvironment, preventing it from mediating cellular activity. Binding of IL-1β to sIL-1RII is nearly irreversible, due to a slow dissociation rate, whereas sIL-1RAcP enhances the binding affinity of both IL-1α and IL-1β to sIL-1RII (Smith *et al.*, **2003**), and can form an inactive complex with surface-expressed IL-1RI bound to IL-1. A neuronal-specific splice variant of IL-1RAcP, termed IL-1RAcPb, has been shown to form a complex with IL-1RI, without leading to recruitment of MyD88 and IRAKs (Smith *et al.*, **2009**).

1.2.2 Anti-IL-1β therapies

Numerous avenues for anti-IL-1β therapy have been exploited by the pharmaceutical industry during the past 15 years (Dumont, **2006**, Braddock *et al.*, **2004**, Dinarello *et al.*, **1991**). Although many have served as tools in experimental models of inflammation, few have been tested in clinical trials, and only three have been approved by the Food and Drug Administration of the USA (FDA). The following paragraphs summarize the main anti-IL-1β inhibitors, in accordance with their mode of action.

1.2.2.1 Inhibition of IL-1β production

Blockers of IL-1β production may target its transcription, processing or release. A popular approach adopted by companies to impede IL-1β processing (Figure 1.5) has been to inhibit caspase-1, also called IL-1-converting enzyme (ICE) due to its ability to cleave off pro-IL-1β into its mature form. Orally active ICE inhibitors have been investigated in humans (Dumont, **2006**). These include peptidomimetics of an active tetrapeptide (Ac-Tyr-Val-Ala-Asp-CHO) (Thornberry *et al.*, **1994**), namely the pyridiazopinedione Pralnacasan (**1.1**, Rudolphi *et al.*, **2003**), the constrained *tert*-glycyl-proline analog (**1.2**, VX-765, Stack *et al.*, **2005**) and the quinoxaline mimetic SNS-11 (**1.3**, O'Brien *et al.*, **2005**) (Figure 1.6). The purinergic receptor $P2X_7R$ has also been targeted to antagonize IL-1β processing and release, because of its involvement in the ATP-dependent activation of ICE and the secretion of IL-1β. Blockers of $P2X_7R$ include adamantane AZD-9056 (**1.4**, Chambers *et al.*, **2010**) and diarylimidazolines SAR-7b (**1.5**, Merriman *et al.*, **2005**). Two fungal metabolites, the terpenoid lactone LL-Z1271α (**1.6**, Ichikawa *et al.*, **2001**) and the picolinate CJ-14,877 (**1.7**, Ichikawa *et al.*, **2001b**; Perregaux *et al.*, **2001**), as well as pyridazines such as K-832 (**1.8**, Tabunoki *et al.*, 2003) displayed IL-1 production inhibition, albeit with unknown mechanisms of action.

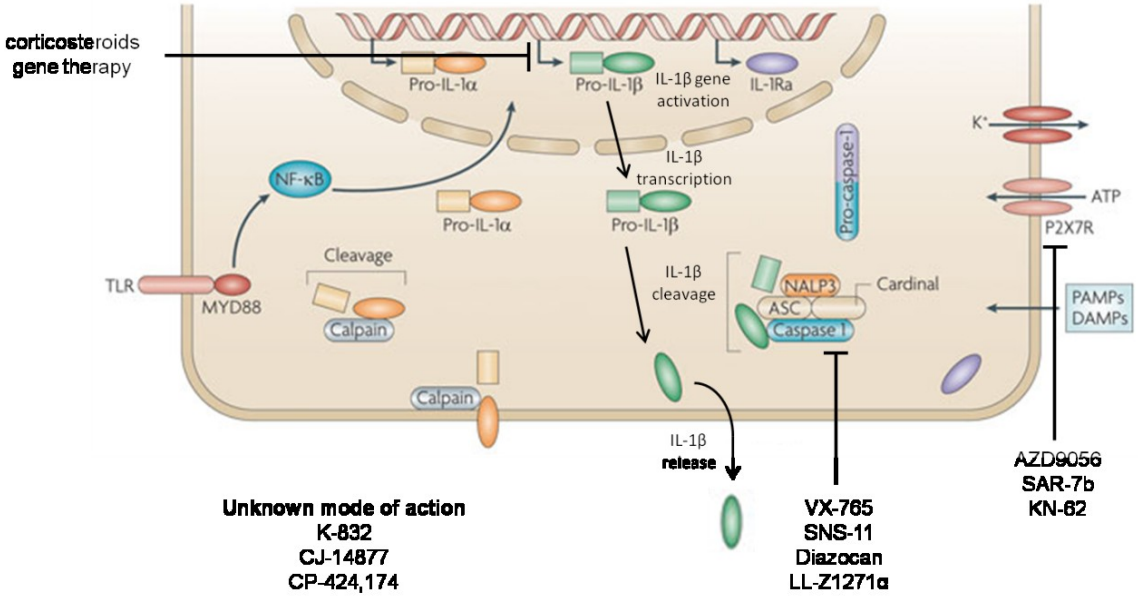

Figure 1.5. Main inhibitors of IL-1β production (adapted from Kopf *et al.*, **2010**).

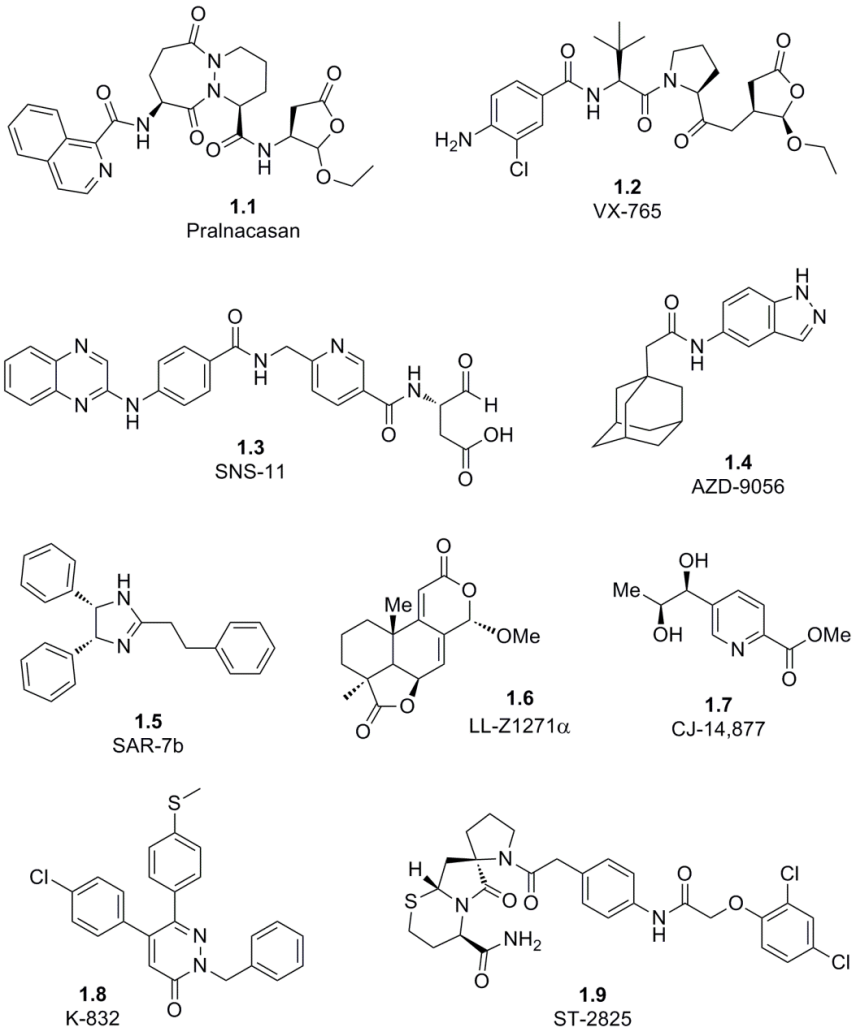

Figure 1.6. Structure of small anti-IL-1β molecules.

1.2.2.2 Inhibition of IL-1β action

After IL-1β is secreted in the extracellular environment, its action can be antagonized by neutralising IL-1β itself or by blocking its receptor (Figure 1.7). As discussed in the previous section, IL-1β can be neutralized by binding to soluble receptors, such as sIL-1RI, sIL-1RII and sIL-1RAcP (Smeets *et al.*, **2003**), which have higher affinity for the cytokine than membrane-bound forms. Phase I clinical studies with shIL-1RII indicated a bioavailability (*f*) of 65% and a serum half-life ($t_{½}$) of 58 hours when administered subcutaneously in 28 patients affected by rheumatoid arthritis (Caldwell, **2002**). A fusion protein consisting of the two extracellular portions of IL-1RII and IL-1RAcP bound to the crystallisable fragment (Fc) of an IgG, termed IL-1 trap, has been developed to sequester IL-1β and IL-1α (Guller *et al.*, **2001**). Several antibodies have been raised against IL-1β and IL-1RI, including Hu007 (Bright *et al.*, **2003**; Bright *et al.*, **2005**), AAL160 (Gram *et al.*, **2001**), ACZ-885 (Gram *et al.*, **2002**) and XOMA052 (Owyang *et al.*, **2011**), which are IL-1β-specific humanised antibody without cross reactivity with IL-1α or IL-1Ra. The murine monoclonal antibodies AF201 and MAB201 (Witte, **2003**) both inhibit the interaction of IL-1RAcP with IL-1β/IL-1RI. Using a murine autoimmunisation protocol, linear and cyclic peptides

corresponding to murine IL-1β regions which come in close proximity to IL-1RI upon binding, have been delivered as immunogens, which produce significant levels of neutralising antibodies against the native murine IL-1β (Geraghty *et al.*, **2005**). The same protocol is under investigation to elicit hIL-1β neutralising antibodies in humans.

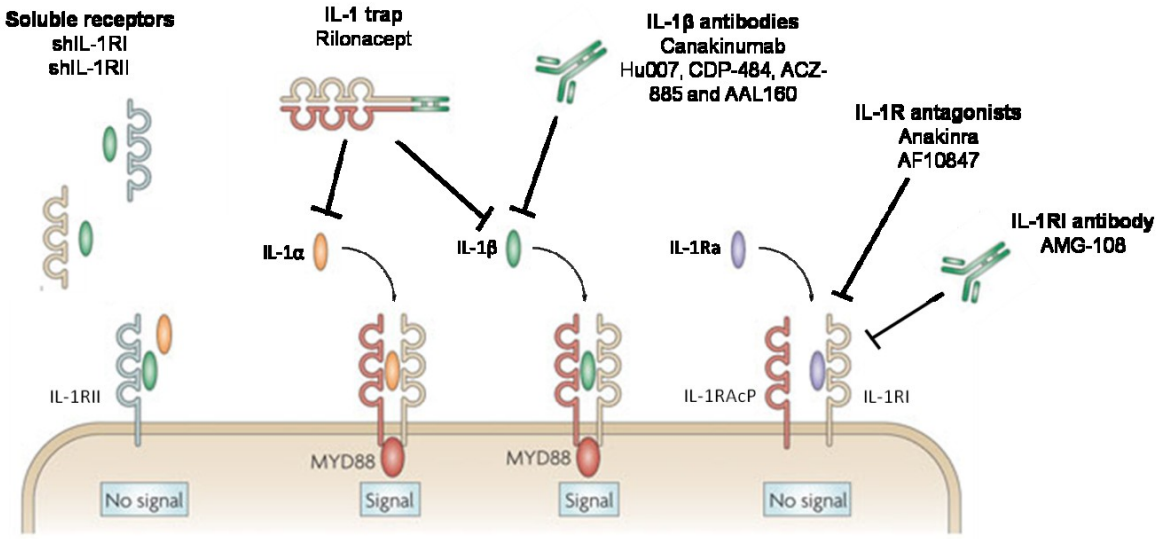

Figure 1.7. Main antagonists of IL-1β action (adapted from Kopf **2010**).

Pharmaceutical companies have also worked to directly block IL-1R. Multiple studies evaluating gene therapy using retroviral constructs encoding human IL-1Ra are currently underway in patients afflicted with RA (Nita **1996**). Synthetic antagonists, such as recombinant hIL-1Ra (Furst **2004**) and the uncosapeptide AF10847 (Brandhuber **2004**) have prevented IL-1β binding to IL-1RI by occupying the binding site. In both cases, failure to interact with the second binding site located in the third Ig-like receptor domain prevented initiation of signaling. Fully human anti-IL-1RI and anti-IL-1RAcP mAbs have been described. The former, AMG108 (Cardiel **2010**; Varnum **2009**), targeted the third Ig domain of IL-1RI, blocking the binding of IL-1β to the receptor without interfering with that of IL-1Ra.

1.2.2.3 Inhibition of IL-1β signaling

Once IL-1β has bound to IL-1RI and formed its receptor complex with IL-1RAcP, the signaling cascades are activated. Inhibitors of IL-1β signaling may thus interfere with several molecular targets. For example, the genes encoding the primary effector protein, MyD88, have been targeted with antisense oligonucleotides (Vickers **2006**). The spiropyrrolothiazin-6-one ST-2825 (**1.9**, Loiarro **2007**) inhibited IL-1β-induced effects both *in vitro* and *in vivo,* presumably by mimicking the loop of the TIR domain of IL-1RI. NF-κB activation has been blocked using mimetics of truncated IRAK-4 proteins, as well as the synthetic D-decapeptide RDP-58 (Travis **2005**), which correspond to the interface between IRAK-1 and TRAF-6. Other primary targets which yielded anti-IL-1β activity include p38 MAPK and IKK-2 inhibitors: however, because numerous components of IL-1β signaling are shared with those of TLRs and the receptors of other cytokines, such approach may lack specificity.

1.2.3 FDA-approved anti-IL-1 biologics

Of the numerous strategies developed to antagonize IL-1β, the three which have been approved by the FDA are biologics sharing common characteristics: similar mode of action, mode of administration and profile of adverse effects (Figure 1.8).

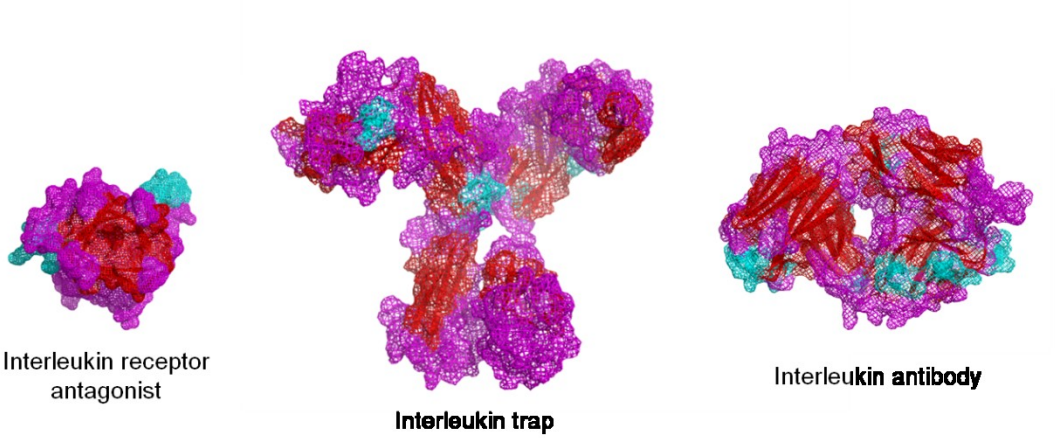

Figure 1.8. Representative crystal structures of FDA-approved anti-interleukin biologics (IL-1Ra: PDB ID 1ILR, Schreuder *et al.*, **1995**; IL-1 trap: PDB ID 3O4O, Wang *et al.*, **2010**; IL-1 mAb: PDB ID 3I2C, Teplyakov *et al.*, **2010**).

1.2.3.1 Anakinra

Anakinra (Kineret®; Amgen, USA) is a 17.3 kDa recombinant protein of the natural human IL-1R antagonist (hIL-1Ra), which differs from the native unglycosylated protein by the addition of an *N*-terminal methionine residue. It was approved by the FDA in 2001 to treat the signs and symptoms of rheumatoid arthritis. Daily injections are needed to sustain the therapeutic effect of anakinra because the average half-life is between 4 and 6 hours and a large excess of drug is needed to block the effect of IL-1β (Furst, **2004**). Consequently, this anti-IL-1 therapy engenders unwanted side effects such as moderate injection-site reactions, increased risk to Gram-positive bacterial infection, immunogenicity and neutropenia (Amgen Product monography, **2008**). The annual cost for an adult patient is evaluated to US$ 18,180 (Kapur *et al.*, **2009**).

1.2.3.2 Rilonacept

IL-1 trap (Rilonacept or Arcalyst®; Regeneron, USA) is a dimeric fusion protein composed of the Fc fraction of human IgG coupled to the extracellular binding motifs of IL-1RI and IL-1RAcP. This technology, which is also in use to trap IL-4, IL-13 and vascular endothelial growth factor (VEGF), works by sequestering the cytokine. Rilonacept was approved by the FDA in 2008 to treat the cryopyrin-associated periodic syndrome (CAPS), and has received the orphan drug approval for familial cold auto-inflammatory syndromes (FCAS) and the Muckle-Wells syndrome (MWS) in adults and children aged 12 years or older. This treatment is administered weekly through subcutaneous injections, and has an average annual cost of US$ 360,000 (Kapur *et al.*, **2009**). In a significant number of patients, Rilonacept induces moderate injection-site reactions, respiratory infections, colitis, gastrointestinal bleeding, and immunogenicity (FDA, **2008**).

1.2.3.3 Canakinumab

Canakinumab (Ilaris®; Novartis, Switzerland) is a fully human monoclonal antibody against IL-1β, weighing 145 kDa. It was approved by the FDA in 2009 to treat patients suffering from the orphan disease CAPS, and more recently from systemic-onset juvenile idiopathic arthritis (SoJIA). This treatment costs approximately US$ 96,000 annually (Whalen *et al.*, **2011**; P&T, **2009**), and must be administered either intravenously or subcutaneously, every eight weeks (Dhimolea, **2010**). Canakinumab has a half-life of 28 to 30 days and a bioavailability of 70% (Dhimolea, **2010**). Canakinumab has been shown to cause certain adverse effects, such as mild injection-site reactions, increased risk to infections and higher occurrence of vertigo (Dhimolea, **2010**).

1.2.3.4 Summary

Therapeutic successes have been achieved with three FDA-approved anti-IL-1β molecules, albeit with several drawbacks due to their appreciable size and weak “drug-like” properties. As biologics, they are relatively expensive and must be injected regularly. Moreover, they completely abrogate IL-1β action, including the desired effects of the cytokine, such as the triggering of the innate immune response, which may impoverish the host defence against microorganism infections. Prolonged IL-1β blockade may also promote the development of insulin resistance, promoting the development of T2D (Somm *et al.*, **2006**). Canakinumab, rilonacept and anakinra are biomacromolecules, which may contain immunogenic epitopes in their sequences. Over time, host organisms may thus produce neutralising antibody against these drugs, necessitating higher doses to attain the same therapeutic effect with higher risks of toxicity. In summary, there remains a clear and unmet medical need to produce small absorbable IL-1R antagonists.

1.3 Our problematic

1.3.1 Small IL-1β antagonists

Although small inhibitors of IL-1R have so far been difficult to generate, they would offer an appreciable number of therapeutic advantages compared to large biologics, such as an improved pharmacokinetic (ADMET) profile. Properties such as light molecular weight, small polar surface area and lower hydrophilicity could improve enteral bioavailability and permit oral administration. Moreover, small molecules are generally more protease resistant, which may prolong duration of action by diminishing metabolism and excretion. They may additionally present lower risk of immunogenicity and toxicity, due to weaker reactivity with enzymes and immune sensors. Small antagonists may likely be more affordable to produce. In addition to benefiting from improved properties related to their size, small IL-1R antagonists may also take advantage of the key features of an allosteric modulator, as discussed below.

1.3.2 Allosteric IL-1R modulators

1.3.2.1 Allosteric modulators

Allosteric modulators are ligands that modify protein responses to agonists, inhibitors and substrates upon binding (Goodey *et al.*, **2008**). Allosteric modulators, by definition, bind to a protein at a site discrete from

the natural substrate binding site, referred to as the orthosteric site. Three general types of allosteric modulators are described in drug discovery: positive, neutral and negative. Upon binding, positive allosteric modulators (PAM) augment the orthosteric ligand effect, neutral allosteric modulators have no observable effect on protein function, and negative allosteric modulators (NAM) usually inhibit the natural ligand action.

Both multi-subunit and monomeric proteins (i.e., receptors and enzymes) can be subjected to allosteric modulation. In contrast to the classical "two-state" concept, receptors are presently thought to exist in a dynamic state, represented by an ensemble of conformers (Hall *et al.*, **2000**). Upon binding of a ligand, local and systemic conformational changes may occur, leading to a variation in the thermodynamic equilibrium of conformers. Ligands may bind preferably to certain receptor forms, and thereby drive the conformational equilibrium toward a "preferred" state (Burgen, **1966**). Modulation of the conformational equilibrium may therefore alter receptor activity and influence protein function.

1.3.2.2 Allostery versus orthostery

Several advantages may be achieved in developing allosteric modulators as therapeutic drugs (Kenakin *et al.*, **2004**). For example, an allosteric modulator may demonstrate functional selectivity (or biased signalisation), exhibiting different biological effects depending on the orthosteric ligand utilized, and blocking or activating selectively certain signaling pathways while not affecting others. Moreover, an allosteric modulator has a saturable effect on its molecular target, such that an excess of this drug would augment duration of action without affecting maximum potency. Allosteric modulators may show subtype specificity, because they may bind at discrete sites, which differ between isoforms. These key characteristics of allosteric modulators may thus confer lower toxicity, higher selectivity and increased specificity.

1.3.2.3 The IL-1R system and allosteric modulation

Allosteric modulation of IL-1R by a small antagonist may have beneficial features. For example, allosteric modulator may circumvent issues of inhibiting primary immune responses to microorganism invasion, which may occur using competitive inhibitors that intercept all IL-1 signalisation. A negative allosteric modulator to the IL-1R complex may thus block certain pathways that lead to pathologic signals and conserve others that participate in essential immunological functions. Subtype-specific modulators may also prevent inhibition of the soluble and alternatively spliced isoforms of the receptor and accessory protein, key natural IL-1β-regulators. Along these lines, a 75 kDa recombinant protein of the major extracellular portion of the IL-1RAcP demonstrated *in vivo* efficacy in a model of autoimmune arthritis without interfering with all IL-1RI-exerted actions (Smeets *et al.*, **2005**).

1.3.3 Peptides as small IL-1R allosteric modulators

1.3.3.1 Interface peptides

Among many strategies to modulate receptor activity, the "interface peptide" approach (Zutshi *et al.*, **1996**; Peczuh *et al.*, **2000**) employs a receptor-derived amino acid sequence to inhibit the inter-domain or protein-protein interactions of the receptor. By interfacing via insertion into an appropriate part of the receptor

itself or via interaction with the subunit, such peptides may displace the equilibrium of conformers and alter biological functions. Such “interface” peptides may be generated using a process termed peptide scanning (Eichler, **2008**), in which short synthetic peptides are based on the protein sequence in a systematic manner which maps sections of the protein using overlapping fragments. Subsequent biological analysis of the peptides allows identification of the regions of the protein responsible for ligand recognition and activity. Such peptides may later serve to develop non-peptidic structures which inhibit the same inter-domain or protein-protein interactions.

1.3.3.2 Successful examples of interface peptides in drug development

Among successful interface peptides, a short peptide derived from the sixth transmembrane domain of human β_2-adrenergic receptor (β_2AR) inhibited homodimerization of the receptor, which could not be inhibited by usual means (SDS, DDT or MR), and blocked adrenergic agonist-promoted stimulation of adenylyl cyclase activity (Hebert *et al.*, **1996**). Likewise, from a library of one- and two-strand peptides, candidates were identified which affected the assembly of proteases 1 and 2 of human immunodeficiency virus 1 (HIV-1), and prevented viral maturation (Babé *et al.*, **1992**; Zutshi *et al.*, **1997**). Octameric peptides were designed specifically to target the dimer interface of human thymidylate synthase (hTS) (Figure 1.9), a homodimeric enzyme that plays a key role in DNA synthesis and is a primary target in anticancer therapy. The peptides bound at a previously unknown allosteric site on hTS, causing inhibition of the intracellular enzyme, thereby reducing cellular growth in both cisplatin-sensitive and -resistant ovarian cancer cells (Cardinale *et al.*, **2011**).

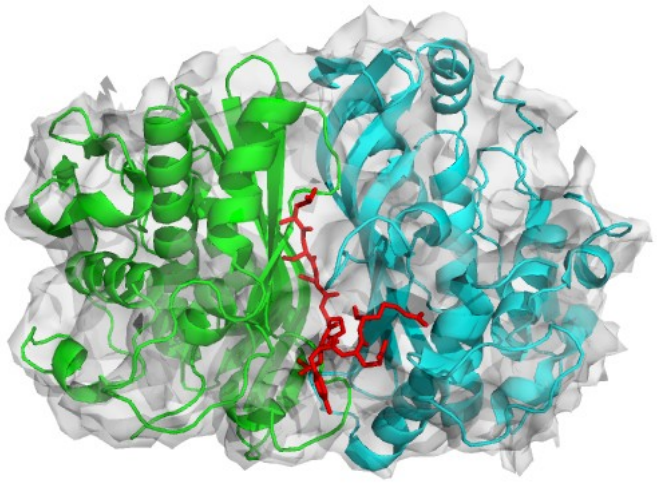

Figure 1.9. Allosteric peptide (red) binding to the interface of a hTS dimer (blue and green) (PDB ID 3N5E, Cardinale *et al.*, **2011**).

1.3.3.3 Peptides as drugs

Peptides display notable advantages as drug candidates (Vlieghe *et al.*, **2010**). Compared to proteins and antibodies, peptides possess a diminished immunogenic potential, lower manufacturing costs, greater

stability during storage, and better organ and tumour penetration, resulting in an ameliorated biodistribution. Therapeutic peptides may also offer benefits over small organic molecules, including: greater efficacy, selectivity and specificity; minimized system toxicity caused by their safer metabolites (amino acids); reduced bioaccumulation owing to their short half-life and greater structural diversity.

Nonetheless, peptides are generally considered to possess limited clinical potential due to their intrinsic physicochemical properties, as interpreted using Lipinski's rule of five (Lipinski *et al.*, **2004**), supplemented by the rules of Veber *et al.* (Veber *et al.*, **2002**). Peptides may have relatively poor drug-like properties including low oral bioavailability (oftenly requiring parenteral administration), short half-life owing to rapid degradation by proteolytic enzymes contained in the digestive and circulatory systems, rapid hepatic and renal clearances, poor ability to cross physiological barriers caused by their large size and hydrophilicity, and high conformational flexibility, occasionally resulting in off-target interactions. Peptides may thus be good entry points in a drug pipeline; however, chemical modification strategies may be necessary to improve their pharmacokinetic properties, particularly when a good enteral absorption is desired such as in cases of chronic inflammatory diseases.

Along these lines, peptides have been employed to modulate IL-1R, because peptides are generated based on receptor fragments, facilitating analysis of the target interaction at the level of individual amino acid, and because their amino acid residues are subject to a wide variation of inter- and intramolecular interactions (dipole-dipole, saline bridges, H-bonds, van der Waals) to favor multiple peptide-protein binding modes. Furthermore, chemical methodology of peptides is well developed and may enable convenient and fast diversification of the scaffold. Finally, natural and short peptides are generally less toxic and immunogenic than their smaller organic and large biologic counterparts, respectively.

1.4 Peptide mimicry

1.4.1 Basis of peptide mimicry

Peptide mimicry has been used to circumvent issues associated with natural peptides as drug candidates. Peptidomimetics (peptide mimics) may be designed to replicate the natural peptide three-dimensional (3D) arrangement of pharmacophores, to retain the affinity for biological targets and to produce analogous biological effects as the parent peptide. Peptide mimic development requires identification of structure-activity relationships (SARs) to define the minimal active sequence (MAS) and the major pharmacophore elements responsible for activity (Vagner *et al.*, **2008**). Conformational constraints may then be applied to probe the topography of the key peptide structural features. Typical modifications employed by medicinal chemists to optimize a natural peptide through peptide mimicry are described in the following sections.

1.4.2 Chemical strategies in peptide mimicry

In the absence of spectroscopic and X-ray crystallographic data concerning the structure of ligand–receptor complexes, the conformation and pharmacophore responsible for the function of the peptide may be elucidated by examination of the activities of various analogues. Such studies may provide an elaborated view point for understanding the form employed for the activity of the natural peptide, as well as valuable leads for building peptide mimics with enhanced physiological properties.

1.4.2.1 Truncation and analysis of global chirality

A lead peptide may be truncated one residue at a time, from the *N*- and *C*-termini, in order to find the MAS, which is desired because shorter peptides reduce the synthetic effort to generate successive analogues and simplify the analysis of their analogue-receptor interactions. Thereafter, the significance of configuration and sequence orientation may be probed by *Ret* design (Ret or retro-enantio; Goodman *et al.*, **1979**; Fletcher *et al.*, **1998**), where three analogues are produced: the enantio peptide, where the chirality of all amino acids is reversed, the retro-peptide where the amino and carboxy termini are exchanged, and the retro-inverso analogue where both modifications are applied at once. Typically, *Ret* isomers have been used to examine the conformation, enzymatic stability and activity of cyclic and linear peptides. In the former case, the *Ret* isomers allowed to lock the absolute three-dimensionnal orientation of the side-chains, independently of the backbone, whereas in linear peptides, they have been used to produce four different topochemical arrangements (Goodman *et al.*, **1979**).

1.4.2.2 Amino acid scans

The relative importance of particular functional groups in the primary peptide sequence may be determined by conducting various systematic scans and testing for biological activity (Vagner *et al.*, **2008**). For example, an alanine scan, in which a library of peptides is generated each possessing one amino acid replaced by an alanine residue, may determine the importance of the side-chain of each residue for molecular recognition and signal transduction contignent on the extent of losses or gains in activity. The importance of stereochemistry may be assessed similarly by scanning the sequence with corresponding enantiomeric amino acids. To distinguish enantiomeric residues in peptides and proteins, L-amino acids are typically written in capital letters whereas their D-counterparts are expressed in lower cases. In L-peptides, introduction of D-amino acids may favour turn conformations and destabilize helices, such that the importance of conformation may be inferred. Further insight into the stereoelectronic and steric requirements of the receptor binding pocket may be gained by modifying the chiral, hydrophobic, steric and acid-base properties of key side-chain moieties. For example, tyrosine may be substituted by phenylalanine to address the importance of the phenol H-bond donor capacity as well as aromatic electron density. Other scanning approaches, including proline and glycine scans, have complementary applications, but will not be discussed here.

1.4.2.3 Local conformational constraints

An additional step which may be taken towards identification of the relationships between biological activity and conformation entails restricting peptide flexibility to determine which conformers are important for activity. This latter corresponds to the conformation adopted by the peptide chain when it binds to its receptor. Organization of the peptide chain to bind to its receptor comes with entropic and enthalpic costs, such that preorganization by conformational restriction may enhance affinity and potency. Certain secondary structures may be energetically preferred (Ramachandran *et al.*, **1968**); i.e., helical, extended and turn conformations (Figure 1.10). These structures are defined by the backbone dihedral angles phi (ϕ), psi (ψ) and omega (ω), respectively about the backbone atoms C'-N-Cα-C', N-Cα-C'-N', as well as the atoms Cα-C'-N-Cα (Figure 1.11).

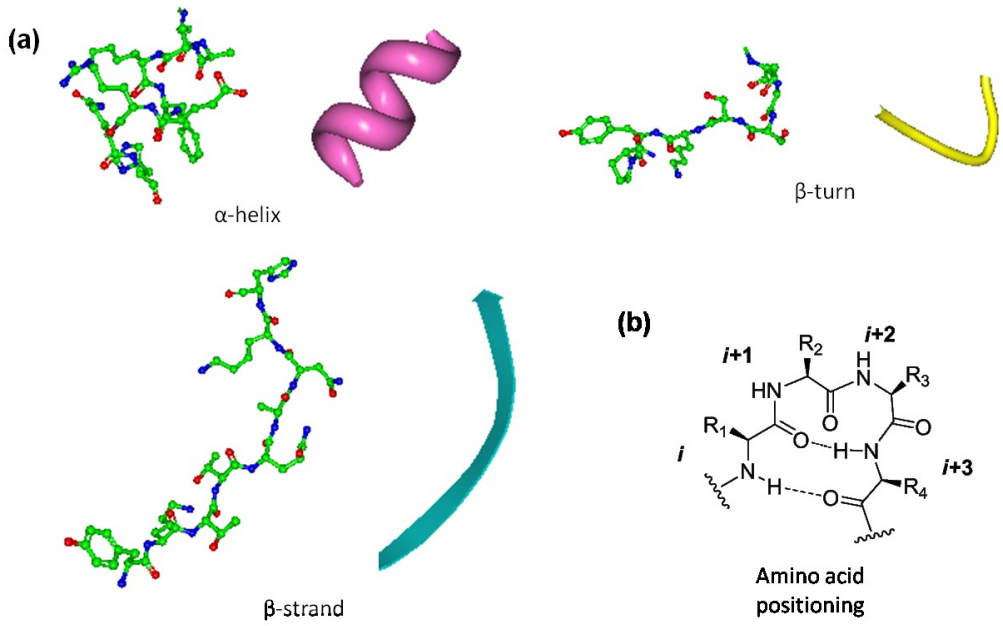

Figure 1.10. (a) Representative helix, strand and turn secondary structures (PDB ID 3I7W, Lewinski *et al.*, **2009**; adapted from Lubell *et al.*, **2012**) and (b) nomenclature of amino acid positioning in secondary structures: *i* defines the first residue of a fold, whereas *i+1* denotes the second residue, and so-on.

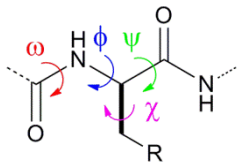

Figure 1.11. Dihedral angles of a peptide chain.

Nonetheless, elucidation of the bioactive conformation of a peptide may be challenging, due to the inherent flexibility of most small linear peptides, but may be facilitated by limiting flexibility through constraint of the dihedral angles by cyclization. Cyclizations from side chain to side chain, side chain to backbone, *C*-terminus to *N*-terminus, backbone to backbone and various combinations have been used to bias the entire or specific sections of the peptide to favour particular conformations. Positional scanning by replacement of amino acids with cyclic counterparts, such as proline and pipecolic acid (Homoproline, Hpr), cyclic urea derivatives, or lactams, places local constraints on the backbone dihedral angles (Figure 1.12) (Maes *et al.*, **2009**; Hopewell *et al.*, **2012**). Alternatively, α-substituted amino acids can be used to bias the backbone conformation towards α-helix, extended or β-turn conformations, depending on the nature of the α-substitution and the nature of the group attached to the first side-chain carbon (χ^1). For example, sterically hindered dialkyl amino acids such as α-aminoisobutyric acid (Aib), α,α-diethylglycine (Deg), and 1-aminocycloalkane-1-carboxylic acids (Acnc, with n=3-8) may favour helices (Figure 1.13) (Grieco *et al.*, **2002**; Marshall *et al.*, **1990**).

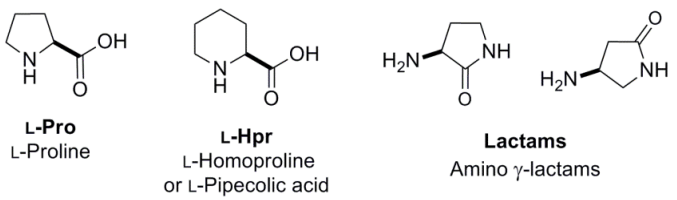

Figure 1.12. Cyclic α-amino acids as local conformational constraints.

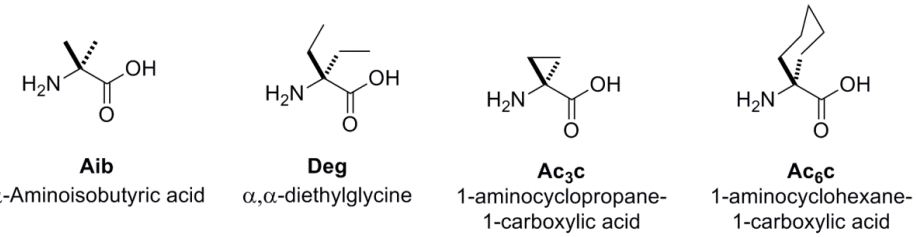

Figure 1.13. Dialkyl α-amino acids as secondary structures stabilizers.

1.4.2.4 Bicycles as global conformational restrictions

Bicyclic templates are commonly used as global rigidifying moieties, because they restrict conformations by a combination of structural constraints and steric interactions (Vagner **2008**). Azabicycloalkanone amino acids are dipeptide surrogates (Hanessian *et al.*, **1997**; Halab *et al.*, **1998**; Gosselin *et al.*, **2000**; Cluzeau *et al.*, **2005**) containing side chain to side chain and side chain to backbone constraints, which may mimic type II' β-turn geometry contingent on stereochemistry. Many azabicycloalkanone derivatives have been made incorporating variations of ring substituent, stereochemistry and size, including [5,5]-pyrrolizidinone, [6,5]-indolizidin-2-one (I^2aa), [6,6]-quino-lizidin-2-one (Q^2aa), [5,6]-indolizidin-9-one (I^9aa), [7,5]-pyrroloazepin-2-one (P^2aa), and [8,5]-pyrroloazocinone (Figure 1.14; Vagner *et al.*, **2008**).

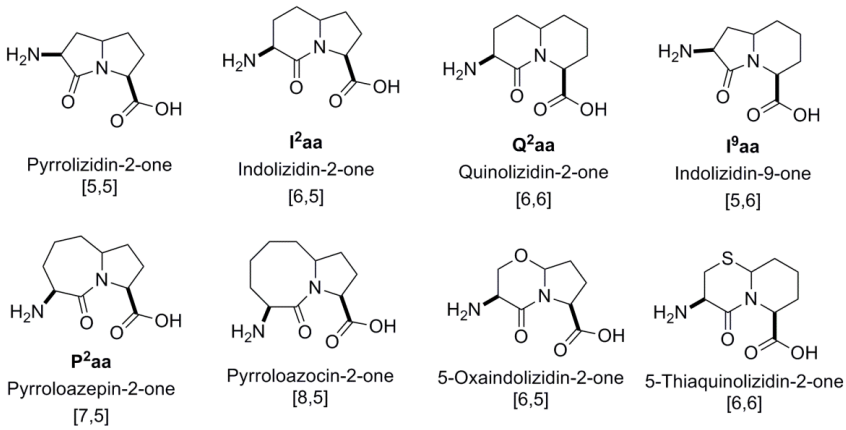

Figure 1.14. Typical azabicycloalkanone amino acids (adapted from Vagner *et al.*, **2008**).

1.4.2.5 Side-chain constraints

Most amino acid side-chains have relatively unhindered rotations about their torsional angles: referred to as χ^1 for the angle between Cα-Cβ bonds, χ^2 for the Cβ-Cγ bond, and so on (Figure 1.11). For example, low

barriers for rotation exist between the three minimum energy conformations about χ^1: *gauche* (–), *gauche* (+) and *trans*. In contact with the receptor, certain side-chain topography may be important for molecular recognition and signal transduction, which can be identified by replacing more flexible amino acids by rigid analogues. For example, hydrogen atoms may be replaced by methyl groups to bias side-chain torsional angle geometry and hinder rotation, such as with β-methyl-2′,6′-dimethyltyrosine (trimethyltyrosine, TMT), 1-amino-2,2'-dimethylcyclopropane carboxylic acid (c_3Val) and β-methylphenylalanine (MePhe), can be utilized (Hruby *et al.*, **2000**). Employing such residues to favour distinct χ^1 side-chain conformations may help elucidate the preferred chain topography.

1.4.2.6 Isosteric replacements

Protease-resistance may be achieved by replacement of amide bonds with non-hydrolysable isosteres (Figure 1.15) (Spatola *et al.*, **1986**; Vagner *et al.*, **2008**). Amide bond isosteres may also restrict flexibility, alter peptide geometry and hydrophilicity through distinct hydrogen bonding patterns and inter-residue length.

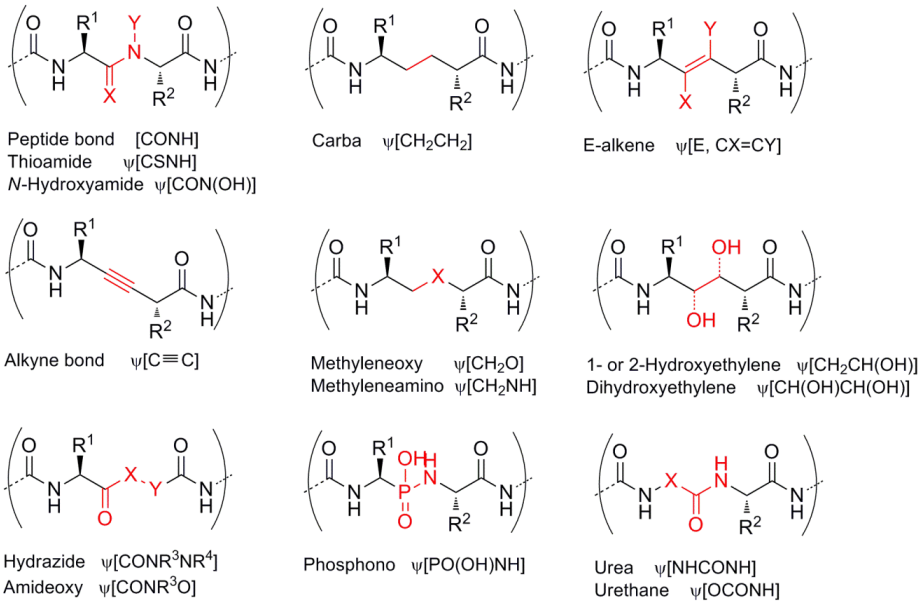

Figure 1.15. Common amide bond isosteres (Vagner *et al.*, **2008**).

1.4.2.7 Other substitutions

Other key strategies used in peptide mimicry feature modifications of the amino acid backbone carbon (Cα). For example, aza-amino acids (carbazic acids) may stabilize secondary structures by adding stereo-electronic restrictions about the Nα (Proulx *et al.*, **2011**). Similarly, peptides bearing β- or γ-amino acids, as well as *N*-alkyl glycines (peptoids), all have been used to alter the conformation and pharmacokinetic properties of peptides (Krauthäuser *et al.*, **1997**). In addition, chemical end capping by *N*-acylation, *C*-esterification and *C*-amidation, glycosylation, pegylation and *N*-alkylation, have been utilized in varying ways to modify conformation and to enhance plasma stability, reduce immunogenicity and retard excretion through the kidneys (Chalmers *et al.*, **1995**).

1.4.3 Challenges in peptide mimicry

In spite of success, peptide mimicry remains a challenging task, because of the difficulties in accurately mimicking larger sections of protein secondary and tertiary motifs (*e.g.* β-sheets) using smaller synthetic surrogates, synthetic challenges and limited guidelines for translating relatively flexible sequences into mimics of particular active conformations. Combination of multiple chemical strategies has thus been essential for optimizing a peptide lead into a more viable drug candidate.

1.5 Previous work

1.5.1 Discovery of 101.10

On the basis of the overall rationale presented above, a library of interface peptides was generated from sequences of the flexible portions of the IL-1RAcP, which were known to interact with IL-1RI (Chemtob *et al.*, **2005**; Quiniou *et al.*, **2008**). Subsequent pharmacological testing, truncation and examination of the enantiomeric sequence resulted in the discovery of a selective D-peptide antagonist of IL-1RI, termed 101.10 (rytvela), which exhibited key features of an allosteric modulator and efficacy in models of acute bouts of inflammation.

In this process, the extracellular loops and interdomain regions of the IL-1RAcP were identified based on the crystal structure and modeling data of the cytosolic portions of the IL-1RI/IL-1β/IL-1RAcP complex. The hydrophobic domains and flexibility profiles of the loops, as well as their homology with other proteins domains were analyzed using various softwares (PROSITE, ProtScale and ProDom) to provide an initial library of fifteen all D-configured, sense or anti-sense peptides (Figure 1.16). These peptides were tested for potential to modulate IL-1β-stimulated PGE_2 formation. Among the candidates, a peptide (101, aprytvela) from the juxtamembranal flexible loop of the accessory protein exhibited promising activity.

Successive D-alanine and *N*-terminal truncation scans were conducted, and resulting analogues were examined for their activity against IL-1β-triggered proliferation of endothelial cells and phosphorylation of downstream effectors p38 MAPK and IκB (Chemtob *et al.*, **2005**). The D-heptapeptide 101.10, (rytvela, D-Arg^1-D-Tyr^2-D-Thr^3-D-Val^4-D-Glu^5-D-Leu^6-D-Ala^7) (Figure 1.17) shown efficacy and potency in a broad variety of *in vitro* IL-1β-dependent assays: proliferation of thymocytes (IC_{50} = 0.2 nM) and human lung fibroblasts (IC_{50} = 2 nM; E_{max} ≥ 90%), as well as PGE_2 synthesis (IC_{50} = 0.5 nM; E_{max} ≈ 50%) (Quiniou *et al.*, **2008**). Radiolabelled ligand binding experiments revealed the noncompetitive nature of 101.10 on inhibition of IL-1β action and on modulation of IL-1β-binding affinity. The effects of 101.10 were selective for IL-1β and did not affect the activity of homologous cytokines of the IL-1 family: no changes in IL-18-iduced TNF-α- and LPS-dependent JNK as well as p38 phosphorylation, nor IL-6-induced Erk1/2 phosphorylation were observed using 101.10. The *in vivo* efficacy of 101.10 was evaluated in animal models of inflammatory conditions and proved superior to corticosteroids and anakinra. In models of hyperthermia, hypotension, trinitrobenzene sulfonic acid (TNBS)-induced inflammatory bowel disease and phorbol myristate acetate (PMA)-triggered contact dermatitis, 101.10 demonstrated robust anti-inflammatory effects. Morevoer, 101.10 failed to bind to IL-1RI-deficient cells and was ineffective *in vivo* in IL-1RI-knockout mice (Quiniou *et al.*, **2008**).

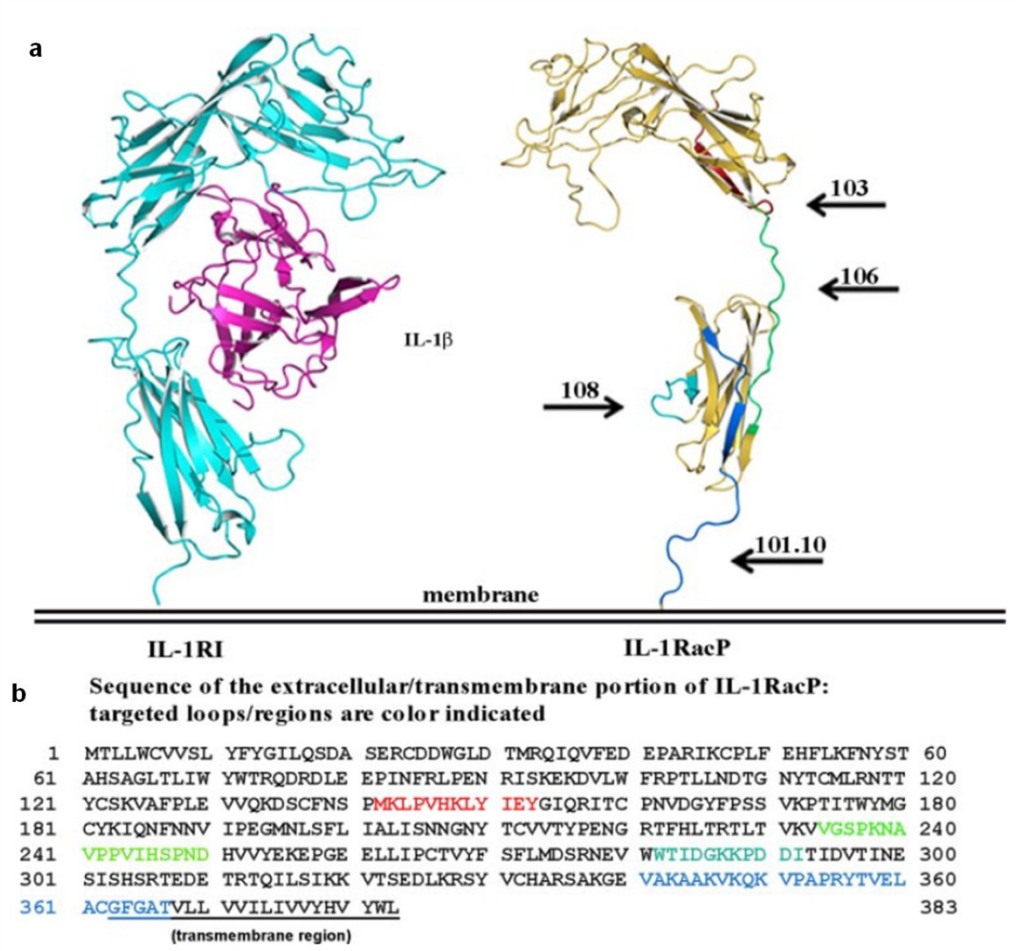

Figure 1.16. Ribbon-like model of IL-1RI/IL-1β/IL-1RAcP complex (a) and primary sequence of the extracellular portion of IL-1RAcP (b). Colored sequences refer to regions that were used to derive interface peptides (Quiniou *et al.*, **2008**).

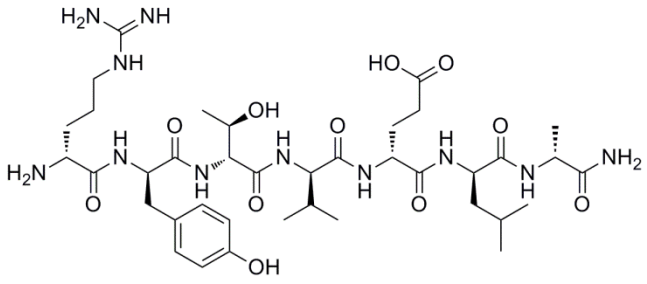

Lead 101.10

D-Arg[1]-D-Tyr[2]-D-Thr[3]-D-Val[4]-D-Glu[5]-D-Leu[6]-D-Ala[7]-NH_2

Figure 1.17. Structure of the lead D-heptapeptide 101.10.

In summary, 101.10 exhibited potent, selective, and reversible non-competitive inhibition of IL-1β activity, without interacting with the ligand binding site, albeit by affecting IL-1β-binding affinity and by interfering variably with different *in vitro* responses to IL-1β. These features distinguished 101.10 as a modulatory

antagonist distinct from the FDA-approved competitive inhibitor anakinra, and the sequestering molecules rilonacept and canakinumab. To improve 101.10 as a drug candidate, efforts were initiated, as described below.

1.5.2 Optimization of 101.10

Modifications were performed on 101.10 to identify the key pharmacophore elements necessary for binding to IL-1RI and to elicit activity (Chemtob *et al.*, **2005**). In attempts to decipher the relative importance of functional groups, systematic conservative replacements of amino acids with analogous residues were conducted at each position along the sequence: i.e., Arg^1 for Cit, Orn and Lys; Tyr^2 for Phe and Trp; Thr^3 for Val and Ser; Val^4 for Pro; Glu^5 for Asp and Gln; Leu^6 for Ile, Met, Val and Ala. Although rytpela exhibited good potency, it was discarded due to low aqueous solubility and poor *in vivo* properties. Successive *N*-terminal truncations identified the region minimum sequence for eliciting antagonistic activity to be Thr^3-Val^4-Glu^5-Leu^6 (Chemtob *et al.*, **2005**).

1.5.3 Project objectives

In light of the earlier findings, the lead peptide 101.10 has been examined further to identify regions of secondary structure necessary for recognition by IL-1RI and activity against IL-1β. Approximately 100 new peptides, peptidomimetics and small analogues of 101.10 have been generated, characterized and tested for biological activity. This master thesis relates specifically my contribution in this effort, and presents current hypotheses concerning the mode of of action of this peptide as well as promising mimics.

1.6 References

Amgen Inc. Product monography for Kineret®, **2008**, 1-31.

Arend, W. P.; Joslin, F. G.; Massoni, R. J. *J. Immunol.* **1985**, *134*, 3868-3875.

Arend, W. P.; Welgus, H. G.; Thompson, R. C.; Eisenberg, S. P. *J. Clin. Invest.***1990**, *85*, 1694-1697.

Arend, W. P. *Cytokine Growth Factor Rev.* **2002**, *13* (4-5), 323-340.

Babé, L. M.; Rosé, J.; Craik, C. S. *Protein Sci.* **1992**, *1* (10), 1244-1253.

Black, R. A.; Kronheim, S. R.; Cantrell, M. *J. Biol. Chem.* **1988**, *263*, 9437-9442.

Braddock, M.; Quinn, A. *Nat. Rev. Drug Discov.* **2004**, *3*, 1-10.

Brandhuber, B. J.; Vigers, G. P. A.; Array BioPharma Inc. Patent US 0014643, **2004**.

Bright, S. W.; Jia, A. Y.; Kuhstoss, S. A.; Manetta, J. V.; Tsurushita, N.; Vasquez, M. J.; Eli Lilly Co. Patent US 0075488, **2005**; and WO 03010282, **2003**.

Brody, D. T.; Durum, S. K. *J. Immunol.* **1989**, *143*, 1183-1187.

Burgen, A. S. V. *Fed. Proc.* **1966**, *40*, 2723-2728.

Caldwell, J. *Proc. Eur. League against Rheum.* **2002**, Abstract FR10098.

Cardiel, M. H.; Tak, P. P.; Bensen, W.; Burch, F. X.; Forejtova, S.; Badurski, J. E.; Kakkar, T.; Bevirt, T.; Ni, L.; McCroskery, E.; Jahreis, A.; Zack, D. J. *Arthritis Res. Ther.* **2010**, *12*, R192.

Cardinale, D.; Guaitoli, G.; Tondi, D.; Luciani, R.; Henrich, S.; Salo-Ahen, O. M. H.; Ferrari, S.; Marverti, G.; Guerrieri, D.; Ligabue, A.; Frassineti, C.; Pozzi, C.; Mangani, S.; Fessas, D.; Guerrini, R.; Ponterini, G.; Wade, R. C.; Costi, M.P. *Proc. Nat. Acad. Sci. USA* **2011**, *108* (34), ES42-49.

Chalmers, D. K.; Marshall, G. R. *J. Am. Chem. Soc.* **1995**, *117*, 5927-5937.

Chambers, L. J.; Stevens, A. J.; Moses, A. P.; Michel, A. D.; Walter, D. S.; Davies, D. J.; Livermore, D. G.; Fonfria, E.; Demont, E. H.; Vimal, M.; Theobald, P. J.; Beswick, P. J.; Gleave, R. J.; Roman, S. A.; Senger, S. *Bioorg. Med. Chem. Lett.* **2010**, *20* (10), 3161-3164.

Chemtob, S.; Quiniou, C.; Lubell, W. D.; Beauchamp, M.; Hansford, K. A. International Patent WO 105830, **2005**.

Cluzeau, J.; Lubell, W. D. *Peptide Sci.* **2005**, *80* (2), 98-150.

Colotta, F.; Dower, S. K.; Sims, J. E.; Mantovani, A. *Immunol. Today* **1994**, *15*, 562-566.

Dhimolea, E. *MAbs.* **2010**, *2* (1), 3-13.

Dinarello, C. A.; Thompson, R. C. *Immunol. Today* **1991**, *12* (11), 404-410.

Dinarello, C. A. *Blood* **1991b**, *77*(8), 1627-52.

Dinarello, C. A. *FASEB J.* **1994**, *8*, 1314-1325.

Dinarello, C. A. *Cytokine & Growth Factor Rev.* **1997**, *8* (4), 253-265.

Dinarello, C. A. *Annu. Rev. Immunol.* **2009**, *27*, 519-550.

Dinarello, C. A. *Blood* **2011**, *117* (14), 3720-32.

Dumont, F. J. *Expert Opin. Ther. Patents* **2006**, *16*(7), 879-912.

Dunn, E. F.; Gay, N. J.; Bristow, A. F.; Gearing, D. P.; O'Neill, L. A.; Pei, X. Y. *Biochemistry* **2003b**, 42, 10938-10944.

Dunne, A.; O'Neill, L. A. J. *Sci. STKE* **2003**, *171*, re3/DC1.

Eichler, J. *Curr. Opin. Chem. Biol.* **2008**, *12*, 707-713.

FDA, Highlights of Prescribing Information, Arcalyst®, **2008**.

Fletcher, M. D.; Campbell, M. M. *Chem. Rev.* **1998**, *98* (2), 763-796.

Furst, D. E. *Clin. Ther.* **2004**, *26*, 1960-1975.

Gabay, C. *Curr. Opin. Invest.Drugs* **2003**, *4*, 593-597.

Gabay, C.; Palmer, G. *Nat. Rev. Rheumatol.* **2009**, *9*, 480-482.

Gabay, C.; Lamacchia, C.; Palmer, G. *Nat. Rev. Rheum.* **2010**, *6*, 232-241.

Garlanda, C.; Anders, H. J.; Mantovani, A. *Trends Immunol.* **2009**, *30*, 439-446.

Geraghty, E.; Zagury, J.-F.; Boissier, M.-C.; Bessis, N.; Vaxconsulting. Patent US 005890, **2005**; and WO 084198, **2005**.

Goodey, N. M.; Benkovic, S. J. *Nat. Chem. Biol.* **2008**, *4*, 474-482.

Goodman, M.; Chorev, M. *Acc. Chem. Res.* **1979**, *12* (1), 1-7.

Gosselin, F.; Lubell, W. D. *J. Org. Chem.* **2000**, *65* (7), 2163-2171.

Gram, H.; Di Padova, F. E.; Novartis A. G. Patent WO0153353, **2001**.

Gram, H.; Di Padova, F. E.; Novartis A. G. Patent WO0216436, **2002**.

Graves, B. J.; Hatada, M. H.; Hendrickson, W. A.; Miller, J. K.; Madison, V. S.; Satow, Y. *Biochemistry* **1990**, *29*, 2679-2684.

Greenfeder, S. A.; Nunes, P.; Kwee, L.; Labow, M.; Chizzonite, R. A.; Ju, G. *J. Biol. Chem.* **1995**, *270*, 13757-13765.

Grieco, P.; Lavecchia, A.; Cai, M.Y.; Trivedi, D.; Weinberg, D.; MacNeil, T.; Van der Ploeg, L. H. T.; Hruby, V. J. *J. Med. Chem.* ***2002****, 45* (24), 5287-5294.

Guler, H.-P.; Caldwell, J.; LittleJohn, T. III; McIlwain, H.; Offenberg, H.; Stahl, N. *Arthritis Rheum*. **2001**, *44*, S370.

Hall, D. A. *Mol. Pharmacol.* **2000**, *58*, 1412-1423.

Hanessian, S.; McNaughton-Smith, G.; Lombart, H.-G.; Lubell, W. D. *Tetrahedron* **1997**, *53* (38), 12789-12854.

Hebert, T. E.; Moffett, S.; Morello, J.-P.; Loisel, T. P.; Bichet, D. G.; Barret, C.; Bouvier, M. *J. Biol. Chem.* **1996**, *271* (27), 16384-16392.

Hopewell, R.; Beauregard, K.; Lubell W. D. *Manuscript in preparation*, **2012**.

Horai, R.; Saijo, S.; Tanioka, H.; Nakae, S.; Sudo, K.; Okahara, A.; Ikuse, T.; Asano, M.; Iwakura, Y. *J. Exp. Med.* **2000**, *191* (2), 313-20.

Ichikawa, K.; Inagaki, T.; Kachi-Tonai, H.; Kojima, Y.; Nakamura, T.-A.; Nishida, H.; Ueno, Y.; Binding, P.; Gabel, C. A.; Lucas, V.; McNiff, P. A.; Kojima, N. *Biochem. Biophys. Res. Comm.* **2001**, *286*, 697-700.

Ichikawa, K.; Hirai, H.; Ishiguro, M.; Kambara, T.; Kato, Y.; Kim, Y. J.; Kojima, Y.; Matsunaga, Y.; Nishida, H.; Shiomi, Y.; Yoshikawa, N.; Kojima, N. *J. Antibiot. Tokyo* **2001b**, *54* (9), 703-709.

Kapur, S.; Bonk, M. E. *Drug Forecast* **2009**, *34* (3), 138-141.

Kenakin, T. *Molec. Interv.* **2004**, *4* (4), 222-229.

Kopf, M.; Bachmann, M. F.; Marsland, B. J. *Nat. Rev. Drug Discov.* **2010**, *9*, 703-718.

Krauthäuser, S.; Christianson, L. A.; Powell, D. R.; Gellman, S. H. *J. Am. Chem. Soc.* **1997**, *119* (48), 11719-11720.

Lachmann, H. J.; Quartier, P.; So, A.; Hawkins, P. N. *Arthritis Rheum.* **2011**, *63* (2), 314-324.

Lewinski, K.; Kurpiewska, K.; Dziubek, K.; Katrusiak, A.; Font, J.; Vilanova, M. *Protein DataBank* ID 3I7W, **2009.**

Lipinski, C. A. *Drug Discov. Today Technol.* **2004**, *1*, 337-341.

Loiarro, M.; Capolunghi, F.; Fantò, N.; Gallo, G.; Campo, S.; Arseni, B.; Carsetti, R.; Carminati. P.; De Santis, R.; Ruggiero, V.; Sette, C. *J. Leukoc. Biol.* **2007**, *82* (4), 801-810.

Lubell, W. D.; Beauregard, K.; Polyak, F. In *Comprehensive Chirality*; Carreira E.; Ed.; Elsevier B.V., Amsterdam, The Netherlands, **2012**, *in press*.

Ma, Y.; Thornton, S.; Boivin, G. P.; Hirsh, D.; Hirsch, R.; Hirsch, E. *Arthritis Rheum.* **1998**, *41*, 1798-805.

Maes, V.; Tourwé, D. In *Aspects of Peptidomimetics, in Peptide and Protein Design for Biopharmaceutical Applications*, Chapter 3, Jensen, K. J., Ed.; John Wiley & Sons, Chichester, UK, **2009**, 294 pages.

March, C. J.; Mosley, B.; Larsen, A.; Cerretti, D. P.; Braedt, G.; Price, V.; Gillis, S.; Henney, C. S.; Kronheim, S. R.; Grabstein, K.; Conlon, P. J.; Hopp, T. P.; Cosman, D. *Nature* **1985**, *315*, 641-647.

Marshall, G. R.; Hodgkin, E. E.; Lansi, D. A.; Smith, G. D.; Zabrocki, J.; Leplawy, M. T. *Proc. Natl. Acad. Sci. USA* **1990**, *87*, 487-491.

Merriman, G. H.; Ma, L.; Shum, P.; McGarry, D.; Volz, F.; Sabol, J.S.; Gross, A.; Zhao, Z.; Rampe, D.; Wang, L.; Wirtz-Brugger, F.; Harris, B. A.; Macdonald, D. *Bioorg. Med. Chem. Lett.* **2005**, *15* (2), 435-438.

Mosley, B.; Urdal, D. L.; Prickett, K. S.; Larsen, A.; Cosman, D.; Conlon, P. J.; Gillis, S.; Dower, S. K. *J. Biol. Chem.* **1987**, *262*, 2941-2944.

Nita, I.; Ghivizzani, S. C.; Galea-Lauri, J.; Bandara, G.; Georgescu, M. I.; Robbins, P. D.; Evans, C. H. *Arthritis Rheum.* **1996**, *39* (5), 820-828.

O'Brien, T.; Fahr, B. T.; Sopko, M. M.; Lam, J. W.; Waal, N. D.; Raimundo, B. C.; Purkey, H. E.; Pham, P.; Romanowski, M. J. *Acta Crystallogr. Sect. F Struct. Biol. Cryst. Commun.* **2005**, *61* (5), 451-458.

Owyang, A. M.; Issafras, H.; Corbin, J.; Ahluwalia, K.; Larsen, P.; Pongo, E.; Handa, M.; Horwitz, A. H.; Roell, M. K.; Haak-Frendscho, M.; Masat, L.; *MAbs* **2011**, *3* (1), 49-60.

Peczuh, M. W.; Hamilton, A. D. *Chem. Rev.* **2000**, *100* (7), 2479–2494.

Perregaux, D. G.; Laliberté, R. E.; Gabel, C. A. *J. Pharmacol. Exp. Ther*. **2001**, *299*, 187-197.

Pharmacy & Therapeutics Committee. *Drugs Ther. Bull.* **2009**, *23* (10), 1-6.

Priestle, J. P.; Schar, H. P.; Grutter, M. G. *Proc. Natl. Acad. Sci. USA* **1989**, *86*, 9667-9671; PDB ID 2I1B.

Proulx, C.; Sabatino, D.; Hopewell, R.; Spiegel, J.; Ramos, Y. G.; Lubell, W. D. *Future Med. Chem.* **2011**, *3* (9), 1139-1164.

Qin, J.; Qian, Y.; Yao, J.; Grace, C.; Li, X. *J. Biol. Chem.* **2005**, *280* (26), 25233-25241.

Quiniou, C.; Sapieha, P.; Lahaie, I.; Hou, X.; Brault, S. Beauchamp, M.; Leduc, M.; Rihakova, L.; Joyal, J.-S.; Nadeau, S.; Heveker, N.; Lubell, W. D.; Sennlaub, F.; Gobeil, F. Jr.; Miller, G.; Pshezhetsky, A. V.; Chemtob, S. *J. Immunol.* **2008**, *180*, 6977-6987.

Ramachandran, G. N.; Sasisekharan, V. *Adv. Protein Chem.* **1968**, *23*, 283-438.

Rudolphi, K.; Gerwin, N.; Verzij, N.; van der Kraan, P.; van der Berg, W. *Osteoarthr.Cartil.* **2003**, *11* (10), 738-746.

Schreuder, H. A.; Rondeau, J. M.; Tardif, C.; Soffientini, A.; Sarubbi, E.; Akeson, A.; Bowlin, T. L.; Yanofsky, S.; Barrett, R. W. *Eur. J. Biochem.* **1995**, *227*, 838-847.

Sims, J. E.; March, C. J.; Cosman, D.; Widmer, M. B.; MacDonald, H. R.; McMahan, C. J.; Grubin, C. E.; Wignall, J. M.; Jackson, J. L.; Call, S. M. *Science* **1988**, *241* (4865), 585-589.

Sims, J. E.; Pan, Y.; Smith, D. E.; Nicklin, M. J. H.; Barton, J. L.; Bazan, J. F.; Kastelein, R. A.; Busfield, S. J.; Ford, J. E.; Lin, H.; Mulero, J. J.; Kumar, S.; Pan, J.; Young, P. R. *Trends Immunol.* **2001**, *22* (10), 536-537.

Smeets, R. L.; Joosten, L. A.; Arntz, O. J.; Bennink, M. B.; Takahashi, N.; Carlsen, H.; Martin, M. U.; van den Berg, M. B.; van de Loo, F. A. *Arthritis Rheum.* **2005**, *52*, 2202-2211.

Smith, D. E.; Hanna, R.; Della, F.; Moore, H.; Chen, H.; Farese, A. M.; MacVittie, T. J.; Virca, G. D.; Sims, J. E. *Immunity* **2003**, *18*, 87-96.

Smith, D. E.; Lipsky, B. P.; Russel, C.; Ketchem, R. R.; Kirchner, J.; Hensley, K.; Huang, Y.; Friedman, W. J.; Boissonneault, V.; Plante, M.-M.; Rivest, S.; Sims, J. E. *Immunity* **2009**, *30* (6), 817-831.

Somm, E.; Cettour-Rose, P.; Asensio, C.; Charollais, A.; Klein, M.; Theander-Carrillo, C.; Juge-Aubry, C. E.; Dayer, J.-M.; Nicklin, M. J. H.; Meda, P. *Diabetologia* **2006**, *49* (2) 387-393.

Spatola, A. F.; Saneii, H.; Edwards, J. V.; Bettag, *A. L.*; Anwer, M. K.; Rowell, P.; Browne, B.; Lahti, R.; Von Voigt- lander, P. *Life Sci.* **1986**, *38*, 1243-1249.

Stack, J. H.; Beaumont, K.; Larsen, P. D.; Straley, K. S.; Henkel, G. W.; Rangle, J. C. R.; Hoffman, H. M. *J. Immunol.* **2005**, *175* (4), 2630-2634.

Subramaniam, S.; Stansberg, C.; Cunningham, C. *Dev. Comp. Immunol.* **2004**, *28*, 415-428.

Tabunoki, Y.; Edano, T.; Murakami, K.; Kobayashi, H.; Koshi, T.; Ohkuchi, M.; Ohshima, S.; Mima, T.; Ishii, T.; Hattori, Y.; Saeki, Y. *Arthritis Rheum.* **2003**, ***48*** **(**Suppl.), S555.

Teplyakov, A.; Obmolova, G.; Rogers, A.; Gilliland, G. L. *Acta Crystallogr.* **2010**, *F66*, 229-232

Thornberry, N. A.; Peterson, E. P.; Zhao, J. J.; Howard, A. D.; Griffin, P. R.; Chapman, K. T. *Biochemistry* **1994**, *33* (13), 3934-3940.

Travis, S.; Yap, L. M.; Hawkey, C.; Warren, B.; Lazarov, M.; Fong, T.; Tesi, R. J. *Inflamm. Bowel Dis.* **2005**, *11* (8), 713-719.

Vagner, J.; Qu, H.; Hruby, V. J. *Curr. Opin. Chem. Biol.* **2008**, *12*, 292-296.

Varnum, B.; Vezina, C.; Witte, A.; Qian, X.; Martin, F. H.; Huang, H.; Elliott, G.; Amgen Inc. Patent US 214559, **2009**.

Veber, D. F.; Johnson, S. R.; Cheng, H.-Y.; Smith, B. R.; Ward. K. W.; Kopple, K. D. *J. Med. Chem.* **2002**, *45* (12), 2615-2623.

Vickers, T. A.; Zhang, H.; Graham, M. J.; Lemonidis, K. M.; Zhao, C.; Dean, N. M. *J. Immunol.* **2006**, *176*, 3652-3661.

Vilcek, J. In *Cytokines and the CNS*, Chapter 2, Ransohoff, R. M.; Benveniste, E. N.; Eds.; CRC Press, Boca Raton, USA, **2006**, 361 pages.

Vlieghe, P.; Lisowski, V.; Martinez, J.; Khrestchatisky, M. *Drug Discov.Today* **2010**, *15* (1/2), 40-56.

Wang, D.; Zhang, S.; Li, L.; Liu, X.; Mei, K.; Wang, X. *Nature Immunol.* **2010**, *11* (10), 905-912.

Webb, A. C.; Collins, K. L.; Auron, P. E.; Eddy, R. L.; Nakai, H.; Byers, M. G.; Haley, L. L.; Henry, W. M.; Shows, T. B. *Lymphokine Res.* **1986**, *5*, 77-85.

Weber, A.; Wasiliew, P.; Kracht, M. *Sci. Signal.* **2010**, ***3*** (105), cm1.

Whalen, J.; Mijuk, G. *Wall Street J.* **2011**, *1*, 1-2.

Witte, A.; Amgen Inc. Patent US 0026806, **2003**.

Zutshi, R.; Brickner, M.; Chmielewski, J. *Curr. Opin. Chem. Biol.* **1996**, 2, 62-66.

Zutshi, R.; Franciskovich, J.; Shultz, M.; Schweitzer, B.; Bishop, P.; Wilson, M.; Chmielewski, J. *J. Am. Chem. Soc.* **1997**, *119*, 4841-4845.

CHAPTER 2

Amino-γ-Lactams

2.1 Introduction

Amino-γ-lactams have been utilized to restrict the mobility, increase selectivity and enhance potency of peptides. Insertion of such lactam residues into a linear peptide may confine the degrees of freedom about the ω and ϕ dihedral angles and diminish the number of rotatable bonds (Freidinger *et al.*, **1980**; Liskamp, **1994**; Loughlin *et al.*, **2010**). Among different types of amino-γ-lactams described, two have been mainly used in peptide science : α-amino-γ-lactam (Agl) and β-amino-γ-lactam (Bgl) (Figure 2.1).

(*S*)-Agl
α-amino γ-lactam

(*S*)-Bgl
β-amino γ-lactam

Figure 2.1. Structure of α- and β-amino-γ-lactams (Agl and Bgl, respectively).

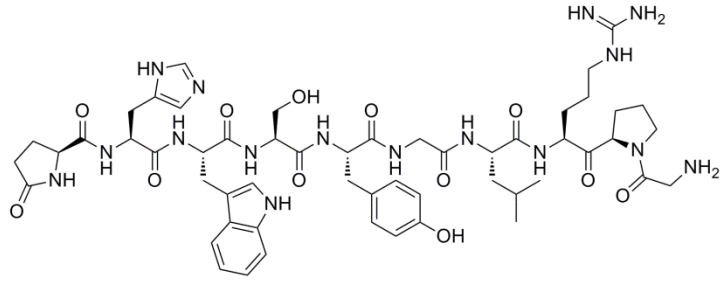

LH-RH, **2.1**
pyro-L-Glu-L-His-L-Trp-L-Ser-L-Tyr-Gly-L-Leu-L-Arg-L-Pro-Gly

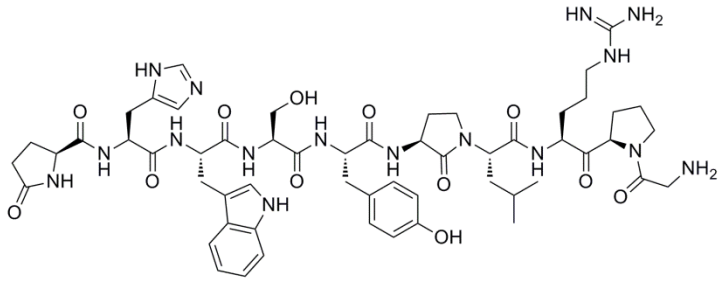

[(*S*)-Agl^6]-LH-RH, **2.2**
pyro-L-Glu-L-His-L-Trp-L-Ser-L-Tyr-(*S*)-Agl-L-Leu-L-Arg-L-Pro-Gly

Figure 2.2. Structure of LH-RH and a (*S*)-Agl^6 analogue.

α-Amino-γ-lactam was first introduced in luteinizing hormone-releasing hormone (LH-RH; **2.1**) by Freidinger and co-workers, producing an analogue (**2.2**) with 8.9 times greater potency than the parent peptide in a pituitary cell culture assay, and exhibited evidence of a bioactive β-turn conformation (Figure 2.2; Freidinger *et al.*, **1980b**). An Agl-containing peptidomimetic (**2.3**) has also demonstrated potent and selective inhibition (K_i = 7 nM) of blood coagulation factor Xa (FXa) in both the rat model of $FeCl_2$-induced carotid artery thrombosis and the rabbit model of jugular vein thrombus formation (Ewing *et al.*, **1999**). The crystal structure of the aminoisoquinoline pyrrolidinonesulfonamide inhibitor named RPR208815 (**2.3**) bound to the human FXa (Figure

2.3) shows the geometrical restrictions produced by the central amino-γ-lactam, necessary to occupy and block the enzyme S1 and S4 pockets (Maignan *et al.*, **2000**).

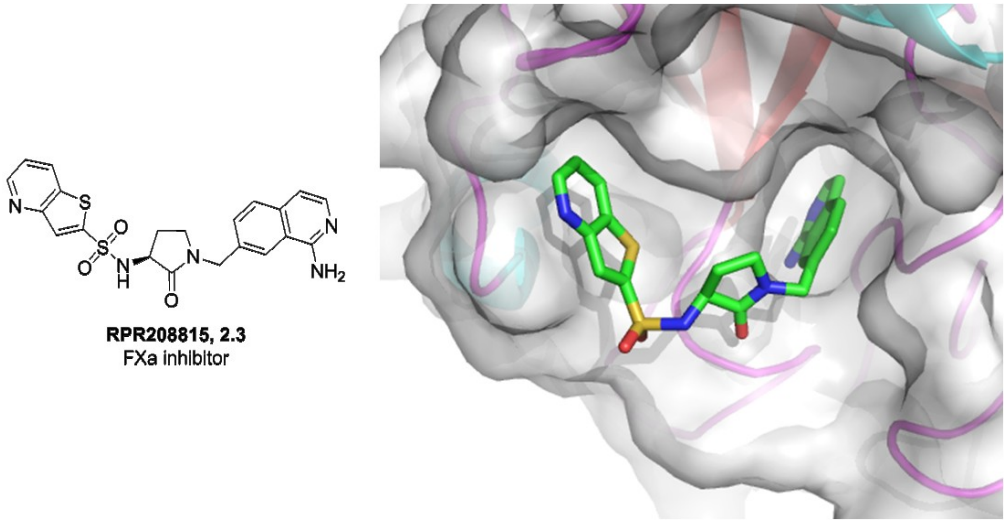

Figure 2.3. Crystal structure of blood coagulation factor Xa complexed with an AgI-bearing inhibitor named RPR208815 (PDB ID 1F0R, Maignan *et al.*, **2000**).

Relative to its α-amino equivalent, β-amino-γ-lactam has been less frequently employed to examine the active conformation of peptides. One notable investigation involves the introduction of a BgI moiety into the minimum peptidic sequence exerting the hypoglycaemic activity of the human growth hormone (hGH), the fragment [6-13]-hGH. Replacement of Asp^{11} for (*S*)-BgI produced an analogue favouring a type II' β-turn (Lee *et al.*, **1997***)* which exhibited extended half-life and preserved biological activity (Ede *et al.*, **1990**; Ede *et al.*, **1991**; Ede *et al.*, **1994**).

AgI and BgI substitutions may be utilized conjointly to take advantage of the distinct orientations of the carbonyl in each lactam ring to study conformational effects. For instance, AgI and BgI have been respectively incorporated into L-prolyl-L-leucyl-glycinamide (PLG), a short peptide modulator of the D_2 dopamine receptors within the central nervous system. These two PLG mimics displayed pharmacological profiles that resembled the parent tripeptide with 100 to 1000 greater potency (Dolbeare *et al.*, **2003**). In addition, amino-γ-lactams have been components of strong chemotherapeutic and antibiotic agents, displaying nanomolar inhibition of serine and cysteine proteases (Scheidt *et al.*, **1998**; Marquis, **2000**; Powers *et al.*, **2002**; Freidinger, **2003**). In these studies, the lactams were hypothesized to act as transition state mimics and both the direction of the carbonyl and the stereochemistry of the amino group affected the ability to inhibit the enzymes tested (Marquis, **2000**; Freidinger, **2003**). Systematic lactam scanning with both AgI and BgI may therefore represent an effective tool for studying conformation and for building complementary mimics of active peptide-based drugs.

2.2 Synthesis of amino-γ-lactams

2.2.1 Previous synthetic approaches

Several strategies have been developed for the insertion of AgI into peptide sequences (Freidinger *et al.*, **1980b**; Wolf *et al.*, **1989**; Schuster *et al.*, **1997**; Wolfe *et al.*, **1997**; Piscopio *et al.*, **1998**; Armstrong, **1998**;

Piscopio *et al.*, **1999**; Freidinger, **2003**; Scott *et al.*, **2004**; Lama *et al.*, **2005**; Galaud *et al.*, **2005**; Bhooma *et al.*, **2006**; Raghavan *et al.*, **2006**; Nöth *et al.*, **2008**). The production of libraries of analogues has however been limited, because the synthesis of the dipeptide lactam has been typically performed in solution before incorporation into the peptide by solid-phase synthesis (Freidinger, **2003**; Scott *et al.*, **2004**). Few solid-phase strategies for lactam synthesis had been elaborated, and most were restricted to the synthesis of dipeptides bearing terminal five- and six-membered rings (Scott *et al.*, **2004**; Lama *et al.*, **2005**), with limited stereocontrol and unsatisfactory yields, precluding any combinatorial usage. In addition, various solution-phase methods have been described to synthesize Bgl-containing peptides (Ede *et al.*, **1990**; Ede *et al.*, **1991**; Ede *et al.*, **1991b**; Boyarskaya *et al.*, **2005**; Dolbeare *et al.*, **2003**): however, to the best of our knowledge, no solid-supported methodologies have been reported prior to our work (Jamieson *et al.*, **2009**).

2.2.2 Our synthetic methodology

In the pursuit of an optimized lead from 101.10, twenty peptidomimetics (**2.8**-**2.27**; Table 2.1 and 2.2) bearing respectively an Agl or Bgl residue of either (*R*)- and (*S*)-configuration were synthesized using two different solid-phase Fmoc-compatible methods. In the Agl and Bgl cases (Scheme 2.1 and 2.2), the approach featured regiospecific *N*-alkylation and lactam annulation onto peptides supported on resin beads employing respectively enantiomerically pure six- and five-membered cyclic sulfamidates (**2.5** and **2.7**) derived from homoserine (**2.4**) and aspartic acid (**2.6**), as chiral educts (Jamieson *et al.*, **2009**; Boutard *et al.*, **2011**). Subsequently, insertion of single and multiple Agl residues into the same peptide was achieved via an analogous method which employed SynPhase® lanterns as solid support (Ronga *et al.*, **2010**).

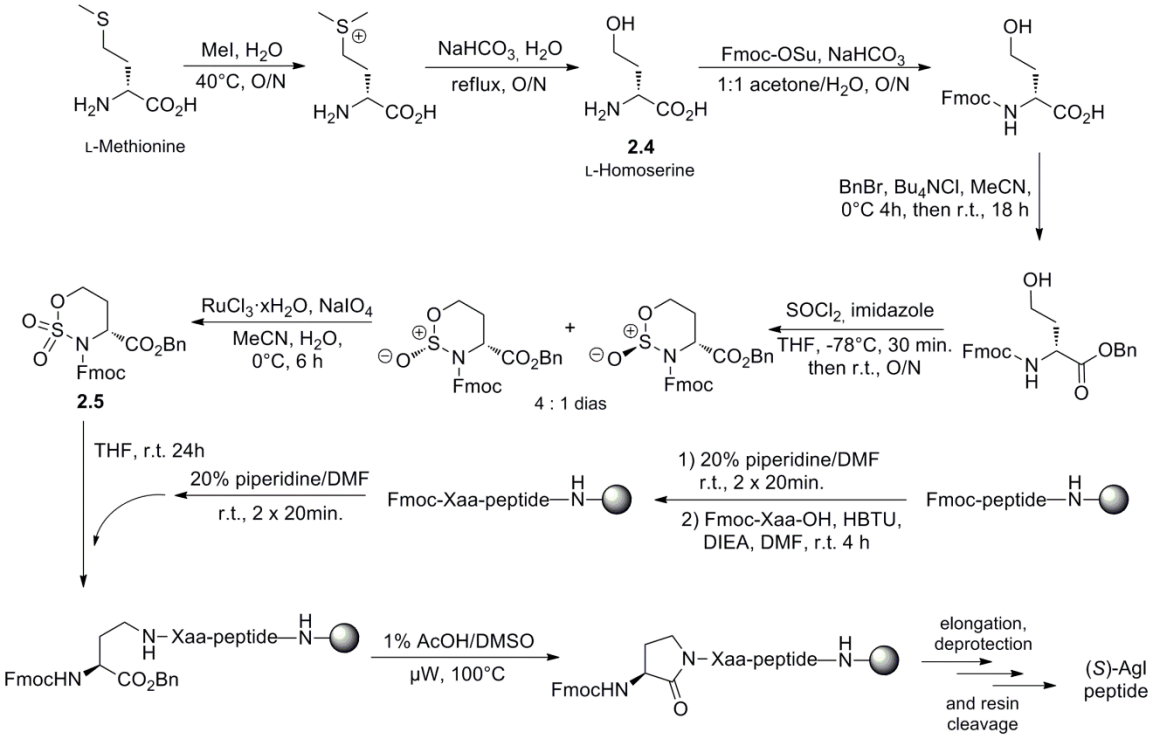

Scheme 2.1. Rink amide resin synthetic approach for Agl-scanning in peptides.

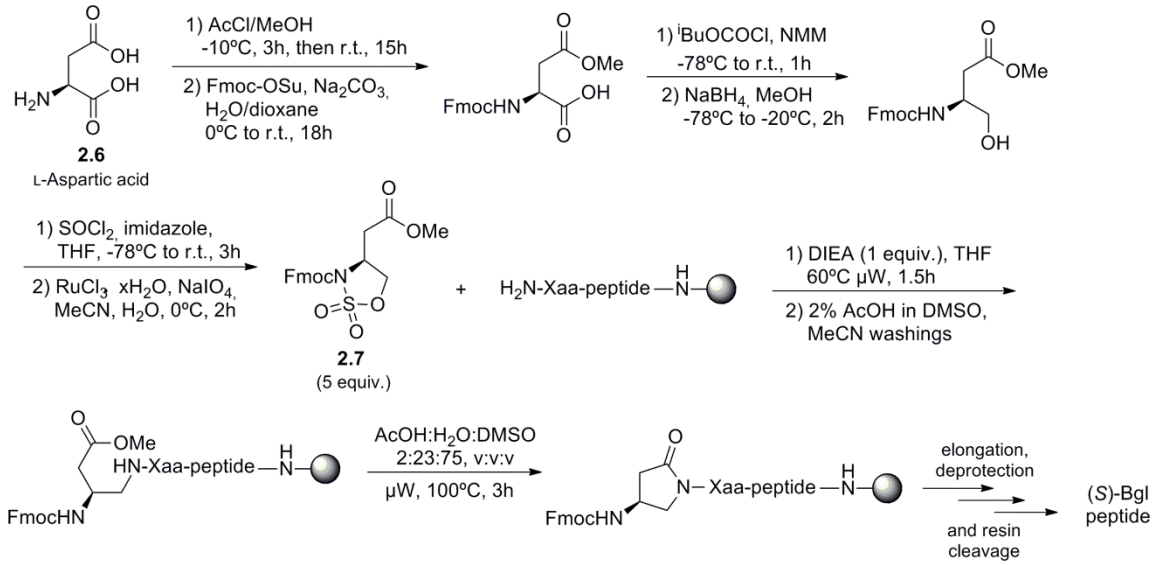

Scheme 2.2. Rink amide resin synthetic approach for Bgl-scanning in peptides.

Employing the resin bead method described above, the Agl analogue **2.8** was resynthesized in the course of this thesis, with improvement on some aspects of the strategy. Specifically, the use of phase-transfer catalysis for the benzylation of L-homoserine and alkylation of the *N*-terminal unprotected peptide without additional bis-alkylation, simplified the synthetic protocols and improved conversions and yields. The lactam peptide **2.8** was recovered in high crude purity and isolated yield, as assessed by analytical RP-HPLC (Table 2.1).

Entry	Peptide	Crude purity %[a]	Purity %[a]	Yield %[b]	HRMS[c]	
					m/z (calcd)	***m/z*** (obsd)
2.8	D-Arg-D-Tyr-(***R***)-**Agl**-D-Val-D-Glu-D-Leu-D-Ala-NH_2	94	> 99	8.4	832.4675	832.4665

Table 2.1. Yields and purities of lactam-containing analogue **2.1** of 101.10. [a] RP-HPLC purity at 280 nm. [b] Yields after purification by RP-HPLC are based on Fmoc loading test for Rink resin. [c] HRMS values from the major protonated molecule, typically $[M+H]^+$.

2.3 Structure-activity relationships of amino-γ-lactams

2.3.1 Conformational analysis

Conformational changes of macromolecules may be assessed using circular dichroism. For example, folding and unfolding of biomolecules (proteins, nucleic acids, and glycosides) may be monitored as changes in circular dichroism (CD) spectra features such as the curve shape and the intensity of positive and negative maxima. Algorithms such as the Chou-Fasman-Prevelige have been used as protein secondary structures prediction software (Prevelige *et al.*, **1989**). Signal in the far-UV region (< 250 nm) may be attributed to peptide amide bonds adopting different types of secondary structures. For instance, a negative n → π* transition band at 195 nm combined with a positive π → π* transition band near 212 nm has been indicative of a disordered

peptide structure, so-called "random coil" (Kelly *et al.*, **2005**). Noteworthy, secondary structures composed of L-amino acids give rise to CD curves that are mirror images of their D-amino acid counterparts.

Entry	Peptide
2.9	**(*R*)-Agl-**D-Tyr-D-Thr-D-Val-D-Glu-D-Leu-D-Ala-NH_2
2.10	D-Arg-**(*R*)-Agl-**D-Thr-D-Val-D-Glu-D-Leu-D-Ala-NH_2
2.11	D-Arg-D-Tyr-D-Thr-**(*R*)-Agl-**D-Glu-D-Leu-D-Ala-NH_2
2.12	D-Arg-D-Tyr-D-Thr-D-Val-**(*R*)-Agl-**D-Leu-D-Ala-NH_2
2.13	D-Arg-D-Tyr-D-Thr-D-Val-D-Glu-**(*R*)-Agl-**D-Ala-NH_2
2.14	D-Arg-D-Tyr-**(*S*)-Agl-**D-Val-D-Glu-D-Leu-D-Ala-NH_2
2.15	D-Arg-D-Tyr-D-Thr-**(*S*)-Agl-**D-Glu-D-Leu-D-Ala-NH_2
2.16	**(*R*)-Bgl-**D-Tyr-D-Thr-D-Val-D-Glu-D-Leu-D-Ala-NH_2
2.17	D-Arg-**(*R*)-Bgl-**D-Thr-D-Val-D-Glu-D-Leu-D-Ala-NH_2
2.18	D-Arg-D-Tyr-**(*R*)-Bgl-**D-Val-D-Glu-D-Leu-D-Ala-NH_2
2.19	D-Arg-D-Tyr-D-Thr-**(*R*)-Bgl-**D-Glu-D-Leu-D-Ala-NH_2
2.20	D-Arg-D-Tyr-D-Thr-D-Val-**(*R*)-Bgl-**D-Leu-D-Ala-NH_2
2.21	D-Arg-D-Tyr-D-Thr-D-Val-D-Glu-**(*R*)-Bgl-**D-Ala-NH_2
2.22	**(*S*)-Bgl-**D-Tyr-D-Thr-D-Val-D-Glu-D-Leu-D-Ala-NH_2
2.23	D-Arg-**(*S*)-Bgl-**D-Thr-D-Val-D-Glu-D-Leu-D-Ala-NH_2
2.24	D-Arg-D-Tyr-**(*S*)-Bgl-**D-Val-D-Glu-D-Leu-D-Ala-NH_2
2.25	D-Arg-D-Tyr-D-Thr-**(*S*)-Bgl-**D-Glu-D-Leu-D-Ala-NH_2
2.26	D-Arg-D-Tyr-D-Thr-D-Val-**(*S*)-Bgl-**D-Leu-D-Ala-NH_2
2.27	D-Arg-D-Tyr-D-Thr-D-Val-D-Glu-**(*S*)-Bgl-**D-Ala-NH_2

Table 2.2. Agl- and Bgl-bearing analogues synthesized by Dr. Andrew G. Jamieson, Dr. Luisa M. Ronga, Dr. Nicolas Boutard and Stéphane Turcotte.

Accordingly, conformational effects of the amino-γ-lactams on peptides were assessed by far-UV-CD spectroscopy in water, performed between 190 and 260 nm. For comparison between different analogues, all CD data were background-substracted and then normalized to mean residue ellipticity, [θ], reported in units of $mdeg \cdot cm^2 \cdot dmol^{-1} \cdot residue^{-1}$. The [θ] values were calculated from θ data directly obtained from the CD instrument, according to equation 2.1 (Whitford, **2005**):

$$[\theta] = MRW \cdot \theta / 10 \cdot d \cdot c$$

Equation 2.1. Conversion of degree of ellipticity to mean residue ellipticity, where [θ] is mean residue ellipticity ($mdeg \cdot cm^2 \cdot dmol^{-1} \cdot residue^{-1}$), MRW corresponds to mean residue weight (molecular weight divided by the number of residues; $g \cdot dmol^{-1} \cdot residue^{-1}$), θ is degree of ellipticity (mdeg), d relates to the cell pathlength (cm), and c is the sample concentration ($g \cdot cm^{-3}$).

CD curves were then interpreted based on established correlations of maxima band values and curve shapes (Figure 2.4; Kelly *et al.*, **2005**; Whitford, **2005**; Shemer, **2009**) with typical secondary structures. For example, the CD spectra of lead peptide 101.10 was compared with selected Agl and Bgl analogues (Figure 2.5).

(a)

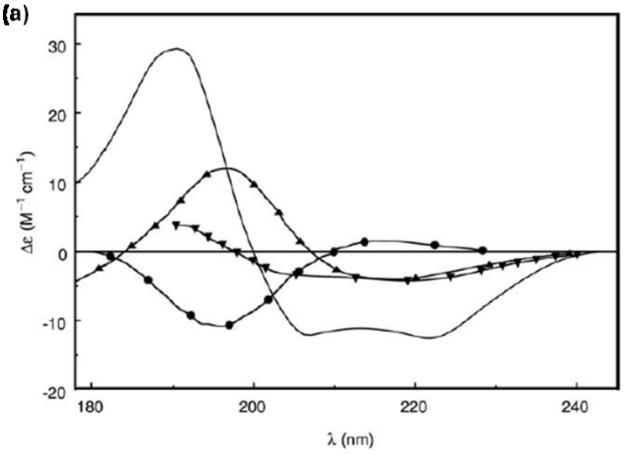

(b)

Secondary structure	Transition bands		
	$\pi_0 \rightarrow \pi^*$	$\pi_1 \rightarrow \pi^*$	$n \rightarrow \pi^*$
α-helix	+ 192	- 208	- 222
β-sheet	+ 195	-	- 218
random coil	- 195	-	+ 215-230
PPII	- 205	-	+ 228
PPI	+ 190	- 205	- 220
type I β-turn	+ 190	- 202	- 220
type II β-turn	-190	+ 205	- 225

Figure 2.4. Representative far-UV CD a) curves and b) transition bands associated with various types of secondary structure. Solid line, α-helix; upside triangles, antiparallel β-sheet; downside triangles, type I β-turn; and circles, random coil (graph reproduced from Woody, **2010**; table values taken from Hutchinson *et al.*, **1994**; Ranjbar *et al.*, **2009**; Moradi *et al.*, **2009**).

The CD curve for the parent peptide (**5.1**; see chapter 5) indicated a disordered structure, as suggested by the positive maxima around 198 nm and the negative shoulder in the longer wavelength. The insertion of a lactam motif into the rytvela core had a pronounced influence on the shape of the CD spectra, contingent on location, stereochemistry and Agl versus Bgl structure. The spectra of analogues bearing an (*R*)-Agl, (*R*)- or (*S*)-Bgl at the third position (**2.8**, **2.18** and **2.24**) were suggestive of a type II' β-turn, displaying one negative and two positive bands near 205 ,195 and 225 nm, respectively. The CD shapes of (*R*)-Agl analogues at the valine, glutamate and leucine positions (data not shown) showed two distinct maxima at 200 and 220 nm, indicating a prevalent type I β-turn fold. Alternatively, the (*S*)-Agl[3] analogue (**2.14**) exhibited a curve shape ressembling that of a random structure, whereas the (*S*)-Agl[4] analogue (**2.15**) produced a spectrum suggesting very discrete amounts of β-turn. The CD curves of the *C*-terminal (*R*)-Bgl analogues at positions 4, 5 and 6 (data not shown) exhibited positive maxima at 195 nm, suggesting a random coil. (*S*)-Bgl analogues induced stronger changes in ellipticity and respectively on peptide conformation than their (*R*)-counterparts. In brief, this ensemble of CD data demonstrated that introduction of Agl or Bgl residues may infer a broad spectrum of secondary structures into 101.10. Ideally, such induced structures may be correlated to good anti-IL-1β biological activty, as described next.

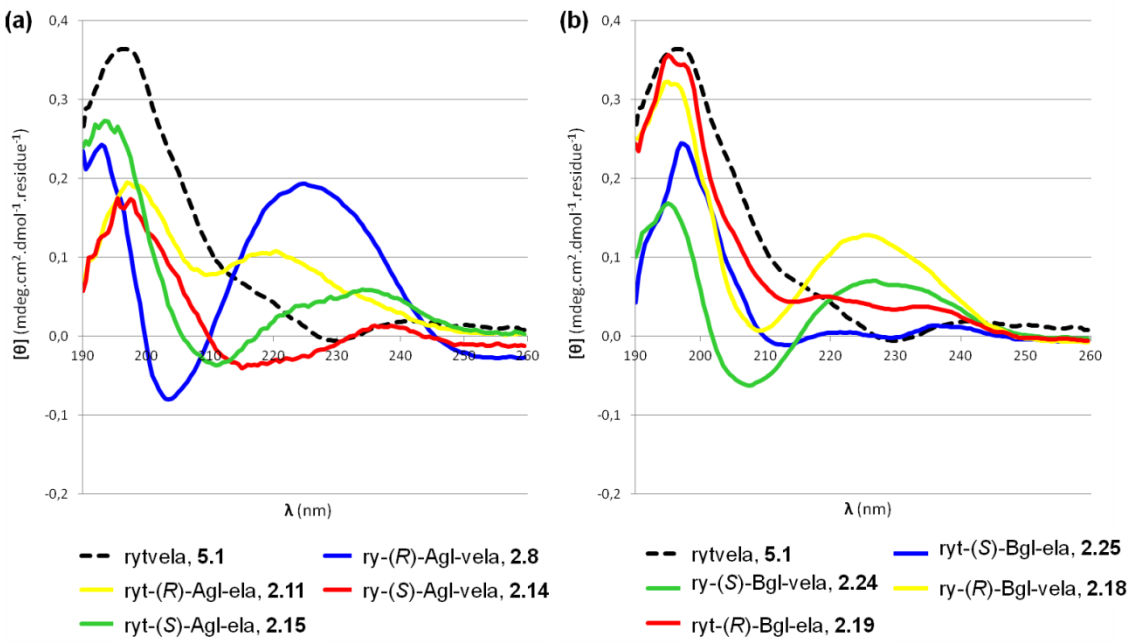

Figure 2.5. CD of 101.10, and a) selected Agl analogues, as well as b) Bgl analogues.

2.3.2 Biological activity

The biological activity of the lactam analogues was ascertained by measuring their influence on IL-1β-induced human thymocyte (TF-1 cell line) proliferation, as assessed by two methods. The first method consisted in the incorporation of [^{3}H]-thymidine into DNA of mitotic cells, and was used to test Agl-bearing peptides (**2.8**-**2.15**; Figure 2.6a). Nonetheless, several inconveniences such as the expensive disposal of radioactive wastes, the poor radionucleus' quantum yield, the labour-intensiveness of the procedure and the relatively low accuracy limited this method. A second assay was thus developed, featuring the intercalation of a cyanine dye (termed CyQUANT NF) into the nuclear and mitochondrial DNA of cells, which generates a 100-fold raise in fluorescence intensity. This second method presented notable advantages, including suitability for high-throughput screening (HTS), greater affordability, a wider dynamic range and higher sensitivity. After optimization and validation with previously obtained data, this later method was subsequently used to test the Bgl analogues (**2.16**-**2.27**; Figure 2.6b). The biological data are reported herein as percentage of control (non-stimulated) proliferation.

In both assays, the lead peptide showed a maximum efficacy of 100%, completely abrogating exogenous IL-1β-induced thymocyte proliferation. Among all analogues, seven maintained inhibitory effects on TF-1 proliferation (**2.9-2.13**, **2.25** and **2.26**), of which five showed a 1.3- to 2.2-fold increase in efficacy compared to 101.10. Introduction of (*R*)-Agl in rytvela caused, in all positions except the third one (analogue **2.8**), an amplification or retention of the activity. Notably, replacement of the *N*-terminal D-Arg^1 residue by (*R*)-Agl (**2.9**) led to the most effective peptidomimetic in the series, causing a 2.2-fold increase in efficacy compared with the parent peptide. In the case of (*S*)-Bgl, only substitutions at positions 4 and 5 (**2.25** and **2.26**) maintained activity. In particular, replacing D-Val^4 for (*S*)-Bgl (**2.25**) produced the most potent of the Bgl library, bearing a 1.3-fold increase in activity. Both (*S*)-Agl (**2.14** and **2.15**) as well as four (*R*)-Bgl derivatives (**2.16, 2.17**, **2.19** and **2.21**) exacerberated the immune cell proliferation.

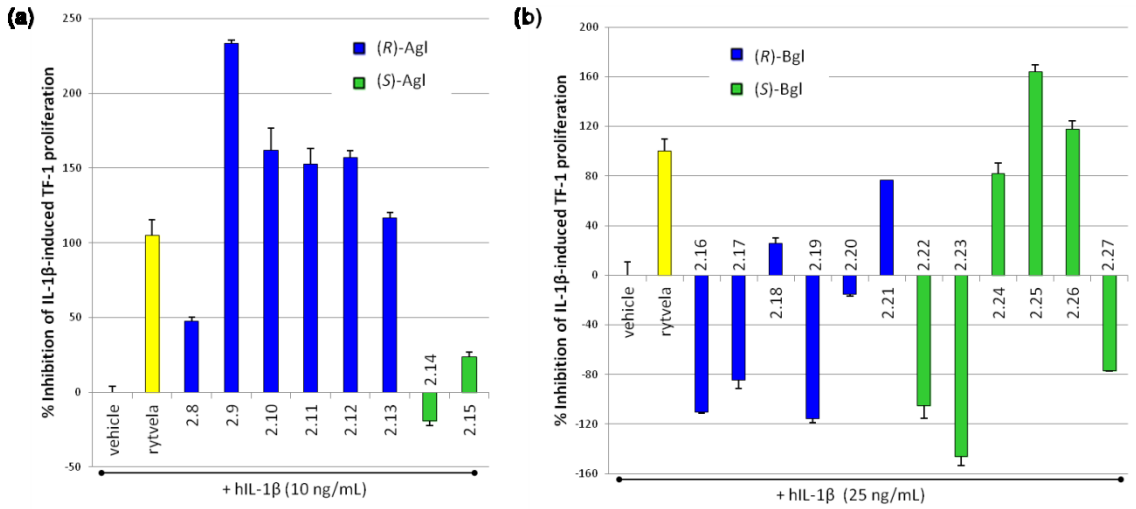

Figure 2.6. Inhibition of IL-1β-induced thymocyte proliferation by a) Agl and b) Bgl analogues. Vehicle column represents cells that were not treated with a peptide, and all columns correspond to cells that were stimulated by an exogenous amount of hIL-1β. The numbers correspond to the entry number of the analogue and the color to the stereochemistry of the lactam. Samples that display more than 100% inhibition of IL-1β-mediated effect are suspected to block the endogenous production of IL-1β in cells as well.

Overall, it seems that the stereochemistry, the position in the sequence and the orientation of the carbonyl of the lactam have a significant influence on the activity of the peptide. For instance, the derivatives containing (*R*)-Agl[4] or (*S*)-Bgl[4] (**2.11** and **2.25**), which share comparable carbonyl orientations and amino group positions, formed the two most active lactam series. Swapping (*S*)-Bgl for (*R*)-Bgl shows little impact on the first three positions, whereas the effect is more drastic on positions 4 to 6. Typically, substitution of D-Thr[3] for a lactam (**2.8**, **2.14** and **2.18**) induced a significant loss of anti-IL-1β efficacy, which may be in part attributed to the loss of the hydroxyl group side-chain.

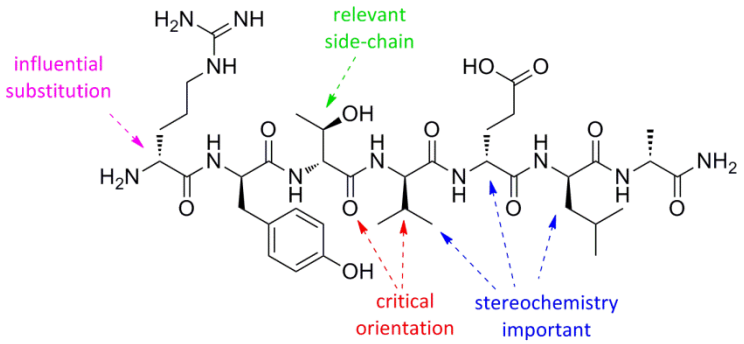

Figure 2.7. Structure-activity relationships observed via amino-γ-lactam scanning of 101.10.

2.4 Concluding remarks

In light of the CD spectra and biological data, some persistent structure-activity relationships were observed (Figure 2.7.). For example, introduction of (*R*)-Agl in the peptide induced higher anti-IL-1β efficacy and stronger turn motifs than most of the Bgl and all of the (*S*)-Agl counterparts. Nonetheless, in the Bgl group, the (*S*)-stereochemistry produced the strongest turn motifs as well as three active analogues. These findings suggest

that the carbonyl and amino group orientation as well as the stereochemistry of the lactam are critical. Replacement of the D-Thr^3 by a lactam caused, in 75% of cases, a β-turn fold associated with a substantial loss in activity. However, this reduction of biological effect may be attributed to the absence of the hydroxyethyl side-chain rather than the rigidification of conformation. This hypothesis will be tested in a subsequent series of 3rd position analogues, the α-amino-β-hydroxy-γ-lactam (Hgl), presented in chapter 3. These results suggest again that a fold induced in the central portion of the peptide may be important for activity, but not at the detriment of side-chain loss. Agl and Bgl scanning of 101.10 have thus proven useful and complementary for enhancing peptide potency and identifying conformational requirements for biological activity.

2.5 Experimental section

2.5.1 General

Unless otherwise specified, starting materials and reagents were obtained from commercial sources and used as received. Rink amide MBHA (100-200 mesh) resin was purchased from Novabiochem (EMD Bioscience, California, USA). L-Homoserine was purchased from Novabiochem (EMD Bioscience, California, USA). Fmoc-amino acids were purchased from Novabiochem (EMD Bioscience, California, USA) or GL Biochem (Shangai, China). *O*-Benzotriazole-*N*,*N*,*N'*,*N'*-tetramethyluronium hexafluorophosphate (HBTU) was purchased from GL Biochem (Shangai, China). Anhydrous solvents (THF, MeCN, DCM and DMF) were obtained from a Seca Solvent Filtration System (GlassContour, Laguna Beach, USA). Triethylamine (TEA) and diisopropylethylamine (DIEA) were purchased from Sigma-Aldrich (Missouri, USA) and distilled from calcium hydride. For reactions requiring anhydrous conditions, glassware, syringes and needles were flame dried immediately prior to use and allowed to cool either in a desiccator or under an atmosphere of dry argon; liquids were added via syringe or cannulation through rubber septa in a system maintained under an atmosphere of argon. The removal of solvents *in vacuo* was achieved using a Büchi rotary evaporator at a pressure of 15 mm Hg, generated by a water aspirator.

2.5.2 Characterization and purification

Flash column chromatography was carried out using SiliaFlash F60 silica (Silicycle, Québec, CA). Precoated glass-backed plates (SiliaPlate S8 TLC Extra Hard Layer F-254, Silicycle, Québec, CA) were used for thin layer chromatography (TLC) and were visualized by either UV fluorescence or staining with molecular iodine, ninhydrin, phosphomolybdic acid (PMA) or $KMnO_4$ solution followed by heating.

Analytical high-performance liquid chromatography (HPLC) and mass spectral (MS) data were obtained using the capLC-MSD Quad (Agilent Technologies) from the Mass Spectrometry Facility of Université de Montréal (Québec, CA), equipped with the electrospray ionization (ESI) and a single quadrupole. Likewise, high resolution mass spectrometry (HRMS) data were recorded with a LC-MSD Time-of-Flight (TOF) (Agilent Technologies, Santa Clara, USA) instrument at the same instrumental facility. Analytical reverse phase (RP)-HPLC analyses were performed on either a Gemini® C18 (5µm, 110Å, 150 mm x 4.60 mm I.D.; Phenomenex, Torrance, USA) or a Synergi® RP-Polar column (4µm, 80Å, 150 mm x 4.60 mm I.D.; Phenomenex, Torrance, USA) with a flow rate of 0.5 mL/min. Unless otherwise specified, linear gradients of acetonitrile or methanol in

water (all HPLC grade solvents), modified with either 0.1% formic acid (FA) or trifluoroacetic acid (TFA), were used. Peptides and analogues were purified via preparative RP-HPLC using a Gemini® C18 (5µm, 110Å, 250 mm x 21.2 mm I.D.; Phenomenex, Torrance, USA) or a Synergi® RP-Polar column (4µm, 80Å, 150 mm x 21.2 mm I.D.; Phenomenex, Torrance, USA) submitted to a specified linear gradient, at a flow rate of 10.6 mL/min. Retention times (t_R) from RP-HPLC are reported in minutes.

2.5.3 Microwave chemistry

Microwave-assisted reactions were preformed in a Biotage Initiator Sixty or Eight microwave apparatus (Biotage AB, Uppsala, SE) with samples prepared in 0.5-2.0mL glass reaction vessels containing a triangular magnetic stirrer bar and sealed with an aluminum-bordered septum cap.

2.5.4 Synthesis of peptides and mimetics by standard Fmoc-SPPS

2.5.4.1 Rink resin swelling and deprotection

Rink amide MBHA resin (300 mg, 0.21 mmol, 0.7 mmol/g) and DMF (7 mL) were charged in a 12 mL plastic filtration tube fitted with a polyethylene filter. The tube was sealed and shaken for 30 min. at room temperature (r.t.). The resin was filtered and taken up in freshly prepared 20% piperidine in DMF solution (7 mL), shaken for 30 min. and filtered. The resin was retreated with 20% piperidine/DMF solution (7 mL) and shaken for another 30 min. The resin was washed by consecutive 1 min. agitations and filtered from DMF (3 x 7 mL), MeOH (3 x 7 mL) and DCM (3 x 7 mL). A positive Kaiser colour test indicated qualitatively the presence of free amine (Kaiser **1970**).

2.5.4.2 Amino acid coupling

The resin was first swollen in DMF (7 mL) for 15 min. In a separate 20 mL-glass vial, a solution of *N*-(Fmoc)amino acid (Fmoc-Xaa-OH, 3 equiv.), HBTU (3 equiv.) and DIEA (6 equiv.) in DMF (7 mL) was stirred for 10 min. and then added to the resin. The resin mixture was shaken for 1 h with Fmoc-D-Ala-OH, 3 h with Fmoc-D-Val-OH, and 4 h with Fmoc-D-Leu-OH, Fmoc-D-Glu(tBu)-OH, Fmoc-D-Thr(tBu)-OH, Fmoc-D-Tyr(tBu)-OH and Fmoc-D-Arg(Pbf)-OH, at room temperature. The resin was filtered and respectively washed by shaking for 1 min. with DMF (3 x 7 mL), MeOH (3 x 7 mL) and DCM (3 x 7 mL). A negative Kaiser colour test result indicated completion of the reaction.

2.5.4.3 Resin capping

In cases in which a coupling did not proceed to completion, the resin was swollen in a solution of acetic anhydride (Ac_2O, 10 equiv.) in DMF (7 mL), treated with DIEA (10 equiv.), shaken for 2 h, filtered, washed by shaking for 1 min. with DMF (3 x 7 mL), MeOH (3 x 7 mL) and DCM (3 x 7 mL) and dried *in vacuo*.

2.5.4.4 Chain alkylation

After swelling the resin, the Fmoc protecting group was removed as described above. For the installation of Agl, the resin was treated by vigorous shaking with a solution of 6-membered sulfamidate (5 equiv.) in THF (7 mL) for 24 h, filtered, washed with THF (3 x 7 mL), MeOH (3 x 7 mL) and DCM (3 x 7 mL) and dried *in vacuo* (Jamieson *et al.*, **2009**). In the case of Bgl, the resin-bound peptide was alkylated by addition of a solution of 5-membered sulfamidate (5 equiv.) in THF (2 mL), after which DIEA (1 equiv.) was added, and heated at 60ºC using microwave irradiation for 1.5 h (Boutard *et al.*, **2011**).

2.5.4.5 Microwave-assisted annulation

The resin was transferred into a 0.5-2 mL glass microwave vial, and treated with a freshly prepared 1% AcOH/DMSO solution (2 mL). The vial was sealed, heated in the microwave at 100 ºC (pressure 1 bar) for 3 h, cooled using a jet of air, washed from the microwave vessel into a 12 mL plastic filtration tube with polyethylene frit, rinsed by shaking for 1 min. using DMF (3 x 7 mL), MeOH (3 x 7 mL) and DCM (3 x 7 mL) and dried *in vacuo*.

2.5.4.6 Peptide cleavage

As described above, the resin was swollen in DMF and the Fmoc group was removed. A positive Kaiser test demonstrated qualitatively the presence of free amine. The resin was shaken in TFA/H_2O/triethylsilane (TES) (7 mL, 95/2.5/2.5, v/v/v) for 2 h at room temperature, filtered, washed with TFA (7 mL) and the combined filtrate and washings were concentrated *in vacuo* up to a volume of 1 mL. The resulting residue was transferred to a 50 mL Falcon centrifuge tube and precipitated by the addition of ice-cold diethyl ether (Et_2O, 40 mL). The mixture containing the precipitate was centrifuged and the diethyl ether was carefully decanted from the tube. The precipitated peptide was washed with cold Et_2O, centrifuged and decanted once more. The resulting white amorphous solid was dissolved in water (10 mL) and freeze-dried to give a white fluffy solid that was analyzed for purity and isolated using the previously specified conditions.

2.5.5 Ultraviolet-circular dichroism

Determination of the aqueous concentration of peptides was performed by UV-quantification using Beer-Lambert law (Equation 2.2; IUPAC, **1997**) :

$$A = \varepsilon \cdot c \cdot l$$

Equation 2.2. Beer-Lambert law, where A relates to the absorbance (a.u.), ε corresponds to the molar absorption coefficient ($L \cdot mol^{-1} \cdot cm^{-1}$), c is the concentration ($mol \cdot L^{-1}$) and *l* the cuvette pathlength (cm).

UV absorbances of aqueous peptide solutions were recorded on a Varian Cary® 300 UV/Vis Spectrophotometer (Varian, California, USA) equipped with a deuterium arc source. Essentially, a spatula tip of the purified peptide is dissolved in 1000 µL of Chromspec-filtered Milli-Q water and transferred to a 1.0 cm spectrophotometric cuvette. The sample absorbance is measured six times at 280 nm, averaged and subtracted from the background signal. The concentration of the solution was calculated using Beer-Lambert law, using the molar absorption coefficient of tyrosine at 280 nm (ε_{Tyr} = 1280 $L \cdot mol^{-1} \cdot cm^{-1}$).

Far-UV-CD spectra of peptides and peptidomimetics were recorded from 190 to 260 nm on a Chirascan CD Spectrometer (Applied Photophysics Ltd., Surrey, UK) using a 1.0-cm pathlength quartz cuvette filled with 20 µM (unless otherwise specified) of compound dissolved in Chromspec-filtered Milli-Q water. All CD curves were subtracted from background signal previously recorded for filtered Milli-Q water. Instrumental settings were fixed as the following: bandwidth of 1 nm, step size of 0.5 nm, sampling time of 2 s. Data are expressed in terms of mean residue ellipticity, [θ] ($mdeg \cdot cm^2 \cdot dmol^{-1} \cdot residue^{-1}$).

2.5.6 Biological activity screening of analogues

2.5.6.1 [^{3}H]-Thymidine incorporation assays

IL-1β-induced proliferation of immune cells was assessed by incorporation of [^{3}H]-thymidine, as previously described (Quiniou *et al.*, **2008**). Basically, human TF-1 cells (CRL-2003, American Type Culture Collection (ATCC), Virginia, USA) were cultured in complete RPMI medium (Wisent, Québec, CA) supplemented with human GM-CSF (2 ng/mL; PeproTech, New Jersey, USA). Cells were splitted ($5x10^4$ cells in 200 µL/well) in a 96-well culture plate (Corning, New York, USA) and deprived of growth factors for 18 h before preincubation with peptide (1 µM) followed by treatment with human IL-1β (10 or 25 ng/mL; PeproTech, New Jersey, USA). After 24 h of incubation, [^{3}H]-thymidine (1 µCi/mL; Amersham, Amersham, UK) was added and the cells were incubated for another 24 h. Cells were harvested, washed twice with PBS (10 mM Na_2HPO_4, 2 mM KH_2PO_4, 137 mM NaCl, 2.7 mM KCl; pH 7.4), and lysed with a 0.1 N NaOH/0.1% Triton X-100 solution. A scintillation cocktail (8 mL/sample; Fisher Scientific, Ontario, CA) was added to the lysate, and after 3 h, radioactivity was measured with a β-ray counter (Beckman Multi-Purpose Scintillation Coulter Counter LS6500; Beckman Coulter, California, USA). Triplicate results were analyzed by one-way analysis of variance (ANOVA) factoring for treatments. Data are presented as mean ± standard error of the mean (SEM).

2.5.6.2 CyQUANT NF intercalation assay

Immune cell proliferation was assessed by DNA intercalation of CyQUANT NF fluorescent dye (Boutard *et al.*, **2011**). Essentially, human TF-1 cells (CRL-2003, American Type Culture Collection, Virginia, USA) were cultured in complete RPMI 1640 (Gibco-Invitrogen, California, USA) supplemented with human GM-CSF (2 ng/ml, PeproTech, New Jersey, USA). Cells (passage 5 and at least 85% viable, as verified by trypan blue dying) were reincorporated into RPMI 1640 medium deprived of phenol red (Gibco-Invitrogen, California, USA) and of growth factors [i.e. fetal bovine serum (FBS) and GM-CSF] for 18 h and split ($5x10^3$ cells in 200µL/well) into a 96-well non-adherent flat bottom culture plate (Sarstedt, Nümbrecht, Germany). Following 15 min. preincubation with peptide (1 µM), the cells were treated with human IL-1β (25 ng/mL, PeproTech, New Jersey, USA) and reincubated. After 48 h, the cells were centrifuged for 7 min. at 300 g, reincorporated into Hank's Buffered Salt Solution (1X HBSS, 50 µL/well; Invitrogen, California, USA) and transferred into a 96-well polystyrene black plate (Corning, New York, USA). An additional 50 µL of a solution made with CyQUANT NF dye (1X component A; Invitrogen, California, USA) and CyQUANT NF delivery agent (1X component B; Invitrogen, California, USA) in 1X HBSS were added to the cells in each well, which were covered with aluminum foil and incubated for 45 min. at 37°C. Fluorescence intensity was measured using a microplate reader (Perkin Elmer Wallac Envision 2104; Perkin Elmer, California, USA) with excitation at 485 nm and emission detection at 530 nm (using FITC 485 and

FITC 535 filters, respectively). Hexaplicate experiments were repeated three times and results were analyzed by one-way analysis of variance (ANOVA) factoring for treatments, and data are presented as mean ± standard error of the mean (SEM).

2.6 References

Armstrong, S. K. *J. Chem. Soc., Perkin Trans. 1* **1998**, *1*, 371-388.

Bhooma, R.; Rodney, J. *J. Org. Chem.* **2006**, *71*, 2151-2154.

Boutard, N.; Turcotte, S.; Beauregard, K.; Quiniou, C.; Chemtob, S.; Lubell, W. D. *J. Pep. Sci.* **2011**, *17*(4), 288-296.

Boyarskaya, N. P.; Prokhorov, D. I.; Kirillova, Y. G.; Zvonkova, E. N.; Shvets, V. *Tetrahedron Lett.* **2005**, *46*, 7359-7362.

Dolbeare, K.; Pontoriero, G. F.; Gutpa, S. K.; Mishra, R. K.; Johnson, R. L. *Bioorg. Med.Chem.* **2003**,*11*, 4103-4112.

Ede, N. J.; Rae, I. D.; Hearn, M. T. W. *Tetrahedron Lett.* **1990**, *31*, 6071-6074.

Ede, N. J.; Lim, N.; Rae, I. D.; Ng, F. M.; Hearn, M. T. W. *Peptide Res.* **1991**, *4*, 171-174.

Ede, N. J.; Rae, I. D.; Hearn, M. T. W. *Aust. J. Chem.* **1991b**, *44*, 891-894.

Ede, N. J.; Rae, I. D.; Hearn, M. T. W. *Int. J. Peptide Protein Res.* **1994**, *44*, 568-581.

Ewing, W. R.; Becker, M. R.; Manetta, V. E.; Davis, R. S.; Pauls, H. W.; Mason, H.; Choi-Sledeski, Y. M.; Green, D.; Cha, D.; Spada, A. P.; Cheney, D. L.; Mason, J. S.; Maignan, S.; Guilloteau, J.-P.; Brown, K.; Colussi, D.; Bently, R.; Bostwick, J.; Kasiewski, C. J.; Morgan, S. R.; Leadley, R. J.; Dunwiddie, C. T.; Perrone, M. H.; Chu, V. *J. Med. Chem.* **1999**, *42* (18), 3557-3571.

Freidinger, R. M.; Veber, D. F.; Hirschmann, R.; Paege, L. M. *Int. J. Pept. Protein Res.* **1980**, *16*, 464-470.

Freidinger, R. M.; Veber, D. F.; Perlow, D. S.; Brooks, J. R.; Saperstein, R. *Science* **1980b**, *210* (4470), 656-658.

Freidinger, R. M. *J. Med. Chem.* **2003**, *46*, 5553-5566.

Galaud, F.; Lubell, W. D. *Biopolymers* **2005**, *80*, 665-674.

Hutchinson, E. G.; Thornton, J. M. *Protein Sci.* **1994**, *3*, 2207-2216.

IUPAC. Compendium of Chemical Terminology : the Gold Book, 2nd edition; McNaught, A. D.; Wilkinson, A. Eds.; Blackwell Scientific Publications, Oxford, **1997**, 450 pages.

Jamieson, A. G.; Boutard, N.; Beauregard, K.; Bodas, M. S.; Ong, H.; Quiniou, C.; Chemtob, S.; Lubell, W. D. *J. Am. Chem. Soc.* **2009**, *131* (22), 7917-7927.

Kaiser, E.; Colescott, R. L.; Bossinger, C. D.; Cook, P. I. *Anal. Biochem.* **1970**, *34*, 595-598.

Kelly, S. M.; Jess, T. J.; Price, N. C. *Biochim. Biophys. Acta* **2005**, *1751*, 119-139.

Lama, T.; Campiglia, P.; Carotenuto, A.; Auriemma, L.; Gomez-Monterrey, I.; Novellino, E.; Grieco, P. *J. Peptide Res.* **2005**, *66*, 231-235.

Lee, T.-H.; Thompson, P. E.; Hearn, M. T. W.; Aguilar, M.-I. *J. Peptide Res.* **1997**, *49*, 394-403.

Liskamp, R. M. J. *Recl. Trav. Chim. Pays-Bas* **1994**, *113* (1), 1-19.

Loughlin, W. A.; Tyndall, J. D. A.; Glenn, M. P.; Hill, T. A.; Fairlie, D. P. *Chem. Rev.* **2010,** *110,* PR32–PR69.

Maignan, S.; Guilloteau, J. P.; Pouzieux, S.; Choi-Sledeski, Y. M.; Becker, M. R.; Klein, S. I; Ewing, W. R.; Pauls, H. W.; Spada, A. P.; Mikol, V. *J.Med.Chem.* **2000**, *43*, 3226-3232.

Marquis, R. W. *Ann. Reports Med. Chem.* **2000**, *35*, 309-320.

Moradi, M.; Babin, V.; Roland, C.; Darden, T. A.; Sagui, C. *Proc. Nat. Acad. Sci. USA* **2009**, *106* (49), 20746-20751.

Nöth, J.; Frankowski, K. J.; Neuenwander, B.; Aubé, J. *J. Comb.Chem.* **2008**, *10*, 456-459.

Piscopio, A. P. D.; Miller, J. F.; Koch, K. *Tetrahedron Lett.* **1998**, *39*, 2667-2670.

Piscopio, A. D.; Miller, J. F.; Koch, K. *Tetrahedron* **1999**, *55*, 8189-8198.

Powers, J. C.; Asgian, J. L.; Ekici, O. D.; James, K. E. *Chem. Rev.* **2002**, *102,* 4639-4750.

Prevelige, P.; Fasman, G. D. In *Prediction of Protein Structure and the Principles of Protein Conformation*, Fasman, G. D., Ed.; Plenum Press, New York, USA; **1989**, *9*, 391-416.

Raghavan, B.; Johnson, R. L. *J. Org. Chem.* **2006**, *71*, 2151-2154.

Ranjbar, B.; Gill, P. *Chem. Biol. Drug Des*. **2009**, *74*, 101-120.

Ronga, L.; Jamieson, A. G.; Beauregard, K.; Quiniou, C.; Chemtob, S.; Lubell, W. D. *Biopolymers* **2010**, *94* (2), 183-191.

Scheidt, K. A.; Roush, W. R.; McKerrow, J. H.; Selzer, P. M.; Hansell, E.; Rosenthal, P. J. *Bioorg. Med. Chem.* **1998**, *6*, 2477-2494.

Schuster, M.; Blechert, S. *Angew. Chem., Int. Ed.* **1997**, *36*, 2036-2056.

Scott, W. L.; Alsina, J.; Kennedy, J. H.; O'Donnell, M. J. *Org. Lett.* **2004**, *6*, 1629-1632.

Shemer, G. In *Circular dichroism*, VDM Verlag, **2009**, 108 pages.

Whitford, D. In *Protein: Structure and Function*, Chapter 10, John-Wiley & Sons, **2005**, 528 pages.

Wolf, J.-P.; Rapoport, H. *J. Org. Chem.* **1989**, *54*, 3164-3173.

Wolfe, M. S.; Dutta, D.; Aubé, J. *J. Org. Chem.* **1997**, *62*, 654-663.

Woody, R. W. *Chirality* **2010**, *22*, E22-E29.

CHAPTER 3

Peptide Core

3.1 Introduction

Nature is typically composed of molecules possessing only one of two possible mirror images (Wallace, **2010**). A corollary of such natural enantio-selection is that the form and function of biologically active peptides is governed by their chirality (Lubell *et al.*, **2012**). Although L-amino acids are predominant, natural entities such as bacterial and amphibian skin peptides contain D-amino acids (Lipmann *et al.*, **1941**; Kreil *et al.*, **1989**; Richter *et al.*, **1990**; Kreil, **1997**); and free D-amino acids have been detected in mammalian tissues and body fluids (Dunlop *et al.*, **1986**; Hashimoto *et al.*, **1993**; Fujii, **2002**). Incorporating amino acids of opposite stereochemistry in the molecular design of peptides has been typically used to improve enzymatic stability and provide access to new molecular topologies (Nomizu *et al.*, **1992**; Zhou *et al.*, **2002**; Mahalakshmi *et al.*, **2006**).

Mirror image conformations are displayed by enantiomeric peptides possessing L- and D- amino acids (Ramachandran *et al.*, **1963**; Ramachandran *et al.*, **1968**; Kumar *et al.*, **2010**). For example, L-peptides have been shown to adopt right-handed α-helices (α_R), and D-peptides left-handed helices (α_L). In addition to chirality, conformation is dictated by entropy, steric factors, hydrophobic effects as well as other electrostatic interactions (Lubell *et al.*, **2012**). Single D-amino acid substitutions in peptides may destabilize α_R-helices (Fairman *et al.*, **1992**; Chen *et al.*, **2002**), and favor extended and turn conformations (Fabiola *et al.*, **2001**; Nagarajan *et al.*, **1997**), in order to minimize steric clashes between side-chains. Peptides with alternating L- and D-amino acids have been demonstrated to adopt specific folds (Mahalakshmi *et al.*, **2006**). For example, gramicidin A, an antimicrobial toxin having the sequence HCO-L-Val-Gly-L-Ala-D-Leu-L-Ala-D-Val-L-Val-D-Val-L-Trp-D-Leu-L-Trp-D-Leu-L-Trp-D-Leu-L-Trp-$NHCH_2CH_2OH$, has been shown to adopt a β-helix secondary structure, which is stabilized by intermolecular hydrogen bonding between strands in a head-to-head dimer (Figure 3.1; Urry *et al.*, **1971**; Veatch *et al.*, **1974**). Certain heterochiral peptides have been demonstrated to form right-handed and left-handed helical segments which self-assemble into head-to-tail tubular dimers (Ghadiri *et al.*, **1993**; Mahalakshmi *et al.*, **2006**; Hanessian *et al.*, **2008**). In particular, even short non-cyclic constructs consisting of bis-D- and L-tripeptides anchored to a *trans*-(1*R*,2*R*)-diaminocyclohexane (C_2 symmetrical turn motif) were shown to adopt energetically favorable local turn conformations and helical superstructures (Hanessian *et al.*, **2008**).

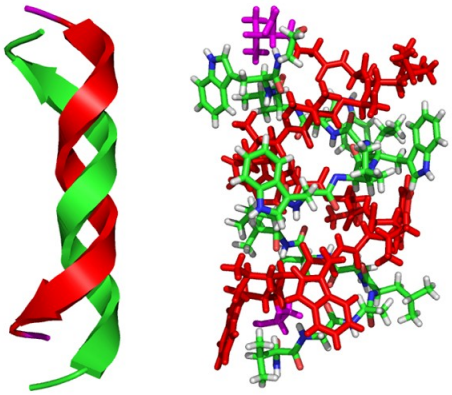

Figure 3.1. β-Helical structure of gramicidin A as depicted in cartoon (a) and stick (b) models (Generated from PDB ID 1AV2; Burkhart *et al.*, **1998**).

In the case of 101.10, substitution of L-amino acids into the minimum active sequence of the peptide (tvel; Chemtob *et al.*, **2005**) was performed to probe the relationship between conformation and bioactivity. In particular, the D-Thr^3-D-Val^4 core was examined because of intriguing results using conformational constraints in this region (e.g. Agl and Bgl, chapter 2; Jamieson *et al.*, **2009**; Boutard *et al.*, **2011**). The β-branched nature of threonine and valine residues may impose van der Waals interactions causing conformational constraints of varying magnitude, depending on sequence chirality. In addition, threonine and valine have low propensity to form helical structures (Chou *et al.*, **1978**). By means of CD and NMR spectroscopy, as well as RP-HPLC, the substitution of D-Thr and D-Val into L-peptides has shown to strongly destabilize the amphipathic KLA-helix by induction of turn-like structures (Krause *et al.*, **2000**). Threonine has shown a high propensity to occupy the *i*+2 position of type I β-turns, as well as the *i*+3 position of type VIII and type II' β-turns (Hutchinson *et al.*, **1994**). Valine commonly occurs at the *i*+2 position of type VIII β-turns and at the *i* position of type I' and II' β-turns (Hutchinson *et al.*, **1994**). Computational studies of the free energy surfaces and solvation energies of Ac-(L-Ala)$_3$-NHMe and Ac-(L-Val)$_3$-NHMe suggested that the weak helical propensity of valine relative to alanine may be in part attributed to low solvation of the valine tripeptide, which could be explained by weaker peptide-water interactions, stronger side-chain rotamer restriction and unfavorable steric interactions (Tobias *et al.*, **1991**).

In the process of developing conformationally restricted analogues of the tetrapeptide Ac-TVAS-NH$_2$ (**3.1**; Figure 3.2), an inhibitor of plasminogen activator inhibitor-1 (PAI-1), an α-branched-α-amino-γ-lactam moiety (**3.2**) has been employed as a Thr-Val dipeptide mimic (Guzzo *et al.*, **2002**). Although the *N*-acetyl-3-amino-3-(1-hydroxyethyl)pyrrolidin-2-one peptide (**3.2**) displayed a biological activity 10-times weaker than its parent peptide (**3.1**), this study substantiated the utility of α-amino-hydroxy-γ-lactams to study bioactive conformations of peptides (Guzzo *et al.*, **2002**).

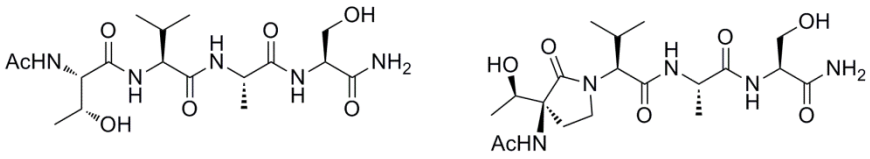

3.1
Ac-TVAS-NH$_2$

3.2
N-acetyl-3-(1-hydroxyethyl)-Agl analogue

Figure 3.2. Tetrapeptide inhibitor of PAI-1 and a Thr-Val restrained dipeptide surrogate.

As alternative constrained threonine residues, 3-hydroxyproline (3-Hyp; Chakraborty *et al.*, **2004**), α-amino-β-hydroxycyclohexanecarboxylic acid (c$_6$Ser, Avenoza *et al.*, **2001**) and α-amino-β-hydroxy-γ-lactam (4-hydroxy-Agl or Hgl; Sicherl *et al.*, **2010**; St-Cyr *et al.*, **2010**; St-Cyr *et al.*, **2010b**) have been utilized in peptide mimics (Figure 3.3). The hydroxyl group and ring in those moieties may stabilize secondary structures, respectively through hydrogen bonding and covalent constraints, limiting the bond rotations to specific sets of dihedral angles.

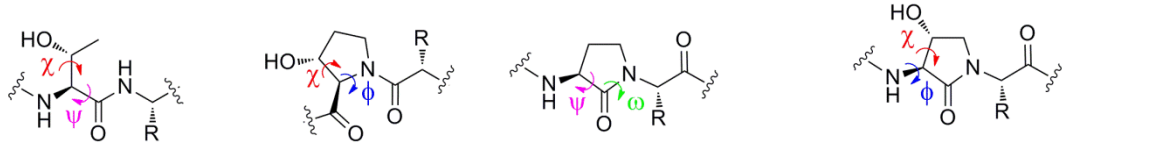

(2*S*, 3*R*)-Thr
(2*S*, 3*R*)-threonine

(2*R*,3*R*)-Hyp
(2*R*,3*R*)-hydroxyproline

(*S*)-Agl
(*S*)-α-amino-γ-lactam

(3*S*,4*R*)-Hgl
(3*S*,4*R*)-α-amino-β-hydroxy-γ-lactam

Figure 3.3. Threonine, 3-hydroxyproline, α-amino-γ-lactam and α-amino-β-hydroxy-γ-lactam.

For example, (3*S*)-hydroxy-L-proline in the Yaa position of the repeating trimer of collagen, Yaa-Xaa-Gly, diminished triple-helix stability compared to L-Pro and 4-L-Hyp. The inductive effect of the hydroxyl group has been suggested to weaken interstrand hydrogen bonds and to cause a C^{γ}-exo pucker of the pyrrolidine ring, leading to interstrand steric hindrance as well as improper ϕ and ψ backbone and χ side-chain torsion angles (Jenkins *et al.*, **2000**; Shoulder *et al.*, **2009**). Although the α-amino-γ-lactam (Agl) may restrict the ψ and ω torsion angles to values approaching 180º and 120º, respectively (Paul *et al.*, **1990**), the absence of side-chain functionality may compromise utility for threonine mimicry. Combining the conformational effects of Agl and the Thr side-chain, α-amino-β-hydroxy-γ-lactam (Hgl) constrains the *C*-terminal amide (i.e., ω), ψ and χ dihedral angles (Toniolo, **1990**), locking the hydroxyl side chain in the gauche (+) or (-) conformers (Hruby *et al.*, **1997**). The analogue [(*R*)-Agl^3]-101.10 (**2.8**; chapter 2) exhibited a CD curve characteristic of a type II' β-turn. Moreover, the crystal structure of *N*-Fmoc-(3*R*,4*S*)-Hgl-Leu-OMe (**3.3**, Figure 3.4; St-Cyr *et al.*, **2010b**) exhibited dihedral angle geometries (ω, ϕ, ψ = 176º, -40º, 116º) similar to that of ideal type II β-turn conformation (ω, ϕ, ψ = 180º, -60º, 120º; Hutchinson *et al.*, **1994**).

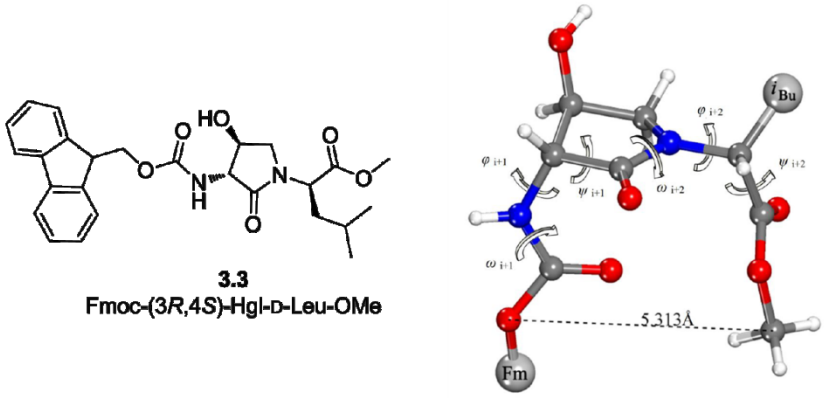

Figure 3.4. β-Turn-like conformation of *N*-Fmoc-(3*R*-amino-4*S*-hydroxy-2-oxopyrrolidizinyl)-D-leucine methyl ester (**3.3**) observed by X-ray diffraction (reproduced from St-Cyr *et al.*, **2010b**).

Considering previous findings regarding the « tvel » core, in particular Agl^3 analogues (**2.8**) of 101.10, a deeper examination of the influences of stereochemistry, side-chain and conformational restriction of the D-heptapeptide rytvela was undertaken. Initially, the chirality at positions 3 and 4 was examined by the synthesis of three diastereomeric derivatives. Subsequently, the hydroxyl side-chain was replaced for an isosteric methyl group, employing valine of L- and D-stereochemistry to provide four double valine diastereoisomers. Finally, the combined consequences of side-chain and geometric constrain on biological activity were investigated by the synthesis of α-amino-β-hydroxy-γ-lactams of (3*R*,4*S*)- and (3*S*,4*R*)-configuration and their introduction at the threonine position of rytvela.

3.2 Synthesis of [Hgl^3]-, [Val^3]- and 101.10 diastereomers

The synthesis of diastereomeric rytvela derivatives was performed using standard Fmoc-SPPS protocols (Jamieson *et al.*, **2009**), and **3.4-3.10** were obtained in high crude and isolated purity, as assessed by analytical RP-HPLC (Table 3.1).

Entry	Peptide	Crude purity %[a]	Purity %[a]	Yield %[b]	HRMS[c]	
					m/z (calcd)	***m/z*** (obsd)
3.4	D-Arg-D-Tyr-L-**Thr**-D-Val-D-Glu-D-Leu-D-Ala-NH_2	96	> 99	9.6	850.4781	850.4780
3.5	D-Arg-D-Tyr-D-Thr-L-**Val**-D-Glu-D-Leu-D-Ala-NH_2	85	94	10.9	850.4781	850.4798
3.6	D-Arg-D-Tyr-L-**Thr**-L-**Val**-D-Glu-D-Leu-D-Ala-NH_2	96	> 99	13.0	850.4781	850.4755
3.7	D-Arg-D-Tyr-D-Val-D-Val-D-Glu-D-Leu-D-Ala-NH_2	84	90	6.6	848.4989	848.4989
3.8	D-Arg-D-Tyr-L-**Val**-D-Val-D-Glu-D-Leu-D-Ala-NH_2	85	94	14.2	848.4989	848.4968
3.9	D-Arg-D-Tyr-D-Val-L-**Val**-D-Glu-D-Leu-D-Ala-NH_2	90	95	7.9	848.4989	848.4975
3.10	D-Arg-D-Tyr-L-**Val**-L-**Val**-D-Glu-D-Leu-D-Ala-NH_2	87	93	9.1	848.4989	848.4982

Table 3.1. Yields and purities of 101.10 and [Val^3]-101.10 diastereomers. [a] RP-HPLC purity at 280 nm. [b] Yields after purification by RP-HPLC are based on Fmoc loading test for Rink resin. [c] HRMS values from the major protonated molecule, typically $[M+H]^+$.

Entry	Peptide
3.11	D-Arg-D-Tyr-**(3*S*,4*R*)-Hgl**-L-Val-D-Glu-D-Leu-D-Ala-NH_2
3.12	D-Arg-D-Tyr-**(3*S*,4*R*)-Hgl**-D-Val-D-Glu-D-Leu-D-Ala-NH_2
3.13	D-Arg-D-Tyr-**(3*R*,4*S*)-Hgl**-D-Val-D-Glu-D-Leu-D-Ala-NH_2
3.14	D-Arg-D-Tyr-**(3*R*,4*S*)-Hgl**-L-Val-D-Glu-D-Leu-D-Ala-NH_2

Table 3.2. Hgl-bearing analogues synthesized by Dr. Daniel J. St-Cyr.

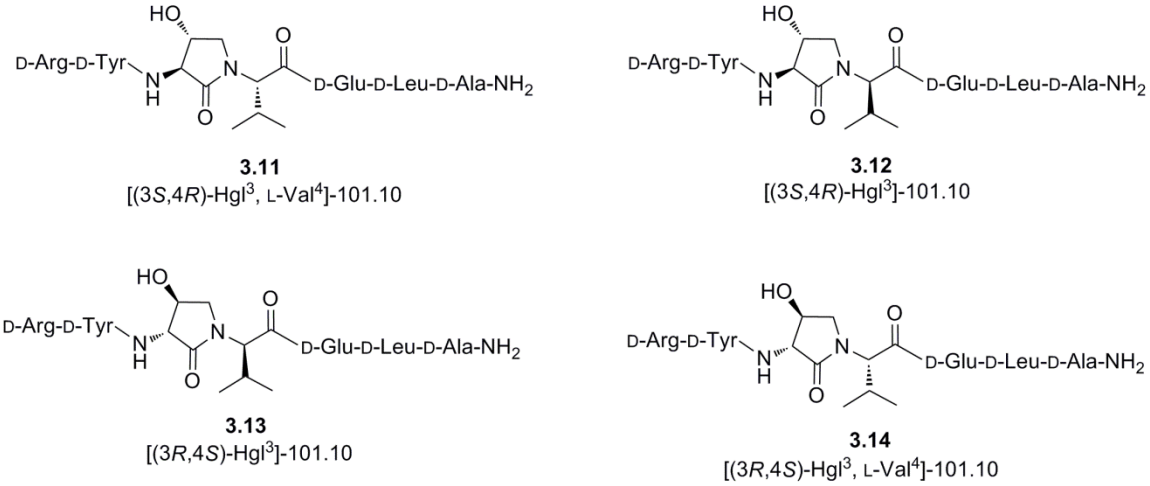

3.11
[(3*S*,4*R*)-Hgl^3, L-Val^4]-101.10

3.12
[(3*S*,4*R*)-Hgl^3]-101.10

3.13
[(3*R*,4*S*)-Hgl^3]-101.10

3.14
[(3*R*,4*S*)-Hgl^3, L-Val^4]-101.10

Figure 3.5. Structure of the analogues of 101.10 featuring Hgl residues (**3.11**-**3.14**).

Using an adaptation of published procedures (St-Cyr *et al.*, **2010**; Sicherl *et al.*, **2010**), analogues of 101.10 featuring α-amino-β-hydroxy-γ-lactam (Hgl) residues (**3.11**-**3.14**) in the place of the central threonine residue were synthesized by Dr. Daniel J. St-Cyr. Essentially, the solution phase synthesis and purification of

Fmoc-Hgl-Val-O*t*-Bu dipeptides from L- or D-*N*-(Fmoc)-oxiranylglycine methyl ester and L- or D- valine *tert*-butyl ester, followed by treatment with TFA afforded the isomerically pure dipeptide acid. Coupling of the latter to the *N*-terminus of the Rink amide resin-bound D-Glu-D-Leu-D-Ala peptide with subsequent elongation, cleavage, and purification following standard SPPS protocols provided peptides **3.11**-**3.14** (Figure 3.5).

3.3 Structure-activity relationships of [Hgl^3]-, [Val^3]- and 101.10 diastereomers

3.3.1 Conformational analysis

The influence of the modifications of 101.10 on the peptide conformation was determined by far-UV-CD spectroscopy in water. As previously discussed, CD curves were measured, presented as mean residue ellipticity versus wavelength, and analyzed using transition band values and backbone dihedral angles of relevant ideal secondary structures (Table 3.3). Typically, poly-L-glutamate at pH 8 (Johnson *et al.*, **1972**; Woody, **2010**), cyclo(L-Ala-L-Ala-Aca) and cyclo(L-Ala-D-Ala-Aca) at pH 7 (Aca = ε-aminocaproic acid; Bandekar *et al.*, **1982**; Woody, **2010**) have been used as CD standards of random coil and β-turns of type I and II, respectively.

Secondary structure	**Transition bands** (nm)			**Dihedral angles** (°)			
	$\pi_0 \rightarrow \pi^*$	$\pi_1 \rightarrow \pi^*$	$n \rightarrow \pi^*$	ϕ_{i+1}	ψ_{i+1}	ϕ_{i+2}	ψ_{i+2}
Type I β-turn	+ 190	- 202	- 220	- 60	- 30	- 90	0
Type II' β-turn	+ 190	- 205	+ 225	60	- 120	- 80	0

Table 3.3. Electronic transition bands and backbone dihedral angles of ideal type I and II' β-turns (Hutchinson *et al.*, **1994**; Woody, **2010**).

Compared to the random coil structure of rytvela (**5.1**), the introduction of a L-amino acid or a second valine at the 3- and 4-positions caused changes in CD shapes (Figures 3.6). In particular, curves indicative of a type I β-turn with negative maxima around 210 and 220 nm were observed for [L-Thr^3]-101.10 (**3.4**), [L-Thr^3, L-Val^4]-101.10 (**3.6**) and [L-Val^3, L-Val^4]-101.10 (**3.10**). On the other hand, curves suggestive of random coil conformations, albeit with a more profound negative maxima around 230 nm, were observed for [D-Thr^3, L-Val^4]- (**3.8**), [D-Val^3, D-Val^4]- (**3.10**), [L-Val^3, D-Val^4]- (**3.11**), and [D-Val^3, L-Val^4]-101.10 (**3.12**). These results suggest that inversion of only the third position stereochemistry may induce a turn conformation contingent on side-chain, suggesting the importance of the hydroxyl group, and that inversion of both 3- and 4-position stereochemistry may augment turn propensity independent of the presence of the hydroxyl group.

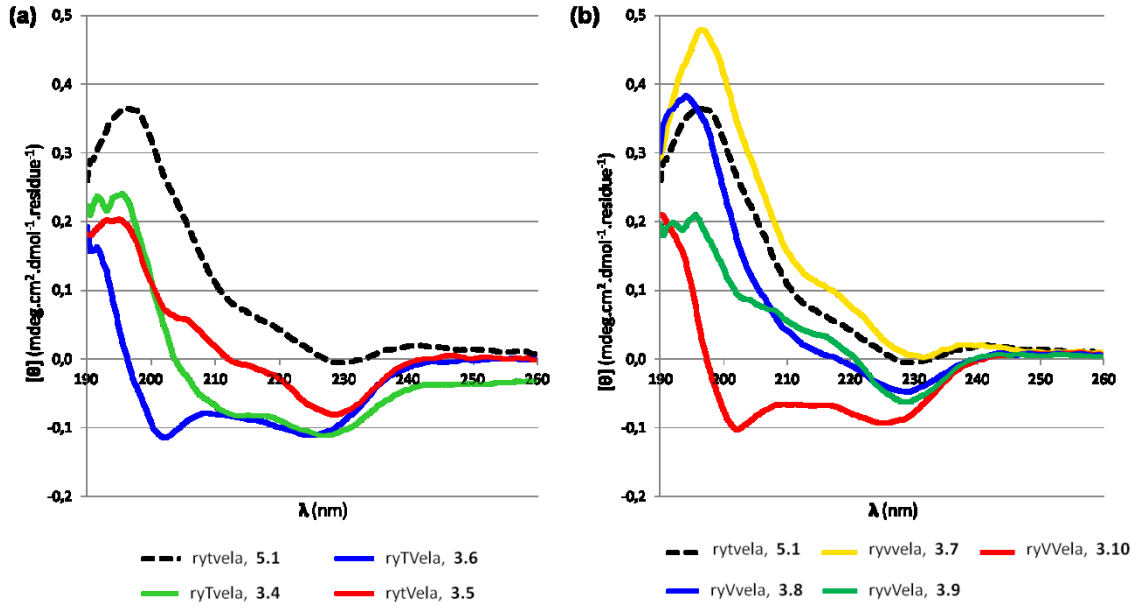

Figure 3.6. CD spectra of a) 101.10 diastereomers **3.4-3.6** and b) Val[3] diastereomers **3.7-3.10**.

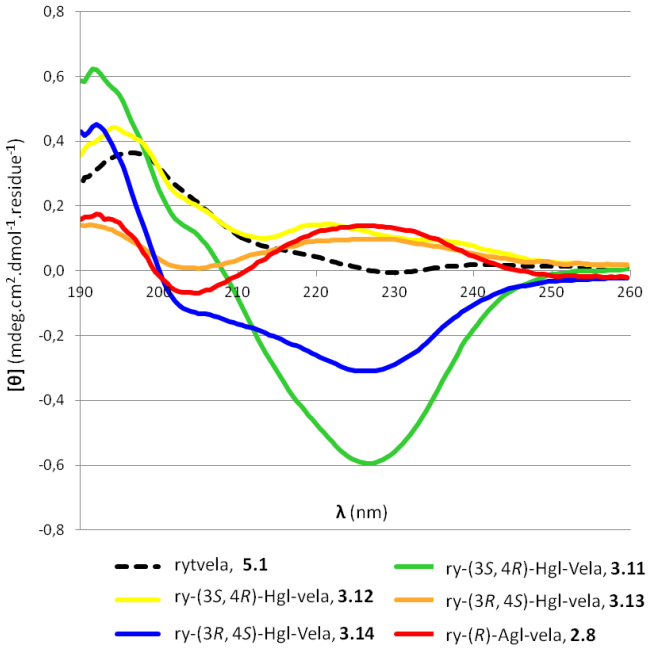

Figure 3.7. CD spectra of 101.10 and α-amino-β-hydroxy-γ-lactam analogues **3.8-3.11**.

In the case of the lactam analogue [(*R*)-Agl[3]]-101.10 (**2.8**), it exhibited a CD curve indicative of a type II' β-turn with negative maximum at 205 nm and positive maximum at 225 nm (Figure 3.7). Introduction of Hgl[3]-D-Val[4] in **3.13** and **3.12** gave similar CD curve shapes as **2.8**, characteristic of a type II' β-turn geometry, albeit with a lower ellipticity, especially for the latter. The CD spectrum of **3.13** corroborated with the X-ray structure described above for the *trans*-Hgl dipeptide (**3.3**), which was characteristic of a type II β-turn (Figure 3.4; St-Cyr *et al.*, **2010b**). The CD curves for [(3*S*,4*R*)-Hgl[3], L-Val[4]]-101.10 (**3.11**) and [(3*R*,4*S*)-Hgl[3], L-Val[4]]-101.10 (**3.14**)

were similar to those observed from respective L-Val^4 analogues (i.e., **3.7** and **3.10**), with a positive and negative bands at 192 nm and 225 nm, respectively, suggestive of a type I β-turn.

Ideal type I and II' β-turns share relatively similar backbone torsion angles, except for ϕ_{i+1} and ψ_{i+1} which differ by 120º and 90º, respectively, and give rise to CD curves that diverge only at the amide n → π* electronic transition (Table 3.3). It is thus not surprising that inverting the stereochemistry of the 3- or 4-position may give rise to either β-turn type conformations.

In summary, CD analysis has shown that the inversion of stereochemistry at the Val^4 position induced in most cases a turn conformation and that similarly, lactams such as Agl and Hgl exhibited CD curves indicative of turn conformations. In addition, subtle effects were observed upon replacement of the threonine hydroxyl group with a methyl substituent and on addition of a hydroxyl group on the Agl ring, suggesting that contributions such as the hydrogen donor and acceptor properties of the alcohol as well as its inductive effects may influence conformation.

3.3.2 Biological activity

The biological activity of the Thr^3-Val^4 analogues of 101.10 was ascertained by measuring their influence on two distinct IL-1β-induced effects. Their potential to modulate the stimulation of human thymocyte (TF-1) proliferation by IL-1β was monitored by the CyQUANT NF fluodye intercalation method, whereas their ability to inhibit activation of the inflammatory pathways of nuclear factor-κB (NF-κB) and mitogen-activated protein kinase (MAPK) by IL-1β was measured using a HEK Blue SEAP reporter gene assay. The latter relies on the expression and secretion of an alkaline phosphatase (SEAP) upon activation of its transcription promoter which is fused to activator protein (AP)-1 and NF-κB transcription binding sites, and is triggered by the binding of IL-1β to its membrane-bound receptor complex (IL-1RI/IL-1RAcP). The quantity of SEAP located in the extracellular medium is determined by adding a mixture containing the enzyme substrate (a dye termed Quanti-Blue), which upon phosphate cleavage undergoes a change of colour, that can be accurately quantified by reading the optical density at 620 nm (OD_{620}). Results are reported as the percentage of inhibition of the IL-1β-induced effect (Figures 3.8 and 3.9).

Six of the seven Thr^3-Val^4 and Val^3-Val^4 diastereomers of 101.10 (**3.5-3.10**) exacerberated IL-1β-stimulated thymocyte proliferation. The only exception, [L-Thr^3]-101.10 (**3.4**), exhibited comparable anti-proliferative activity (22% inhibition) to that of rytvela (19%). The Agl analogue **2.8** and all four Hgl-containing mimetics (**3.11**-**3.14**) displayed anti-proliferative activity. Relative to 101.10, the (3*S*)-Hgl analogues **3.11** and **3.12** exhibited respectively 4.4- and 3.2-fold improved activity and the (3*R*)-Hgl isomers **3.13** and **3.14** retained similar anti-IL-1β activity. [(*R*)-Agl^3]-101.10 (**2.8**) exhibited activity better than 101.10, yet lower than the (3*S*)-Hgl peptides relative to the Hgl series, suggesting that the (3*R*)-amino configuration is important to achieve inhibition of thymocyte proliferation.

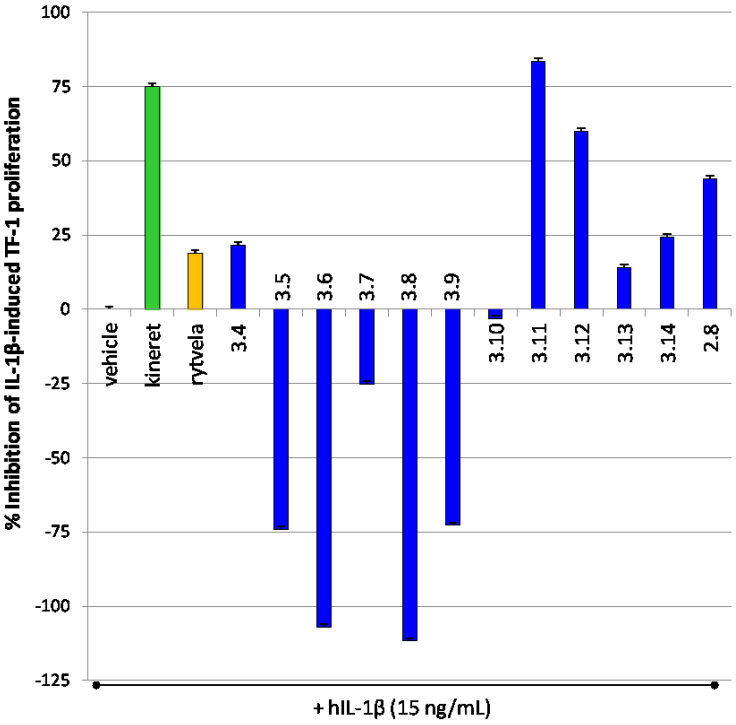

Figure 3.8. Inhibition of IL-1β-induced thymocyte proliferation by Thr^3-Val^4 analogues, as assessed by fluodye intercalation.

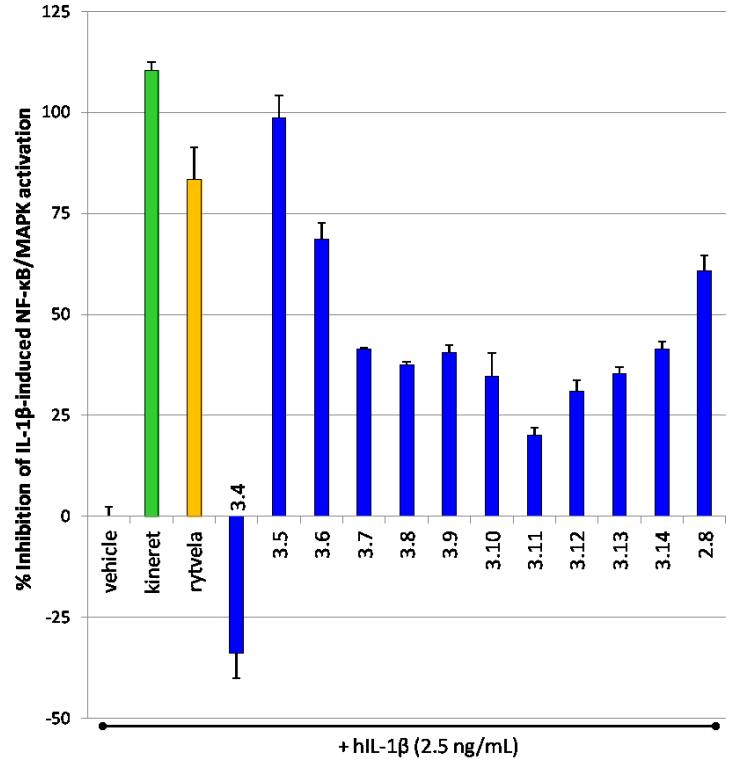

Figure 3.9. Inhibition of IL-1β-induced NF-κB and MAPK activation by Thr^3-Val^4 analogues, as measured via the HEK Blue SEAP reporter gene assay.

Contrary to the results obtained in the thymocyte proliferation assay, only [L-Thr^3]-101.10 (**3.4**) failed to block NF-κB/MAPK activation. In this test, [L-Val^4]-101.10 (**3.5**) and [L-Thr^3-L-Val^4]-101.10 (**3.6**) were the most potent, exhibiting 99% and 69% anti-inflammatory activity, respectively. The Val^3 analogues exhibited modest levels (35-41%) of inhibition of IL-1β-mediated triggering of NF-κB/MAPK pathways. Although neither the Agl nor Hgl analogues exhibited improved activity relative to rytvela (83% inhibition) in the NF-κB/MAPK assay, they did exhibit 20-61% inhibition, with the (*R*)-Agl analogue **2.8** displaying higher activity than the Hgl counterparts.

The different activities of the analogues towards inhibition of IL-1β-induced thymocyte proliferation and NF-κB/MAPK activation is notable and may be attributed to several factors: a) the two assays are measuring the effects of analogues at two different phases of the IL-1β-mediated response; b) the two assays are monitoring distinct physiological effects of IL-1β, namely immune cell proliferation (part of the adaptive immune response) and activation of inflammatory pathways (part of the inflammatory/destructive reaction); and c) the conformational changes induced upon binding of a peptide to the IL-1RI may be distinct from one analogue to the other, and may thus modulate the receptor differently causing biased signaling. Therefore, the divergent results may attest of the functional selectivity of different pharmacophores for causing anti-immune and anti-inflammatory effects.

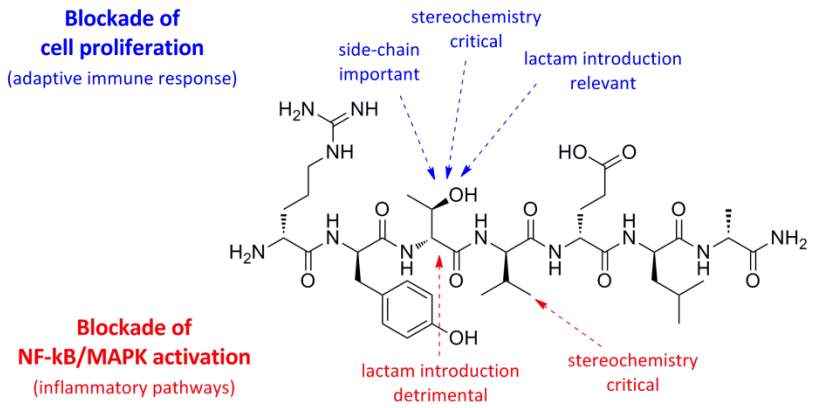

Figure 3.10. Structure-activity relationships observed using [Hgl^3]-, [Val^3]- and 101.10 diastereomers.

3.4 Concluding remarks

Attempting to correlate the relationships between structure, conformation and biology of 101.10, a series of Thr^3-Val^4 analogues were prepared, and CD studies were performed and complemented by two *in vitro* assays. Notably, many analogues demonstrated divergent bioactivity and differing states of efficacy in the two assays. Peptidomimetics that blocked more efficiently NF-κB/MAPK activation contained either L-Val^4 or (3*R*)-Hgl^3 residues and exhibited β-turn-like CD curves. Alternatively, the analogues that showed the highest inhibition of IL-1β-induced immune cell proliferation possessed L-Thr^3 and (3*S*)-Hgl^3 residues, and also displayed CD spectra indicative of β-turns. In general, substitution of D-Thr^3 by L- or D-Val^3 caused a loss of activity in both assays, suggesting that the hydroxyl side-chain is important for eliciting bioactivity. With respect to changes in stereochemistry, L-Thr^3 (**3.4**) and L-Val^4 (**3.5**) exhibited respectively losses of activity in the NF-κB/MAPK activation and proliferation relative to 101.10, differentiating the anti-IL-1β effects. Finally, conformational constraint from the application of lactams generally gave peptidomimetics with inhibitory activity to both NF-

κB/MAPK activation and proliferation, albeit their potency relative to 101.10 was contingent on the assay employed as well as ring system structure and stereochemistry.

Selected Thr^3-Val^4 analogues are currently being tested for their inhibitory potency (IC_{50}) toward NF-κB/MAPK activation and in *in vivo* inflammatory models, such as IL-1β-mediated hyperthermia and contact dermatitis, as well as oxazolone-induced arthritis. These ongoing studies may help clarify the structure-activity relationships between the Thr^3-Val^4 subunit of rytvela and explored IL-1β-mediated pathways.

3.5 Experimental section

3.5.1 General

See experimental section of chapter 2.

3.5.2 Characterization and purification

Refer to experimental section of chapter 2.

3.5.3 Synthesis of peptides and mimetics by standard Fmoc-SPPS

See experimental section of chapter 2.

3.5.4 Ultraviolet-circular dichroism

Refer to experimental section of chapter 2.

3.5.5 Biological activity screening of analogs

3.5.5.1 CyQUANT intercalation assay

Same as experimental section of chapter 2.

3.5.5.2 HEK Blue SEAP reporter gene assay

Activation of the NF-κB pathway upon interaction with IL-1β or IL-33 receptor complex at the membrane was assessed via HEK-Blue SEAP reporter gene assay (InvivoGen, California, USA). Basically, HEK Blue IL-33/IL-1β sensor cells (stably expressing the SEAP reporter gene; InvivoGen, California, USA) were cultured in growth medium made of complete Dulbecco's modified Eagle medium (DMEM; 4.5 g/L glucose, 2 mM L-glutamine, 100 mM sodium pyruvate, 10% fetal bovine serum, 50 U/mL penicillin, 50 µg/mL streptomycin; Gibco (Invitrogen), Ontario, CA) supplemented with selection antibiotics (30 µg/mL Blasticidin, 200 µg/mL HygroGold and 100 µg/mL Zeocin; InvivoGen, California, USA). Upon reaching almost 70% confluency, HEK Blue cells were reincorporated into complete DMEM medium and split ($2.5x10^4$ cells in 180 µL/well) into 96-well membrane-treated flat bottom culture plates (#3595, Corning Life Sciences, Massachusetts, USA). Cells were pre-treated

with 10 µL of peptide or peptidomimetic (1 µM) for 15 min., after which 10 µL of human IL-1β (2.5 ng/mL, PeproTech, New Jersey, USA) was added. After 24 h of incubation, 40 µL of supernatant was added to a UV-transparent 96-well plate (#3635, Corning Life Sciences, Massachusetts, USA) already filled with 160 µL of resuspended Quanti-Blue dye (InvivoGen, California, USA). The plate was covered and incubated for 20 min. The level of SEAP was measured by reading absorbance (or optical density, OD) at 620 nm using a multiplate reader equipped with a monochromator (Perkin Elmer Wallac Envision 2104; Perkin Elmer, California, USA). Hexaplicates results were normalized over complete DMEM background signal and analyzed by one-way analysis of variance (ANOVA) factoring for treatments, and data are presented as mean ± standard error of the mean (SEM).

3.6 References

Avenoza, A.; Barriobero, J. I.; Cativiela, C.; Fernandez-Recio, M. A.; Peregrina, J. M.; Rodriguez, F. *Tetrahedron* **2001**, *57*, 2745-2755.

Bandekar, J.; Evans, D. J.; Krimm, S.; Leach, S.J.; Lee, S.; McQuie, J. R.; Minasian, E.; Nemethy, G.; Pottle, M. S.; Scheraga, H.A. *Int. J. Pept. Protein Res.* **1982**,*19*, 187-205.

Banerjee, A.; Raghothama, S. R.; Karle, I. L.; Balaram, P. *Biopolymers* **1996**, *39* (3), 279-285.

Boutard, N.; Turcotte, S.; Beauregard, K.; Quiniou, C.; Chemtob, S.; Lubell, W.D. *J. Pep. Sci.* **2011**, *17*(4), 288-296.

Burkhart, B. M.; Li, N.; Langs, D. A.; Pangborn, W. A.; Duax, W. L. *Proc. Natl. Acad. Sci. USA* **1998**, *95*, 12950-12955.

Chakraborty, T. K.; Srinivasu, P.; Vengal Rao, V.; Kiran Kumar, S.; Kunwar, A. C. *J. Org. Chem.* **2004**, *69*, 7399-7402

Chemtob, S.; Quiniou, C.; Lubell, W.D.; Beauchamp, M.; Hansford, K.A. International Patent WO 105830, **2005**.

Chen, Y.; Mant, C. T.; Hodges, R. S. *J. Pep. Res.* **2002**, *59* (1), 18-33.

Chou, P. Y.; Fasman, G. D. *Ann. Rev. Biochem.* **1978**, *47*, 251-276.

Dunlop, D. S.; Neidle, A.; McHale, D.; Dunlop, D. M.; Lajtha, A. *Biochem. Biophys. Res. Commun.* **1986**, *141*, 27-32.

Fabiola, G. F.; Bobde, V.; Damodharan, L.; Pattabhi, V.; Durani, S. *J. Biomolec. Struc. Dyn.* **2001**, *18* (4), 579-594.

Fairman, R.; Anthony-Cahill, S. J.; DeGrado, W. F. *J. Am. Chem.Soc.* **1992**, *114*, 5458-5459.

Fisher, G. H.; Petrucelli, L.; Gardner, C.; Emory, C.; Frey, W. H.; Amaducci, L.; Sorbi, S.; Sorrentino, G.; Borghi, M.; D'Anielli, A. *Mol. Chem. Neuropathol.* **1994**, *23*, 115-124.

Fujii, N. *Origins Life Evol. B.* **2002**, *32* (2), 103-127.

Ghadiri, M. R.; Granja, J. R.; Milligan, R. A.; Mckee, D. E.; Khazanovich, N. *Nature* **1993**, *366*, 324-327.

Guzzo, P. R.; Trova, M. P.; Inghardt, T.; Linschoten, M. *Tetrahedron Lett.* **2002**, *43*, 41-43.

Hanessian, S.; Vinci, V.; Fettis, K.; Maris, T.; Viet, M. T. P. *Org. Chem.* **2008**, *73* (4), 1181-1191.

Hashimoto, A.; Kumashiro, S.; Nishikawa, T.; Oka, T.; Takahashi, K.; Mito, T.; Takashima, S.; Doi, N.; Mizutani, Y.; Yamazaki, T.; Kaneko, T. Ootomo, E. *J. Neurochem.* **1993**, *61*, 348-351.

Hruby, V. J.; Li, G.; Haskell-Luevano, C.; Shenderovich, M. *Biopolymers* **1997**, *43* (3), 219-266.

Hutchinson, E. G.; Thornton, J. M. *Protein Sci.* **1994**, *3*, 2207-2216.

Jamieson, A. G.; Boutard, N.; Beauregard, K.; Bodas, M. S.; Ong, H.; Quiniou, C.; Chemtob, S.; Lubell, W. D. *J. Am. Chem. Soc.* **2009**, *131* (22), 7917-7927.

Jenkins, C. L.; Bretscher, L. E.; Guzei, I. A.; Raines, R. T. *J. Am. Chem. Soc.* **2003**, *125*, 6422-6427.

Johnson, W. C. Jr.; Tinoco, I. Jr. *J. Am. Chem. Soc.* **1972**, *94*, 4389-4390.

Krause, E.; Bienert, M.; Schmieder, P.; Wenschuh, H. *J. Am. Chem. Soc.* **2000**, *122,* 4865-4870.

Kreil, G.; Barra, D.; Simmaco, M.; Erspamer, V.; Erspamer, G. F.; Negri, L.; Severini, C.; Corsi, R.; Melchiorri, P. *Eur. J. Pharmacol.* **1989**, *162*, 123-128.

Kreil, G. *Annu. Rev. Biochem.* **1997**, *66*, 337-345.

Kumar, A.; Ramakrishnan, V. *Syst. Synth. Biol.* **2010**, *4*, 247-256.

Leeson, P. D.; Williams, B. J.; Rowley, M.; Moore, K. W.; Baker, R.; Kemp, J. A.; Priestley, T.; Foster, A. C.; Donald, A. E. *Bioorg. Med. Chem. Lett.* **1993**, *3*, 71-76.

Lipmann, F.; Hotchkiss, R. D.; Dubos, J. *J. Biol. Chem.* **1941**, *141*, 163-167.

Lubell, W. D.; Beauregard, K.; Polyak, F. In *Comprehensive Chirality*; Carreira E.; Ed.; Elsevier B.V., Amsterdam, The Netherlands, **2012**, *in press*.

Mahalakshmi, R.; Balaram, P. In *D-Amino Acids : A New Frontier in Amino Acid and Protein Research;* Konno, R.; Ed.; Nova Science, Hauppauge, USA, **2006**, 415-430.

Nagarajan, V.; Pattabhi, V.; Johnson, A.; Bobde, V.; Durani, S. *J. Peptide Res.* **1997**, *49*, 74-79.

Nomizu, M.; Utani, A.; Shiraishig, N.; Kibbeyg, M. C.; Yamada, Y.; Roller, P. P. *J. Biol. Chem.* **1992**, *267* (20), 14118-14121.

Okumura, K.; Inoue, K.; Fukamizu, M. Japan Patent JPN 46041305, **1971**.

Paul, P. K. C.; Burney, P. A.; Campbell, M. M.; Osguthorpe, D. J. *J. Comput. Aided Mol. Des.* **1990**, *4*, 239-253.

Pouny, Y.; Shai, Y. *Biochemistry* **1992**, *31*, 9482-9490.

Quiniou, C.; Sapieha, P.; Lahaie, I.; Hou, X.; Brault, S. Beauchamp, M.; Leduc, M.; Rihakova, L.; Joyal, J.-S.; Nadeau, S.; Heveker, N.; Lubell, W.D.; Sennlaub, F.; Gobeil, F. Jr.; Miller, G.; Pshezhetsky, A.V.; Chemtob, S. *J. Immunol.* **2008**, *180*, 6977-6987.

Ramachandran, G. N.; Ramakrishnan, C.; Sasisekharan, V. *J. Mol. Biol.* **1963**, *7*, 95-99.

Ramachandran, G. N.; Sasisekharan, V. *Adv. Protein Chem.* **1968**, *23*, 283-438.

Richter, K.; Egger, R.; Negri, L.; Corsi, R.; Severino, C.; Kreil, G. *Proc. Natl. Acad. Sci. USA* **1990**, *87*, 4836-4839.

Scholz, D.; Billich, A.; Charpiot, B.; Ettmayer, P.; Lehr, P.; Rosenwirth, B.; Schreiner, E.; Gstach, H. *J. Med. Chem.* **1994**, *37*, 3079-3089.

Shoulders, M. D.; Raines, R. T. *Annu. Rev. Biochem*. **2009**, *78*, 929-958.

Sicherl, F.; Cupido, T.; Albericio, F. *Chem. Commun*. **2010**, *46*, 1266-1268.

St-Cyr, D. J.; Jamieson, A. G.; Lubell, W. D. *Org. Lett.* **2010**, *12* (8), 1652-1655.

St-Cyr, D. J.; Maris, T.; Lubell, W. D. *Heterocycles* **2010b**, *82* (1), 729-737.

Tobias, D. J.; Brooks, C. L. *Biochemistry* **1991**, *30*, 6059-6070.

Toniolo, C. *Int. J. Pept. Protein Res.* **1990**, *35*, 287-300.

Urry, D.W.; Goodall, M.C.; Glickson, J.D.; Mayers, D. F. *Proc. Natl. Acad. Sci. USA* **1971**, *68* (8),1907-1911.

Veatch, W. R.; Fossel, E.T.; Blout, E. R. *Biochemistry* **1974**, *13* (26), 5249-5256.

Wallace, R. *Nature Precedings* **2010**, *8* (1), 1-7.

Woody, R. W. *Chirality* **2010**, *22*, E22-E29.

Zhou, N.; Luo, Z.; Luo, J.; Fan, X.; Cayabyab, M.; Hiraoka, M.; Liu, D.; Han, X.; Pesavento, J.; Dong, C.-Z.; Wang, Y.; An, J.; Kaji, H.; Sodroski, J. G.; Huang, Z. *J. Biol. Chem.* **2002**, *277* (20), 17476-17485.

CHAPTER 4

Indolizidinone Amino Acids

4.1 Introduction

Indolizidin-2-one amino acids (I^2aa; Figure 4.1a) are bicyclic lactams that include an Ala-Pro-type dipeptide unit with an all-carbon backbone. The popularity of these azabicyclo[3.4.0]nonane amino acids has quickly progressed after a [6,5]-fused thiaindolizidinone (called BTD, **4.1**) was shown to serve as a type II' β-turn mimic, contingent upon ring-fusion and backbone stereochemistry, which was comparable to D-Ala-L-Pro dipeptide (**4.2**; Nagai *et al.*, **1985**; Nagai *et al.*, **1993**). However, the higher acidic stability of I^2aa compared to its thia and oxa counterparts has rendered it an attractive rigid [6,5]-fused peptidomimicry system.

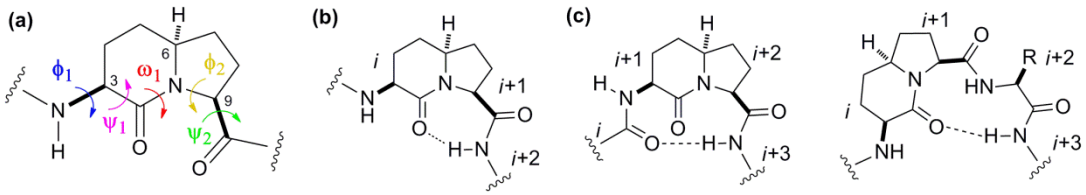

Figure 4.1. (3*S*,6*S*,9*S*)-I^2aa as dihedral angles constraint (a), and typical residue position in γ-turn (b) and β-turn motifs (c) (adapted from Halab *et al.*, **2000**).

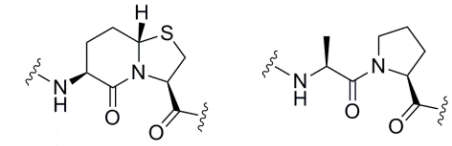

BTD, 4.1
(2*R*,6*S*,8*S*)-thiaindolizidinone

4.2
D-Ala-L-Pro

Figure 4.2. Structure of type II' β-turn mimics [6,5]-thiaindolizidinone and D-Ala-L-Pro dipeptide.

The I^2aa heterocycle restricts three contiguous dihedral angles, ϕ_2, ψ_1 and ω_1. Moreover, the torsion angles ϕ_1 and ψ_2 are confined by *gauche* interactions with the ring system (Figure 4.1a; Hanessian *et al.*, **1997**; Halab *et al.*, **2000**). The conformational preferences elicited by these restrictions have been studied by spectroscopic and crystallographic methods supported by computational analysis. Using *N*-acetyl-I^2aa-9-methylamide models, force fields evaluating the frequency of hydrogen bond formation have calculated that the minimal energy conformers of the dipeptide may preferentially adopt a γ- or β-turn (Lombart *et al.*, **1996b**; McDonald *et al.*, **1996**; Takeuchi *et al.*, **1998**). For example, the dihedral angles for both (3*S*,6*S*,9*S*)- and (3*S*,6*R*,9*S*)-I^2aa *N*-acetyl-methylamide dipeptides were respectively characteristics of inverse and classical γ-turns, as well as type II' and II β-turns (Table 4.1; Cluzeau *et al.*, **2007**). The circular dichroism spectrum of Dnp-Gly-(3*S*,6*S*,9*S*)I^2aa-Gly-*p*-NA (Dnp = *N*-2,4-dinitrophenyl; *p*-NA = *para*-nitroanillide) exhibited a curve bearing a positive band at 305 nm and a negative maximum at 350 nm, indicative of a type II' β-turn (Lombart *et al.*, **1997**; Halab *et al.*, **2000**). The close similarity between the dihedral angles obtained from the X-ray diffraction of *N*-Boc-I^2aa-esters crystals (Lombart *et al.*, **1996**; Polyak *et al.*, **1998**; Polyak *et al.*, **2000**) and that of ideal turn conformations (Table 4.1) corroborated the high turn-propensity of these azabicycloalkanes (Ball *et al.*, **1990**, Nagai *et al.*, **1993**). Together, these investigations have denoted the positioning preferences of I^2aa, namely at the *i* and *i*+1 residue of a γ-turn, and at the *i* and *i*+1 or at the *i*+1 and *i*+2 positions of a β-turn (Figure 4.1b and c; Lombart *et al.*, **1996b**; Halab *et al.*, **2000**).

Secondary structure	Transition bands (nm)			Dihedral angles (°)			
	$\pi_0 \rightarrow \pi^*$	$\pi_1 \rightarrow \pi^*$	$n \rightarrow \pi^*$	ϕ_{i+1}	ψ_{i+1}	ϕ_{i+2}	ψ_{i+2}
classical γ-turn	+ 198	- 212	+ 230	75	- 64	-	-
type II' β-turn	+ 190	- 205	+ 225	60	- 120	- 80	0
PPI	+ 190	- 205	- 220	- 75	160	-	-
PPII	- 205	-	+ 228	- 75	145	-	-

Table 4.1. Electronic transition bands and backbone dihedral angles of ideal classical γ-turn, type II' β-turn, PPI and PPII (Rose *et al.*, **1985**; Hutchinson *et al.*, **1994**; Uray *et al.*, **2000**; Moradi *et al.*, **2009**; Woody, **2010**).

Since 1994, azabicyclo[3.4.0]alkanone amino acids have been regularly used to study peptide conformation-activity relationships (Figure 4.3.). For example, replacement of the D-Phe-Pro dipeptide residues with (3*R*,6*R*,9*R*)- and (3*S*,6*S*,9*S*)-I^2aa (**4.4**) in the cyclic peptide drug gramicidin S (GS, *cyclo*[Val-Orn-Leu-D-Phe-Pro]$_2$, **4.3**) produced analogues which were shown by CD and NMR spectroscopy to adopt the type II' β-turn/anti-parallel β-sheet structure of the parent peptide. Moreover, the [$I^2aa^{4\text{-}5,4'\text{-}5'}$]-GS analogues (**4.4**) displayed anti-microbial activity, albeit with higher minimal inhibitory concentration (MIC) against Gram-negative bacteria and fungi than the parent compound (Roy *et al.*, **2002**). In addition, unsaturated (3*S*,6*S*)-I^2aa equivalent **4.6** has been used to probe the bioactive conformation of thyrotrophin-related hormone (TRH). Relative to the poorly active [Cha^2]-TRH analogue (**4.5**), the azabicyclo[4.3.0]non-2-ene derivative **4.6** improved 3.4- and 4.7-times the receptor affinity and potency in stimulating inositol phosphate second messenger, respectively (Laakkonen *et al.*, **1996**; Li *et al.*, **1996**), offering potential therapeutic avenues to treat thyroid disorders. In the development of calcitonin gene-related peptide (CGRP) antagonists as potential treatments of neuronal pain, [D^{31}, $I^2aa^{33\text{-}34}$, F^{35}]-$CGRP_{27\text{-}37}$ (**4.8**) displayed 7-fold improved potency relative to the active peptide fraction [D^{31}, F^{34}, F^{35}]-$CGRP_{27\text{-}37}$ (**4.7**), in an inhibition assay of α-CGRP-induced production of cyclic adenosine monophosphate (cAMP; Boeglin *et al.*, **2007**).

In preliminary studies, [D-Pro^4]-101.10 exhibited anti-inflammatory activity, both *in vitro* and *in vivo*. An Ala-Pro-type bicyclic scaffold such as I^2aa was thus employed to investigate the spatial arrangement of pharmacophores, stereochemistry and conformation at the 3- and 4-positions of rytvela. Accordingly, a series of analogues of 101.10 were synthesized bearing a central indolizidin-2-one amino acid and proline residues.

4.2 Synthesis of indolizidinone amino acids

4.2.1 Previous synthetic approaches

A number of strategies (Cluzeau *et al.*, **2005**) have been adopted to construct indolizidin-2-one amino acids, in which obtaining the correct absolute stereochemistry at all three carbon centers was the key issue. Although the best starting material appears as cyclic amino acid templates such as proline or pyroglutamic acid, the first syntheses of I^2aa relied on acyclic precursors. For example, a diastereoselective synthesis employed a Sköllkopf alkylation to prepare a linear diamino acid dicarboxylate precursor (**4.9**), which upon reductive amination and lactam formation gave a separable mixture of the (3*S*,6*S*,9*S*)-[5,6]-fused bicycle (**4.10**), along with

the (3*R*,6*R*,9*R*)-enantiomer and a racemic mixture of the diastereomers (Scheme 4.1; Mueller *et al.*, **1994**). A similar linear precursor (**4.11**) was prepared by a Horner-Emmons olefination and enantioselective hydrogenation using a chiral rhodium catalyst, and used subsequently in a reductive amination/lactamization sequence to furnish the desired bicyclic lactam (**4.12**, Scheme 4.2; Wang *et al.*, **2001**). Anodic amide oxidation and 5-position functionalization has given 5-vinylproline methyl ester (**4.13**), which after coupling to *N*-Boc-vinylglycine **4.14,** olefin metathesis and hydrogenation provided the *N*-Boc-(3*S*,6*S*,9*S*)-I^{2}aa **4.15** (Scheme 4.3; Beal *et al.*, **2000**).

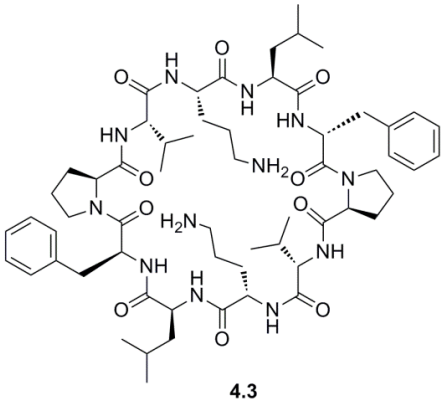

4.3
Gramicidin S
cyclo[Val-Orn-Leu-D-Phe-Pro]$_2$

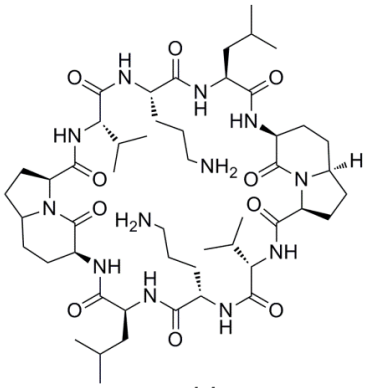

4.4
[(3*S*,6*S*,9*S*)-I^{2}aa$^{4\text{-}5,4'\text{-}5'}$]-GS

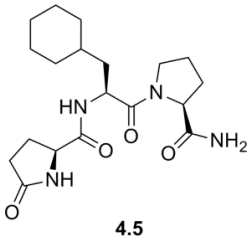

4.5
[Cha^2]-TRH
pGlu-Cha-Pro-NH$_2$

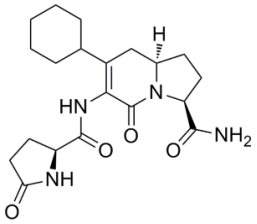

4.6
4-cyclohexyl-[(3*S*,6*S*,9*S*)-I^{2}aa^{2,3}]-TRH

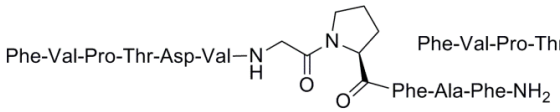

4.7
[D^{31}, P^{34}, F^{35}]-CGRP$_{27\text{-}37}$

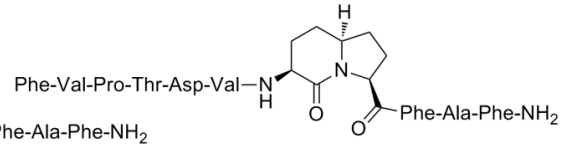

4.8
[D^{31}, (3*S*,6*S*,9*S*)-I^{2}aa$^{33\text{-}34}$, F^{35}]-CGRP$_{27\text{-}37}$

Figure 4.3. (3*S*,6*S*,9*S*)-I^{2}aa analogues of gramicidin S, cyclohexylalanine-thyrotropin-related hormone ([Cha^2]-TRH) and modified calcitonin gene-related peptide ([D^{31}, P^{34}, F^{35}]-CGRP$_{27\text{-}37}$).

Many published synthetic approaches towards the indolizidin-2-one amino acids have met the challenges of creating the bicycle with good stereocontrol by employing enantioselective and diastereoselective methods (Hanessian *et al.*, **1996**; Kim *et al.*, **1997**; Hanessian *et al.*, **2000**; Mulzer *et al.*, **2000**; Wang *et al.*, **2001**; Hanessian *et al.*, **2003**) as well as by application of amino acids derived from the chiral pool (Mueller *et al.*, **1994**; Lombart *et al.*, **1996**; Polyak *et al.*, **1998**; Halab *et al.*, **2000**; Beal *et al.*, **2000**). However, methods are more rare

which provide selective and combinatorial access to all stereoisomers of the bicycle in good yields (at most 80%) (Lombart *et al.*, **1996**; Mulzer *et al.*, **2000**).

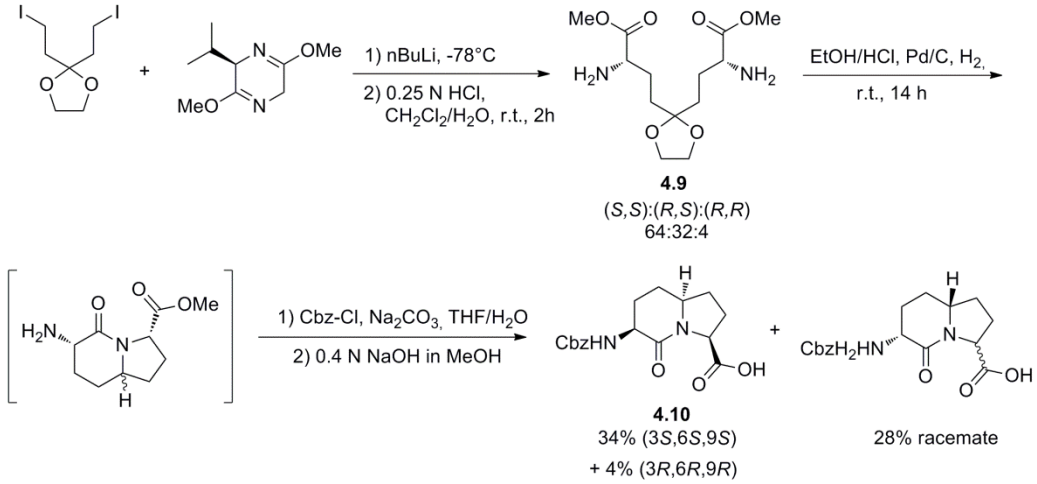

Scheme 4.1. Synthesis of I^{2}aa via Sköllkopf alkylation and reductive amination (Mueller *et al.*, **1994**).

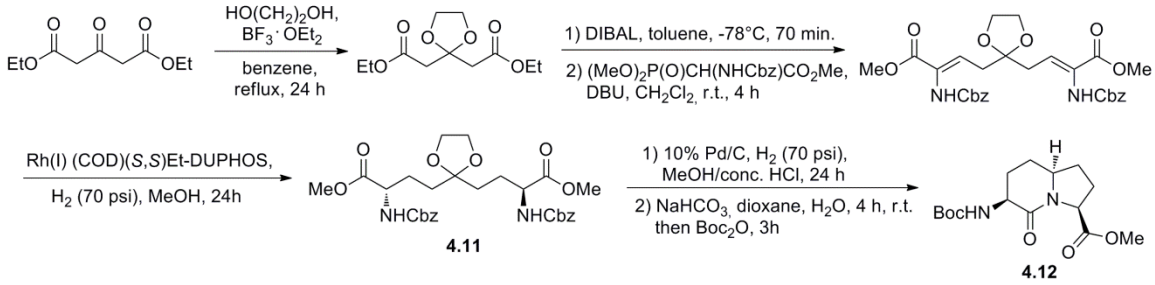

Scheme 4.2. Synthesis of I^{2}aa via Horner-Emmons olefination and asymmetric hydrogenation (Wang *et al.*, **2001**).

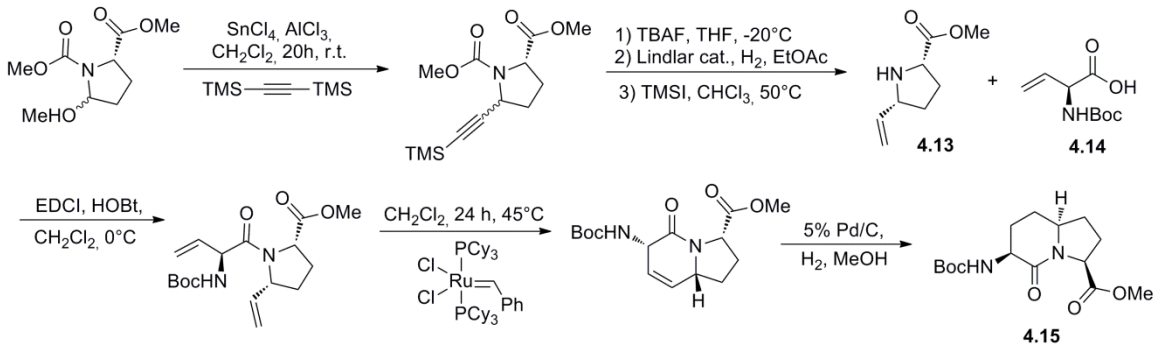

Scheme 4.3. Synthesis of I^{2}aa via anodic amide oxidation and ring-closing metathesis (Beal *et al.*, **2000**).

4.2.2 Our synthetic methodology

(3*R*,6*R*,9*R*)-Indolizidinone amino acid **4.17** was synthesized in solution from D-glutamic acid (**4.16**) using a Claisen condensation/reductive amination/lactam cyclization sequence (Scheme 4.4; Lombart *et al.*, **1996**). A modification of the original published method (Lombart *et al.*, **1996**) was employed in the hydrogenation of the symmetric ketone: instead of a bulk reactor, flow-through hydrogenation was performed in a H-Cube® apparatus,

which produces molecular hydrogen from the electrolysis of water. This change resulted in a reduction of the reaction time from 2-3 days down to 30 min. The safety of the operation was improved by circumventing the use of a pressurized hydrogen tank. Conversions and yields were similar if not superior to that of published method (81%; Lombart *et al.*, **1996**).

The Boc group of (3*R*,6*R*,9*R*)-indolizidinone *N*-(Boc)amino acid was substituted for a Fmoc *N*-protecting group (Boeglin *et al.*, **2007**). N-Fmoc-(3*R*,6*R*,9*R*)-indolizidinone amino acid **4.18** was introduced at the Thr^3-Val^4 positions of 101.10, employing standard peptide synthesis protocols on Rink amide MBHA resin (Scheme 4.5). The indolizidinone peptides were recovered in 47-96% crude purity, as assessed by analytical HPLC, and generally isolated in > 95% purity in 5.3-14.5% yield (Table 4.2). For comparison, three peptides containing a Pro^4 residue were prepared using standard SPPS protocols (Table 4.2.).

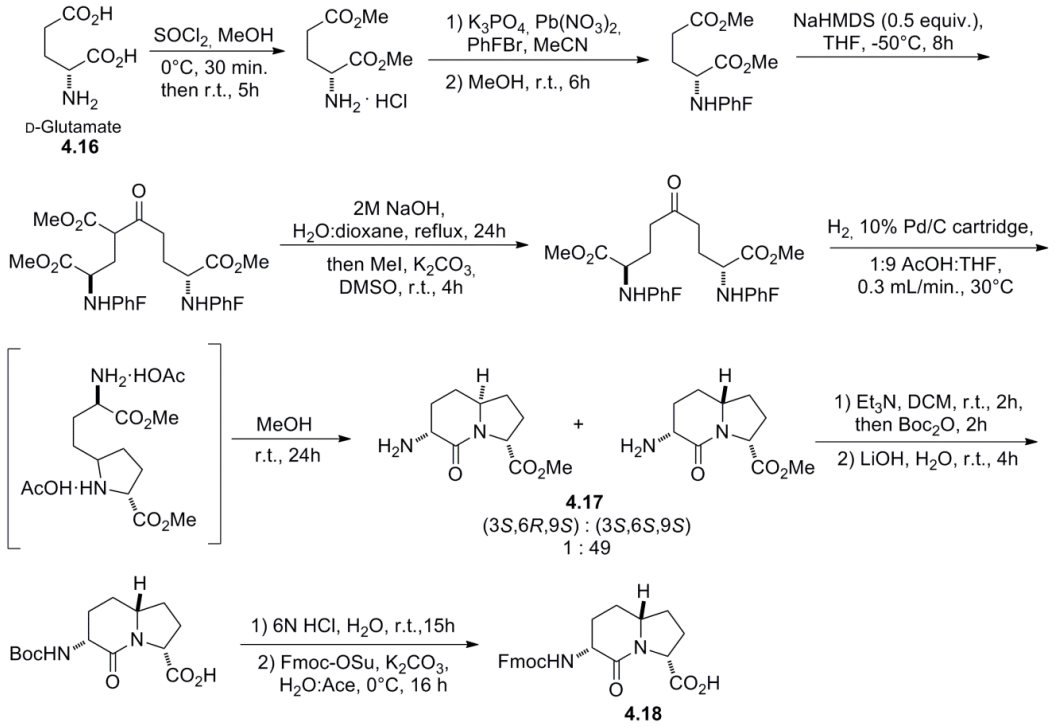

Scheme 4.4. Solution-phase synthesis of the indolizidin-2-one dipeptide building block.

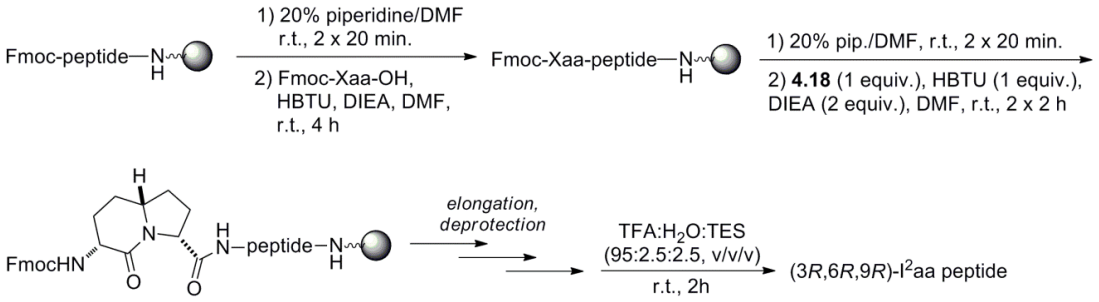

Scheme 4.5. Anchoring of *N*-Fmoc-(3*R*,6*R*,9*R*)-I^{2}aa on Rink MBHA resin following standard SPPS protocols.

Entry	Peptide	Crude purity %[a]	Purity %[a]	Yield %[b]	HRMS[c]	
					m/z (calcd)	***m/z*** (obsd)
4.19	D-Arg-D-Tyr-**(3*R*,6*R*,9*R*)-I^{2}aa**-D-Glu-D-Leu-NH_2	80	99	8.4	759.4148	759.4114
4.20	D-Arg-D-Tyr-**(3*R*,6*R*,9*R*)-I^{2}aa**-D-Glu-D-Leu-D-Ala-NH_2	47	95	5.3	830.4519	830.4493
4.21	D-Arg-D-Tyr-D-Thr-**D-Pro**-D-Glu-D-Leu-D-Ala-NH_2	85	92	10.2	848.4625	848.4619
4.22	D-Arg-D-Tyr-D-Thr-**L-Pro**-D-Glu-D-Leu-D-Ala-NH_2	96	> 99	14.5	848.4625	848.4598
4.23	D-Arg-D-Tyr-D-Thr-**D-Pro**-D-Glu-D-Leu-NH_2	88	> 99	7.0	777.4254	777.4273

Table 4.2. Yields and purities of I^{2}aa- and Pro-containing analogues of 101.10. [a] RP-HPLC purity at 280 nm. [b] Yields after purification by RP-HPLC are based on Fmoc loading test for Rink resin. [c] HRMS values from the major protonated molecule, typically $[M+H]^+$.

Entry	Peptide[a]
4.24	D-Arg-D-Tyr-**(3*S*,6*S*,9*S*)-I^{2}aa**-D-Glu-D-Leu-D-Ala-NH_2

Table 4.3. [(3*S*,6*S*,9*S*)-I^{2}aa]-101.10 synthesized by Carine Bourguet.

4.3 Structure-activity relationships of indolizidinone amino acids

4.3.1 Conformational analysis

The ability of proline and indolizidin-2-one amino acid residues to elicit folding in 101.10 analogues **4.19**-**4.24** was assessed by far-UV-CD spectroscopy in water. The CD data were reported as mean residue ellipticity, [θ] (Figure 4.4), and analyzed according to typical CD electronic transition values (Table 4.1).

Examination of the CD spectra of analogues possessing proline or I^{2}aa moieties showed limited changes in curve shape from the parent peptide. For example, [(3*R*,6*R*,9*R*)-I^{2}aa]-101.10 (**4.20**) exhibited a CD curve similar to the parent peptide, indicative of a disordered structure. Truncating the alanine of this analogue (**4.19**) resulted in the deepening of the negative shoulder at 202 nm, suggesting discrete amounts of PPII. The CD spectra of the (3*S*,6*S*,9*S*)-I^{2}aa (**4.24**) displayed a positive band at 198 nm and a negative band at 222 nm, characteristic of a PPI helical structure. Replacing D-Val for L- or D-Pro with or without removal of D-Ala (**4.21**-**4.23**) produced curves featuring two negative maxima at 203 and 225-230 nm intersperced with a positive apex centered at 215-220 nm, indicating the presence of a type I β-turn. Overall, these results suggested that a central Pro or a I^{2}aa residue of the (*S*)-stereochemistry induced more profound changes in the CD curve of the parent peptide than their (*R*)-counterparts, and that most of these analogues elicited a turn or a polyproline-type helical conformation, albeit in discrete amounts for some mimetics.

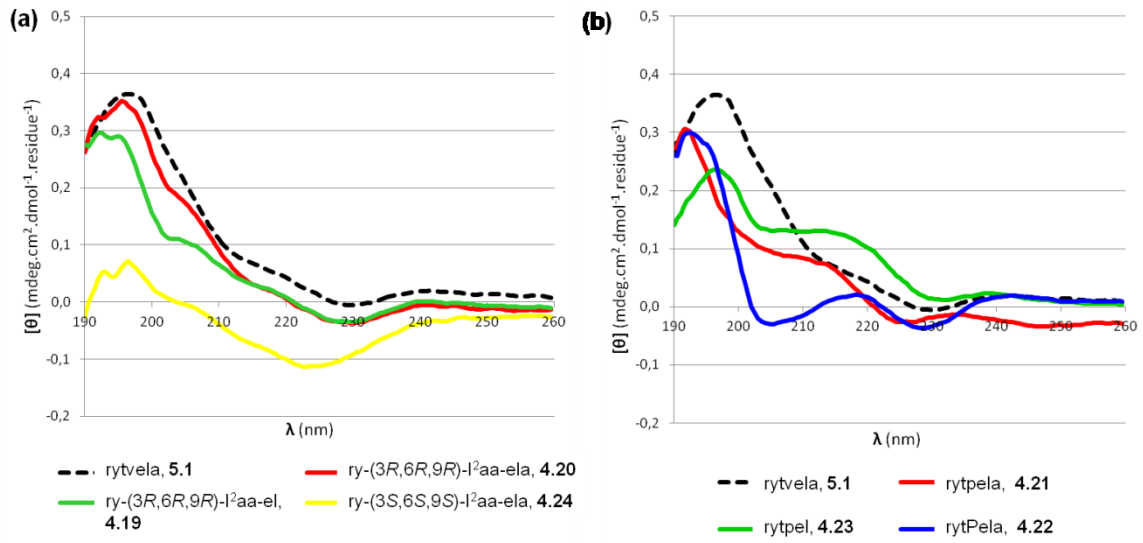

Figure 4.4. CD of 101.10 and a) selected l^2aa and b) Pro^4 analogues.

Although the CD spectrum of [(3*R*,6*R*,9*R*)-$l^2aa^{3,4}$, ΔAla^7]-101.10 (**4.19**) indicated the slight presence of PPII, discerning between PPII and unfolded states has been typically problematic, because both structures lack hydrogen bonding, are highly dynamic and are indistinguishable by ^{1}H-NMR spectroscopy (Bochicchio *et al.*, **2002**). In nature, type II poly-L-proline is a left-handed helix composed of three prolyl residues per turn with defined backbone dihedral angles (ϕ, ψ, ω = −75°, 145°, 180°), commonly found in elastomeric proteins such as collagen and elastin. In the Ramachandran plot, the PPII structure is located very close to type II β-turn and extended conformations (Bochicchio *et al.*, **2001**), and in circular dichroism, only a slight shift in the n→π* and π_0→π* electronic transitions as well as a faint peak at 220 nm may distinguish PPII from random coil. The PPII has thus been considered an extended structure coexisting with unordered conformations as well as turn motifs. Other extensive studies have noted the close resemblance between CD spectra of unordered, PPII and collagen (Tiffany *et al.*, **1968**), and suggested that the so-called random coil may consist in short segments (4-6 residues) of PPII helices mixed with sharp bends, a motif referred to as "PPII helix-coil" (Bochicchio *et al.*, **2002**). In order to unambigously reveal PPII as the dominant solution conformer of a peptide, further spectroscopic studies including vibrational circular dichroism (vCD), Raman optical activity (ROA) and low-temperature CD, must be conducted. However, none of these techniques were in our hands, and only suppositions about the incidence of PPII in the ensemble of aqueous conformers of [(3*R*,6*R*,9*R*)-l^2aa analogue **4.19** could be made.

4.3.2 Biological activity

The anti-IL-1β activity of the indolizidin-2-one and proline analogues (**4.19**-**4.24**) was measured in human thymocyte proliferation and NF-κB and MAPK pathways activation (Figure 4.5), as described in previous chapters.

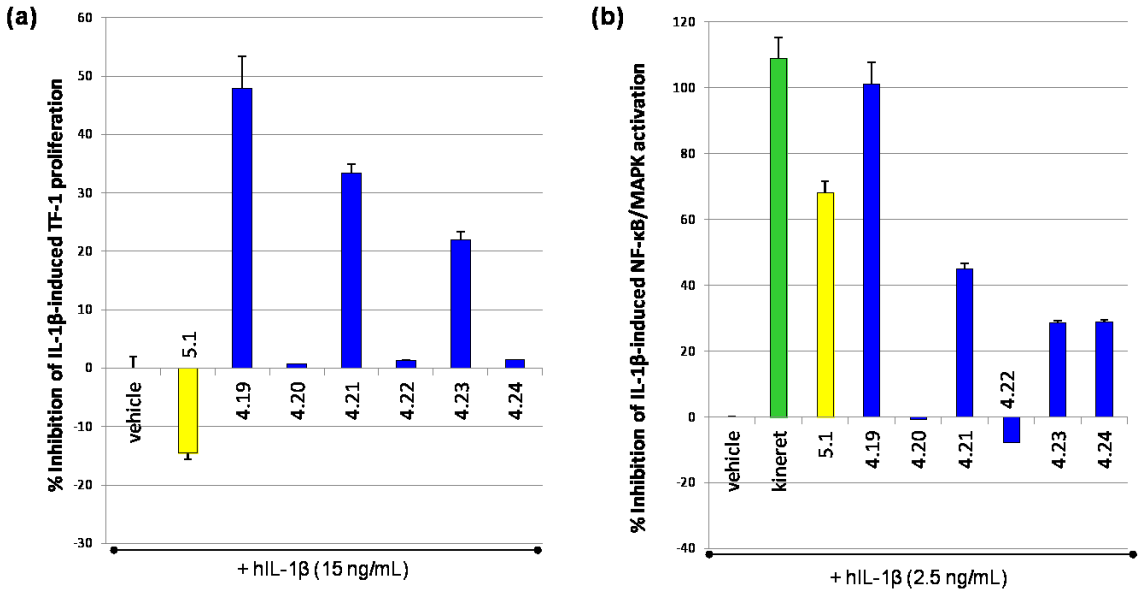

Figure 4.5. Inhibition of IL-1β-induced thymocyte proliferation (a) and NF-κB/MAPK activation (b) by I^{2}aa (**4.19**, **4.20**, **4.24**) and Pro^{4} analogues (**4.21**-**4.23**), as measured by fluodye intercalation and HEK Blue SEAP reporter gene assays, respectively.

The non-redundancy in anti-IL-1β activities of rytvela will be discussed in more details in chapter 5. The replacement of valine by D-proline (**4.21**) had a beneficial effect in the SEAP reporter gene test, regardless of the truncation of the *C*-terminal residue (**4.23**), exhibiting an average increase in 40% of IL-1β inhibition. On the contrary, employing L-proline produced a peptide (**4.22**) with approximately no observable influence on IL-1β effects. The (3*S*,6*S*,9*S*)-I^{2}aa mimetic **4.24** demonstrated no significant effect on immune cell proliferation, and a modest 29% reduction of NF-κB/MAPK pathway induction; results that were similar to its enantiomeric bicyclic analogue (**4.20**), which produced no significant change in both assays. Removal of the alanine yielded the most active analogue of this series, [(3*R*,6*R*,9*R*)-$I^{2}aa^{3,4}$, ΔAla^{7}]-101.10 (**4.19**), exhibiting 1.4- and 4-fold increase in anti-IL-1β actions compared to rytvela (**5.1**). Overall, the biological screening of these analogues suggested that the (*R*)-stereochemistry either for the proline or the bicycloalkane retained or improved anti-IL-1β activity compared to rytvela.

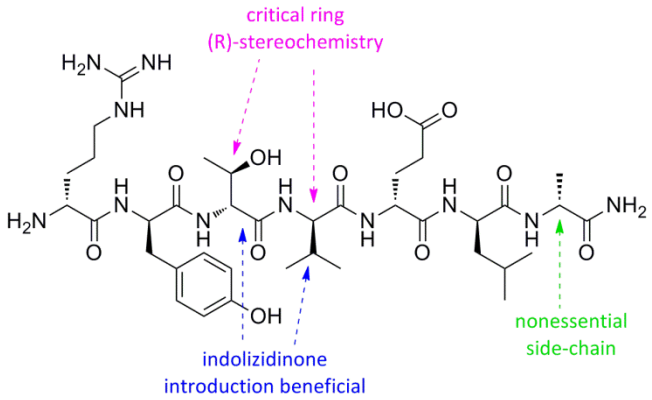

Figure 4.6. Structure-activity relationships regarding the $I^{2}aa^{3,4}$ and Pro^{4} analogues of 101.10.

4.4 Concluding remarks

Introducing a proline at the fourth position of 101.10 produced peptides (**4.21**-**4.23**) that demonstrated increasingly more intense CD curves characteristic of a type I β-turn, whereas introducing a I^2aa dipeptide at the third and fourth positions yielded analogues (**4.19**, **4.20**, **4.24**) revealing the increasing presence of polyproline-like folds, contingent on the stereochemistry. For example, using the (3*S*,6*S*,9*S*)-scaffold may push the amide bond towards the *cis*-conformation, which favour PPI helices (Moradi *et al.*, **2009**). On the contrary, both (3*R*,6*R*,9*R*)-bicycles elicited CD curves suggestive of PPII structures, which are typically formed by *trans*-amide isomers. Stereochemistry of the scaffolds turned out to be crucial on the bioactivity: for example, employing the D-proline or (3*R*,6*R*,9*R*)-azabicycloalkanone produced analogues (**4.19**, **4.22**, **4.24**) with higher anti-IL-1β *in vitro* activities than their L- and (3*S*,6*S*,9*S*)-counterparts (**4.22**, **4.24**). Truncating the alanine in the peptides resulted in more intense transition bands in the CD spectra and good to superior anti-IL-1β activities, relative to 101.10 and heptamers. Particularly, ry-(3*R*,6*R*,9*R*)-I^2aa-el (**4.19**) was the only mimetic of all series to demonstrate consistently high inhibition of both IL-1β-mediated effects.

The structure-activity relationships regarding the $I^2aa^{3,4}$ and Pro^4 analogues of 101.10 (Figure 4.6) correlate with the trends observed for the Thr^3-Val^4 and Hgl^3 mimetics (chapter 3). In all cases, the D- and (*R*)-configurations at the central 3- and 4-positions appear crucial to impart activity against IL-1β.

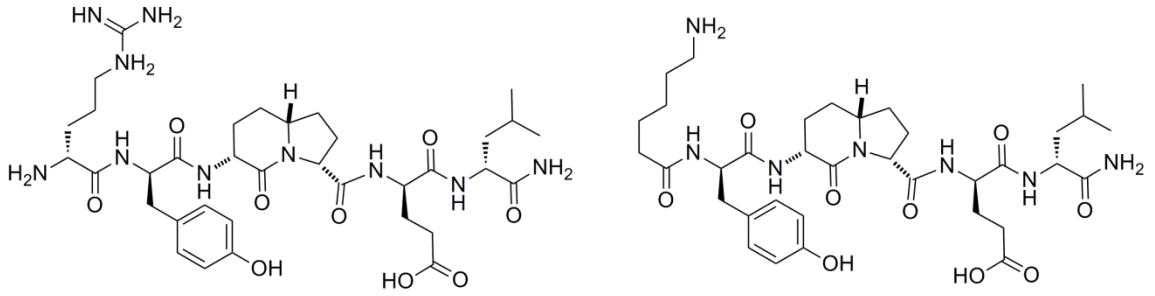

4.19
[(3*R*,6*R*,9*R*)-$I^2aa^{3,4}$, ΔAla^7]-101.10

4.25
[aminohexanoyl^1, (3*R*,6*R*,9*R*)-$I^2aa^{3,4}$, ΔAla^7]-101.10

Figure 4.7. New aminoalkanoyl derivative (**4.25**) of [(3*R*,6*R*,9*R*)-$I^2aa^{3,4}$, ΔAla^7]-101.10 (**4.19**) which displayed promising anti-IL-1β efficacy as well as physicochemical properties relative to rytvela.

Among all, [(3*R*,6*R*,9*R*)-$I^2aa^{3,4}$, ΔAla^7]-101.10 (**4.19**) emerged as a small, potent anti-IL-1β analogue of the parent peptide, from which a subsequent library of α- and β-amino-γ-lactams as well as aminoalkanoyl derivatives was synthesized, and interesting preliminary biological data were obtained. Moreover, further pharmacological characterization of these analogues compared to rytvela has been recently undertaken, including *in vitro* assessment of solubility, permeability and biostability, as well as *in silico* calculation of ADMET properties such as lipophilicity, ionizability and polar surface area. For example, the insertion of the indolizidin-2-one amino acid into the 101.10 sequence has improved the partition coefficient (C log P) from -3.0558 to -2.6836, and the Connolly solvent excluded volume (molecular surface) from 581.023 to 530.578 Å^3, as obtained via the chemical standard properties calculator of the GAMESS software. In addition, the *in vitro* permeability of [aminohexanoyl^1, (3*R*,6*R*,9*R*)-$I^2aa^{3,4}$, ΔAla^7]-101.10 (**4.25**; Figure 4.7) was 7- and 1.6-times higher than rytvela (**5.1**) at pH of 4.0 and 7.4, respectively, as measured in a parallel artificial membrane permeability assay (PAMPA). In light of these findings, the optimization of 101.10 employing (3*R*,6*R*,9*R*)-indolizidin-2-one as a rigid

surrogate has resulted into a small IL-1β antagonist that displayed improved *in vitro* efficacy, permeability, and chemophysical properties, as well as a CD curve typical of a poly-D-proline type II fold.

4.5 Experimental section

4.5.1 General

See experimental section of chapter 2.

4.5.2 Characterization and purification

Refer to experimental section of chapter 2.

4.5.3 Solution-phase synthesis of l^2aa dipeptide

Essentially, the solution-phase synthesis of the indolizidin-2-one scaffold was performed as previously described (Lombart *et al.*, **1996**), except for the hydrogenation step.

4.5.4 Hydrogenation chemistry

Flow-through hydrogenations were conducted in a H-Cube® continuous-flow hydrogenation reactor (Thales Nano, Budapest, Hungary) equipped with an autosampler, liquid handler, hydrogen generator, product collector and multi-chambers hydrogenation head. Upon mixing with a pressurized flow of hydrogen, sample solutions are pushed through a teflon-coated system toward a packed catalyst cartridge (CatCart®, Thales Nano, Budapest, Hungary), where heating and pressure can attain 100 bar and 100°C, respectively. Precisely, a solution of (2*R*,8*R*)-dimethyl-5-oxo-2,8-bis[*N*-(PhF)amino]azelate (7.6 mg, 0.016 mmol) in anhydrous THF (2.7 mL) and glacial AcOH (0.3 mL) was stirred for 10 min., filtered through a Chromspec 0.2 µm filter, and transferred into a 5-mL glass sample vial. The H-Cube® system was washed for 10 min. with the eluting solvent (10% AcOH in THF), after which the 10 wt% Pd/C cartridge (30 mm, CatCart®, Budapest, Hungary) was primed for 10 min. The azelate sample solution was injected at 0.3 mL/min., and subsequently eluted for 30 min. in the collection vials using the same flow rate, at a hydrogen pressure around 40 bar and 30°C. The combined collection solutions were dried *in vacuo* after which the residual solids were dissolved in MeOH (1 mL) and stirred for 24 h. The solvolysed product, (3*R*,6*R*,9*R*)-aminoindolizidinone methyl ester **4.17**, was evaporated to a residue that was directly used in the next reaction.

4.5.5 Synthesis of peptides by standard Fmoc-SPPS

See experimental section of chapter 2.

4.5.6 Ultraviolet-circular dichroism

Refer to experimental section of chapter 2.

4.5.7 Biological screening of analogues

See experimental section of chapters 2 and 3.

4.6 References

Ball, J. B.; Alewood, P. F. *J. Mol. Recogn.* **1990**, *3*, 55-64.

Beal, L. M.; Liu, B.; Chu, W.; Moeller, K. D. *Tetrahedron* **2000**, *56*, 10113-10125.

Bochicchio, B.; Pepe, A.; Tamburro, A. M. *Matrix Biol.* **2001**, *20*, 243-250.

Bochicchio, B.; Tamburro, A. M. *Chirality* **2002**, *14*, 782-792.

Boeglin, D.; Hamdam, F. F.; Melendez, R. E.; Cluzeau, J.; Laperrière, A.; Héroux, M.; Bouvier, M.; Lubell, W. D. *J. Med. Chem.* **2007**, *50,* 1401-1408.

Cluzeau, J.; Lubell, W. D. *Biopolymers* **2005**, *80* (2), 98-150.

Halab, L.; Gosselin, F.; Lubell, W. D. *Pep. Sci.* **2000**, *55*, 101-122.

Hanessian, S.; McNaughton-Smith, G. *Bioorg. Med. Chem. Lett.* **1996**, *6*, 1657-1662.

Hanessian, S.; McNaughton-Smith, G.; Lombart, H.-G.; Lubell, W. D. *Tetrahedron* **1997**, *53*, 12789-12854.

Hanessian, S.; Balaux, E.; Musil, D.; Olsson, L.-L.; Nilsson, I. *Bioorg. Med. Chem. Lett.* **2000**, *10*, 243-247.

Hanessian, S.; Sailes, H.; Munro, A.; Therrien, E. *J. Org.Chem.* **2003**, *68*, 7219-7233.

Kim, H.-O.; Kahn, M. *Tetrahedron Lett.* **1997**, *38*, 6483-6484.

Laakkonen, L.; Li, W.; Perlman, J. H.; Guarnieri, F.; Osman, R.; Moeller, K. D.; Gershengorn, M. C. *Mol. Pharm.* **1996**, *49*, 1092-1096.

Lee, H. J.; Choi, K. H.; Ahn, I. A.; Ro, S.; Jang, H. G.; Choi, Y. S.; Lee, K. B. *J. Mol. Struct.* **2001**, *569*, 43-54.

Lee, H. J.; Lee, M. H.; Choi, Y. S.; Park, H. M.; Lee, K. B. *J. Mol. Struct.* **2003**, *631*, 101-110.

Li, W.; Moeller, K. D. *J. Am. Chem. Soc.* **1996**, *118,* 10106-10112.

Lombart, H.-G.; Lubell, W. D. *J. Org. Chem.* **1996**, *61,* 9437-9446.

Lombart, H.-G.; Lubell, W. D. In *Peptides: Chemistry, Structure and Biology*; Kaumaya, P. T. P.; Hodges, R. S., Eds.; Escom: Leiden, The Netherlands, **1996b**, 695-696.

Lombart, H.-G.; Lubell, W. D. Thèse de doctorat, Université de Montréal, **1997**.

Mandal, P. K.; Kaluarachchi, K. K.; Ogrin, D.; Bott, S. G.; McMurray, J. S. *J. Org. Chem.* **2005**, *70* (24), 10128-10131.

McDonald, D. Q.; Still, W. C. *J. Org. Chem.* **1996**, *61*, 1385-1391.

Moradi, M.; Babin, V.; Roland, C.; Darden, T. A.; Sagui, C. *Proc. Nat. Acad. Sci. USA* **2009**, *106* (49), 20746-20751.

Mueller, R.; Revesz, L. *Tetrahedron Lett.* **1994**, *35* (24), 4091-4092.

Mulzer, J.; Schuelzchen, F.; Bats, J.-W. *Tetrahedron* **2000**, *56*, 4289-4298.

Nagai, U.; Sato, K. *Tetrahedron Lett.* **1985**, *26* (5), 647-650.

Nagai, U.; Sato, K.; Nakamura, R.; Kato, R. *Tetrahedron* **1993**, *49*, 3577-3592.

Polyak, F.; Lubell, W. D. *J. Org. Chem.* **1998**, *63*, 5937-5949.

Polyak, F.; Lubell, W. D. In *Peptides: Chemistry, Structure and Biology*; Fields, G.; Barany, G., Eds.; Escom: Leiden, The Netherlands, **2000**, 150-152.

Reynolds, C. H.; Hormann, R. E. *J. Am. Chem. Soc.* **1996**, *118*, 9395-9401.

Rose, G. D.; Gierasch, L. M.; Smith, J. D. *Adv. Protein Chem.* **1985**, *37*, 1-109.

Roy, S.; Lombart, H.-G.; Lubell, W.D.; Hancock, R.E.; Farmer, S.W. *J. Pept. Res.* **2002**, *60* (4), 198-214.

Takeuchi, Y.; Marshall, G. R. *J. Am. Chem. Soc.* **1998**, *120,* 5363-5372.

Thormann, M.; Hofmann, H. J. *J. Mol. Struct*. **1999**, *469*, 63-76.

Tiffany, M. L.; Krimm, S. *Biopolymers* **1968**, *6*, 1767-1770.

Uray, K.; Kajtar, J.; Vass, E.; Price, M. R.; Hollosi, M.; Hudecz, F. *Arch. Biochem. Biophys.* **2000**, *378* (1), 25-32.

Wang, W.; Xiong, C.; Hruby, V. J. *Tetrahedron Lett.* **2001**, *42* (18), 3159-3161.

CHAPTER 5

Salts, Contaminants and Retro-Enantio Analogues

5.1 Introduction

Ionizable molecules dissociate into two or more ions in solution. Typically, the simpler ion of a metal complex or a charged amino acid is designated as the counter-ion. In principle, every acid or base can partake in salt formation, including pharmaceuticals such as peptides and proteins. Emerging evidence has demonstrated that a drug's counter-ion is an important facet of the pharmaceutical (Berge *et al.*, **1977**; Stahl *et al.*, **2002**; Kunz, **2010**), and may be tuned to impart desired chemical, biological and physical characteristics to the drug. Even in a medium of high dielectric constant, counter-ions may modulate drug efficacy, receptor engagement, cell or nuclear penetration, and changes in protein conformation, contingent on the specific type of ion used. Various salts produced from the same drug rarely diverge pharmacologically; however, their physicochemical properties may be influenced, including dissolution rate, solubility, permeability, stability and hygroscopicity (Berge *et al.*, **1977**; Stahl *et al.*, **2002**).

The counter-ion has been proposed to assist in the passive transport of drugs. For example, a hydrophobic counter-ion, such as trifluoroacetate or hexafluorophosphate, may help overcome the energy barriers required to insert into the internal lipophilic phase of the phospholipid bilayer membrane (Esbjorner *et al.*, **2007**). Changes in counter-ion may similarly affect the ampiphilicity of a drug with pH, and facilitate passage in the gastrointestinal (GI) tract upon oral absorption (Baciu *et al.*, **2006**). Studies on the octanol/water partitioning of charged species, including zwitterions and ordinary ampholytes, have demonstrated that ionic molecules must be accompanied by their ion-pair to enter a lipid phase such as octanol (Adjei *et al.*, **1993**). Counter-ion may thus effect drug partitioning, as observed in lipophilicity profiles (log D versus pH graph). For example, the log D of the dipeptide L-Trp-L-Phe was systematically higher in a 1.0 M KCl solution than in pure aqueous solution, and switching for a 1.0 M $NaClO_4$ solution reduced significantly the log D compared to the KCl electrolyte, yet maintained a value better than the aqueous level (Avdeef, **2001**).

Different salts may improve stability of a parent compound by a variety of mechanisms (Kunz, **2010**). For example, sparingly soluble salts may be used in the formulation to reduce the dissolution of a drug in solution, and thereby avoid degradation in the medium. For example, penicillin G (BenPen), a broadly used antibiotic, displays characteristic solution instability; however, degradation was minimized by respectively employing procaine, benzathine, and hydrabamine as counter-cation (Schwartz *et al.*, **1960**). Counter-ions may also affect the dissolution rate of a drug by shifting the dissolution equilibrium of the solute. Salts will usually speed dissolution by acting as their own buffers to alter the pH of the inner diffusion layer, which contributes to increase the solubility of the parent compound. For ions typically encountered in physiological systems (Cl^-, K^+, Na^+), the common ion effect may, however, hamper dissolution of the salt, due to the pre-existing abundance of the ion in the medium (Shozo *et al.*, **1980**). In general, salts possess greater absorption and higher oral exposure than their free acid/base counterparts, and their usage in drug formulation has been beneficial for a large array of drugs (Kerns *et al.*, **2008**).

Different types of ions may affect distinctly the solubility and stability of secondary and tertiary structures of proteins (Horowicz, **1964**). The order of extent of these effects correlates with the original Hofmeister series (Hofmeister, **1890**; Collins *et al.*, **1985**), which ranked ions according to their ion-pairing effectiveness (also referred to as their "salting in" capacity). Accordingly, fluorine and sulfate detain the weakest ion-pairing capability; phosphate, formate and acetate exhibit medium ion-pairing capability; and larger halides, trifluoroacetate, chlorate and perchlorate show the strongest ion-pairing effectiveness (Kunz, **2010**).

Only some anions and cations are pharmaceutically acceptable (FDA-approved) for employment in drug formulation, because of their physicochemical properties. The most common counter-anions occurring in the Cambridge Structural Database (Haynes *et al.*, **2005**) are chloride (45.5%), bromide (21.2%), nitrate (4.4%), sulfate (dianionic; 2.4%), tosylate (1.8%), phosphate (monoanionic; 1.5%), L-tartrate (monoanionic; 1.3%), maleate (1.1%) and acetate (Figure 5.1).

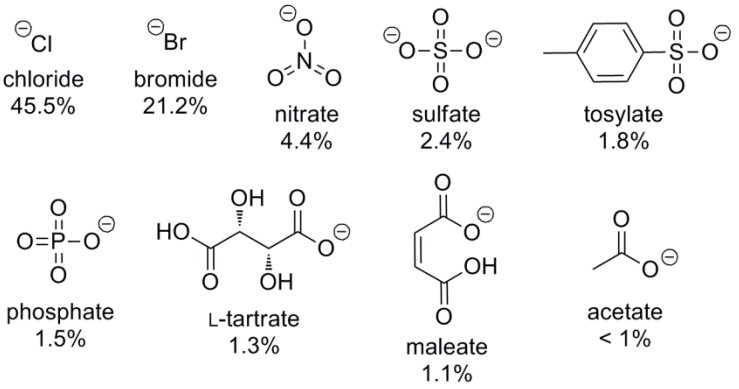

Figure 5.1. Most common counter-anions occurring in the Cambridge Structural Database (Haynes *et al.*, **2005**).

In the context of 101.10, counter-ion effects may influence the properties of the cationic peptide. Although accurate determination of the ionic state of 101.10 at a physiologically relevant pH may be accomplished by measurement of the isoelectric point of the peptide via potentiometric titration, significant amounts of material would be required. Alternatively, the ionization state of 101.10 at a pH of 4 (0.1% FA in H_2O) may be ascertained by examination of the MS data, in which the bicationic specie (charged arginine and amino-termini, uncharged glutamate) accounted for 60% of the *m/z* signal compared to 40% for the monocation. At least one anion may thus be presumed to associate with 101.10 in solution. Concern for the counter-ion of 101.10 was raised after diverging biological activities were obtained from different synthetic sources of the peptide, for which HPLC-MS analyses of different samples revealed differences in purity depending on the source. For example, a sample of 101.10 purchased from Elim Biopharmaceuticals (**5.9**, Table 5.3), was shown by HPLC-MS analysis to contain 61% of rytvela, 24% of ytvela, and 15% of rytvelaa, all as their respective trifluoroacetate salts (data not shown). In the synthesis of peptides, the chiral amino acid building blocks may contain appreciable quantities of its enantiomer, such that impure samples of peptides may also contain inseparable diastereoisomers, which elute at similar retention times.

In order to decipher the active pharmaceutical ingredient and optimal counter-ion, pure rytvela was synthesized following Good Manufacturing Practices (GMP) for peptide synthesis, and transformed into three different salts: formate (FA), acetate (OAc) and trifluoroacetate (TFA). Furthermore, the main synthetic impurities were synthesized and purified using standard solid-phase peptide synthesis procedures. In addition, the retro, enantio, and retro-enantio isomers of 101.10 were prepared to probe the residue configuration and backbone direction requirements to impart bioactivity (see section 1.4.2.1).

5.2 Synthesis, ion-exchange and CZE analysis of analogues

5.2.1 GMP synthesis of rytvela

The optical purity of the Fmoc-amino acid building blocks was initially assessed by examining specific rotations at 589 nm, which correlated with their theoretical values. The initial loading of the resin was determined in two parallel assays (employing DBU and piperidine), which yielded similar values. Completion of the coupling of the first amino acid was also measured by the two same assays. Although the measured value differed slightly from that expected, chain elongation was initiated. Considering a manufacturing scale of rytvela, the synthesis was targeted on 0.3 mmol, employing ecofriendly solvents, such as *iso*-propanol and di-*iso*-propylether, instead of their shorter alkyl counterparts. After each deprotection and coupling step, a Kaiser test was performed. In the middle of the sequence, a small quantity of resin was cleaved and analyzed by HPLC-MS to ascertain the sample quality.

Relative to standard SPPS procedures, reduced equivalents of di-*iso*-propylethylamine (DIEA) were used during coupling steps to reduce the occurrence of *in situ* Fmoc-deprotection by the base, and double coupling of amino acid. The double coupling problem was observed in the sample from Elim Biopharmaceuticals, in which the D-octapeptide rytvelaa was detected. In the synthesis of rytvela on an automatic peptide synthesizer using typical amounts of base, some double coupling of alanine was also observed. The large presence of the truncated D-hexapeptide ytvela in the chromatogram of 101.10 obtained from commercial and internal sources indicated that the last amino acid, Fmoc-D-Arg(Pbf)-OH, was difficult to couple. In our hands, this coupling required the resin to be submitted to a second reaction with freshly made solutions, for a longer period of time.

The crude purity of this rytvela was calculated as 85% using HPLC-MS with UV detection at 280 nm (**5.1**; Table 5.1), contaminated with 5% of truncated peptide, ytvela (**5.2**). The crude yield was approximated at 94%. A more profound characterization of the impurities contained in the crude sample of 101.10 was made by HPLC-MS (Table 5.2) using an optimized stepwise elution gradient. In total, 35.4 mg of more than 99% pure and 39.7 mg of 95 to 98.9% pure rytvela (**5.1.1**) were synthesized. Noteworthy, these two rytvela samples possessed a crystalline solid state rather than the usual amorphous fluffy solids observed for the Elim (**5.9**) and crude 101.10 samples (**5.10**).

Entry	Peptide	Crude purity %[a]	Purity %[a]	Yield %[b]	HRMS[c]	
					m/z (calcd)	***m/z*** (obsd)
5.1	D-Arg-D-Tyr-D-Thr-D-Val-D-Glu-D-Leu-D-Ala-NH_2	85	> 99	17.4	850.4781	850.4747
5.2	D-Tyr-D-Thr-D-Val-D-Glu-D-Leu-D-Ala-NH_2	85	92	9.7	694.3770	694.3784
5.3	D-Tyr-D-Thr-D-Val-D-Glu-D-Leu-D-Ala-D-Ala-NH_2	N/A	99	N/A	765.4141	765.4149
5.4	D-Arg-D-Tyr-D-Thr-D-Val-D-Glu-D-Leu-D-Ala-D-Ala-NH_2	70	95	14.2	921.5152	921.5171
5.5	D-Arg-D-Tyr-D-Thr-D-Val-D-Glu-D-Leu-NH_2	85	95	6.5	779.4410	779.4430
5.6	L-Arg-L-Tyr-L-Thr-L-Val-L-Glu-L-Leu-L-Ala-NH_2	71	94	11.8	850.4781	850.4778
5.7	D-Ala-D-Leu-D-Glu-D-Val-D-Thr-D-Tyr-D-Arg-NH_2	74	95	11.3	850.4781	850.4753
5.8	L-Ala-L-Leu-L-Glu-L-Val-L-Thr-L-Tyr-L-Arg-NH_2	88	93	12.8	850.4781	850.4756

Table 5.1. Yields and purities of GMP rytvela, Ret analogues and co-synthesized contaminating peptides. [a] RP-HPLC purity at 280 nm. [b] Yields after purification by RP-HPLC are based on Fmoc loading test for Rink resin. [c] HRMS values from the major protonated molecule, typically $[M+H]^+$.

Peak	t_R (min.)[a]	Fraction	A_{214} (a.u.)[b]	Specie[c]
1	2.50	1-2	-0.11	injection peak
2	5.70	4-5	+0.28	unidentified
3	11.00	10-12	+0.07	unidentified
4	13.25	14-16	+2.00	rytvela
5	17.70	19	+0.18	ytvela
6	23.65	25	+0.50	unidentified

Table 5.2. RP-HPLC profile of the crude GMP sample of rytvela on a Synergi® RP-Polar column (80 Å, 4 µm, 150 mmx 21.2 mm I.D.). Eluting conditions employed were a flow rate of 10.6 mL/min. and a linear gradient composed as: 0-5 min. at 5% B; 5-20 min. from 5% to 20% B; 20-25 min. at 20% B; then washing and reconditioning (solvent A: H_2O + 0.1% FA; solvent B: MeCN + 0.1% FA). [a] Retention times of each peak. [b] Maximum peak absorbance at 214 nm. [c] Protonated specie identified by ESI-MS.

Entry	Peptide[a]	Counter-ion
5.1.1	D-Arg-D-Tyr-D-Thr-D-Val-D-Glu-D-Leu-D-Ala-NH_2	FA
5.1.2	D-Arg-D-Tyr-D-Thr-D-Val-D-Glu-D-Leu-D-Ala-NH_2	TFA
5.1.3	D-Arg-D-Tyr-D-Thr-D-Val-D-Glu-D-Leu-D-Ala-NH_2	OAc
5.2.1	D-Tyr-D-Thr-D-Val-D-Glu-D-Leu-D-Ala-NH_2	FA
5.2.2	D-Tyr-D-Thr-D-Val-D-Glu-D-Leu-D-Ala-NH_2	TFA
5.3	D-Tyr-D-Thr-D-Val-D-Glu-D-Leu-D-Ala-D-Ala-NH_2	TFA
5.4	D-Arg-D-Tyr-D-Thr-D-Val-D-Glu-D-Leu-D-Ala-D-Ala-NH_2	TFA
5.5	D-Arg-D-Tyr-D-Thr-D-Val-D-Glu-D-Leu-NH_2	FA
5.6	L-Arg-L-Tyr-L-Thr-L-Val-L-Glu-L-Leu-L-Ala-NH_2	FA
5.7	D-Ala-D-Leu-D-Glu-D-Val-D-Thr-D-Tyr-D-Arg-NH_2	FA
5.8	L-Ala-L-Leu-L-Glu-L-Val-L-Thr-L-Tyr-L-Arg-NH_2	FA
5.9	101.10 from ELIM Biopharmaceuticals	TFA
5.10	crude 101.10 from our GMP synthesis	TFA

Table 5.3. Salts of different purified analogues and of various sources of 101.10.

5.2.2 Ion-exchange of rytvela

After purification on a preparative Synergi® RP-Polar column using eluting solvents containing 0.1% formic acid, the counter-anion of rytvela (**5.1.1**) was assumed to be formate. To exchange formate to trifluoroacetate (stronger ion-pairing agent) or acetate (weaker ion-pairing agent; Dai *et al.*, **2005**), two solid-phase extraction methods were examined: ion-exchange and reverse-phase chromatography (Roux *et al.*, **2008**). The first method called **m**ixed-mode **c**ation e**x**change (MCX), relies on interactions between cations contained in the mobile phase and benzenesulfonate anion bound to a polystyrene (PS)/divinylbenzene (DVB) stationary phase. The peptide salt was loaded onto the resin, washed with neutral pH water to elute off any formate attached, and was eluted with the ammonium salt of the desired counter-ion: ammonium trifluoroacetate or

acetate. The eluated peptide bound to trifluoroacetate/acetate was then lyophilized. In practice, elution of rytvela on the MCX resin required, however, an excess of ammonium salt which could not be evaporated with the eluate, resulting in issues of isolating the desired peptide salt. In principle, this may be addressed by dialysis; instead, the reverse-phase chromatography method was explored.

This latter alternative method was performed on a C18 reverse-phase resin, which relies on the principle that relatively hydrophobic peptides stay bound to the stationary phase when the counter-ion is eluted with near 100% aqueous mobile phase. Increasing the amount of organic solvent in the mobile phase containing a strong acid of the desired counter-ion (i.e. trifluoroacetic acid or acetic acid) elutes the peptide bound to the new counter-anion. The correct peptide salt is then isolated by freeze-drying. The C18 reverse-phase resin ion-exchange method proved more efficient with rytvela, due to the use of voltatile acids instead of salts, as well as the relative strength of interactions between the C18 phase and the peptide compared to the electrostatic interactions between the MCX anion and the peptide cation.

Both methods comprised technical limitations, such as the loading capacity of the cartridge limiting the experimental scale, and the recovery of the desired salt precluded by the loss of some peptide bound tightly to the sorbent and/or eluted in the washing step. An alternative approache would be to purify the crude peptide on the preparative Synergi® RP-Polar column and use eluting solvents containing 0.1% TFA or AcOH, or using the same column to exchange the formate salt. However, these methods are not without inconveniences such as the use of a large quantity of solvent and material loss on the column.

5.2.3 Capillary electrophoresis analysis of the relative amount of counter-anions

Capillary zone electrophoresis (CZE) is a technique introduced in the 1960s to separate species based on their charge, frictional forces and hydrodynamic radius in the interior of a small capillary filled with an eletrolyte (Terabe *et al.*, **1984**). The resolution of ionic compounds by capillary electrophoresis will depend on the differential migration of analytes, called electrophoretic migration velocity (u_p), in an applied electric field. In the capillary bounded by two electrodes, the analyte is attracted toward the electrode of the opposite charge, at the same time as it is pulled by the electroosmotic flow (EOF). The balance of these forces determines the resolution between different species.

To separate peptides and proteins, capillary electrophoresis has emerged as a high-resolution technique (Messana *et al.*, **1997**; Kasicka, **2001**), complementary to HPLC, because both techniques rely on different physicochemical properties. Capillary electrophoresis coupled to indirect UV-absorption detection has become an efficient and reliable method for the quantitation of small anions. In this indirect detection method, UV-absorbing co-ions are added in the electrophoretic buffer to provide background UV signal during elution of the UV-inactive anion, resulting in a negative absorbance peak. For example, sodium phthalate has been used as the UV-absorbing background electrolyte and cetyltrimethylammonium bromide (CTAB) as the EOF modifier for distinguishing peptide acetates from trifluoroacetates (Sazelova *et al.*, **2006**).

The relative amounts of the three counter-ions in different samples of rytvela (**5.1.1**-**5.1.3**) were thus measured using a published indirect-UV detection CZE method for the quantification of trifluoroacetate (Little **2007**) and of acetate (Altria *et al.*, **1997**). Calibration curves for each anion were first constructed with concentrations ranging from 0.05 to 10 mM, using sodium trifluoroacetate, ammonium acetate and ammonium

formate as the corresponding salts. Representative examples of electropherograms were obtained for each salt (**5.1.1**-**5.1.3**; Figure 5.2). The CZE calibration results were conducted in triplicates, and characteristics such as elution time, area under the curve (AUC), and peak shape were reproduced with high precision. Formate exhibited the highest electrophoretic velocity, due to its small radius, large charge to mass ratio and strong limiting ionic conductivity (λ_0, 69.3 $S \cdot cm^2 \cdot mol^{-1}$; Cummings *et al.*, **2009**), whereas acetate showed the slowest migration, possibly due to its weaker negative charge and limiting ionic conductivity (40.9 $S \cdot cm^2 \cdot mol^{-1}$; Cummings *et al.*, **2009**). The median velocity of trifluoroacetate may be explained by its averaged higher limiting ionic conductivity (approximated between 26.37 and 72.65 $S \cdot cm^2 \cdot mol^{-1}$ by several methods; Miyauchi *et al.*, **1992**) and stronger negative charge relative to acetate. These results demonstrated the reliability and the quality of resolution of the different anions, promoting the use of this method for quantifying the relative amount of each anion in different salts of the D-heptapeptide rytvela, as prepared above.

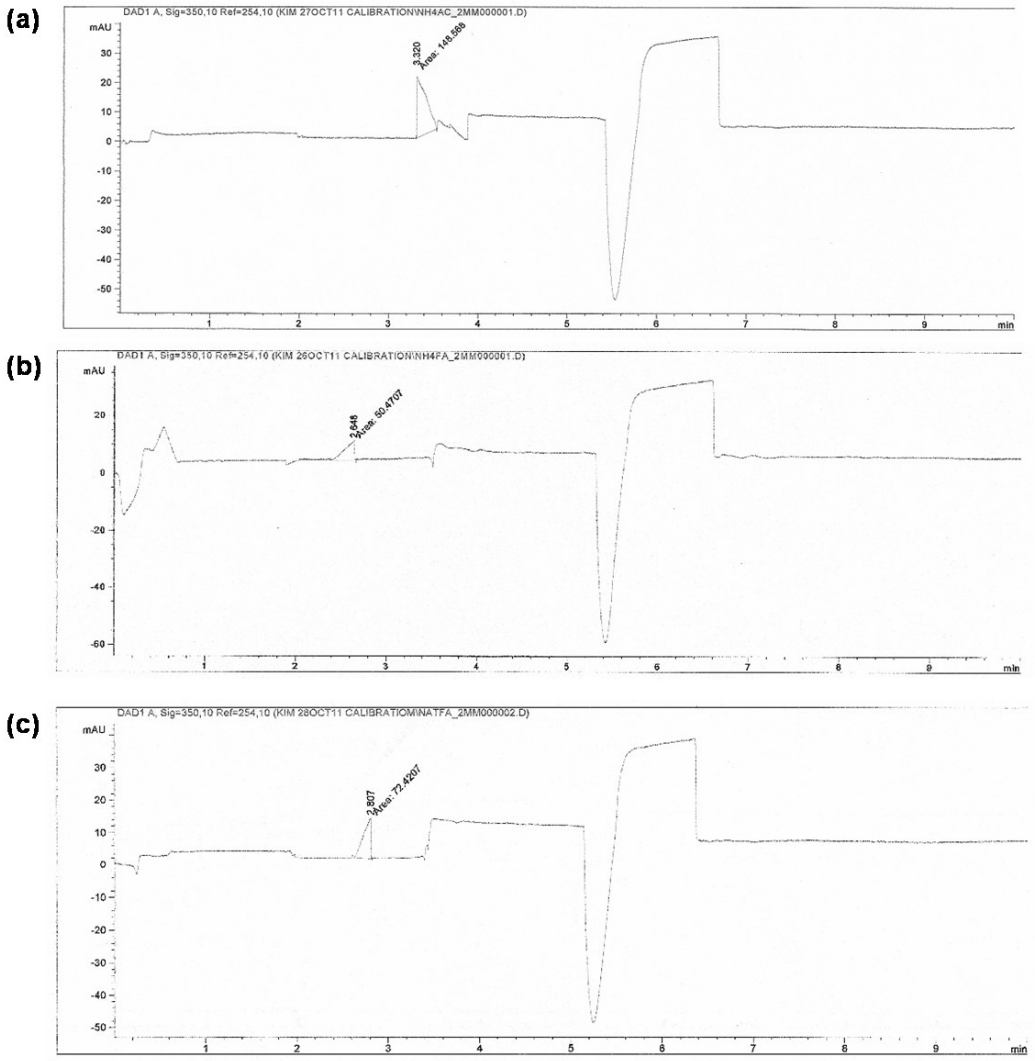

Figure 5.2. Representative CZE electropherograms of 2.0 mM solutions of NH_4OAc (a), NH_4FA (b), and NaTFA (c), recorded with a BGE composed of 5 mM KHP, 50 mM MES, and 0.5 mM TTAB.

Although the exact ratio of counter-ion over peptide could not be determined and the electrophoretic mobility of the counter-ions slightly changed due to ion-pairing effect of the peptide, the CZE electropherograms

of the three salts of rytvela (Figure 5.3) reproducibly provided relative purity of the salt form. The presence of about 5% of formate and 15% of unidentified species was found in the acetate salt. Only trifluoroacetate was detected in the TFA salt sample. Around 10% of trifluoroacetate was noticed in the formate sample. As quantified, the samples were used to examine the influence of counter-ion on the bioactivity and conformation of rytvela.

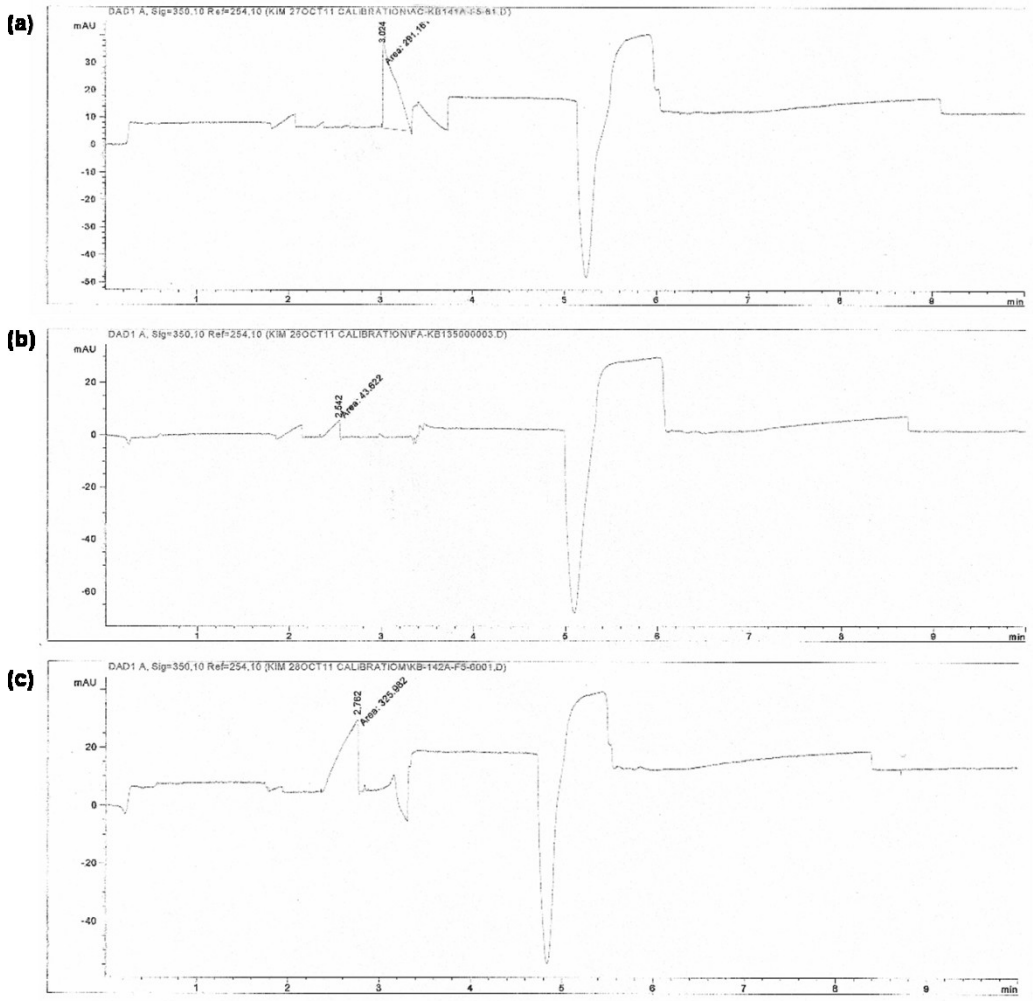

Figure 5.3. CZE electropherograms of different rytvela salt samples (acetate (a), formate (b), and trifluoroacetate (c)), recorded with a BGE composed of 5 mM KHP, 50 mM MES, and 0.5 mM TTAB.

5.3 Conformation and biological activity of analogues

5.3.1 Aggregation and solvent effects

Indications of aggregation at high concentration were obtained in the course of the synthesis of rytvela, when efforts were unsuccessful in dissolving the bulk of crude peptide after precipitation with ether. Aggregates may form in proteins or peptides by non-native intermolecular hydrophobic interactions, between unburied hydrophobic amino acid stretches. Aggregation, contrarily to folding, is a second or higher-order process, which is favoured at higher concentration. Constituted of hydrophobic amino acids (Tyr, Thr, Val, Leu, Ala), rytvela may

aggregate prior to folding or interaction with surrounding molecules at high concentrations. The extent of aggregation was determined by measuring the far-UV-CD curve of rytvela at aqueous concentrations ranging from 1 to 100 µM (Figure 5.4a). In addition, the structure-inducing solvent trifluoroethanol (TFE) (Sonnichsen *et al.*, **1992**) was employed to study the extent of rytvela folding in an alternative environment (Figure 5.4b). The CD curves of the present study were compared to electronic transition band values and backbone torsion angles of ideal secondary structures (Table 5.4).

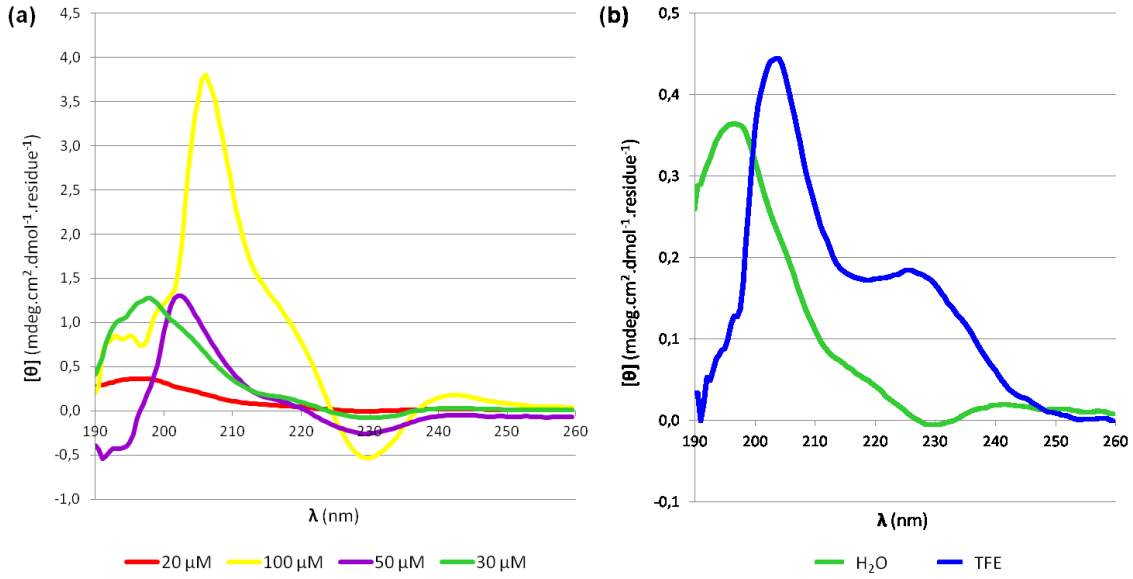

Figure 5.4. CD curves of rytvela formate salt (**5.1.1**) at different aqueous concentrations (a) and in different solvents at a concentration of 20 µM (b).

Secondary structure	**Transition bands** (nm)			**Dihedral angles** (°)			
	$\pi_0 \rightarrow \pi^*$	$\pi_1 \rightarrow \pi^*$	$n \rightarrow \pi^*$	ϕ_{i+1}	ψ_{i+1}	ϕ_{i+2}	ψ_{i+2}
random coil	- 195	-	+ 215-230	-	-	-	-
PPII helix	- 205	-	+ 228	- 75	145	-	-
Type I' β-turn	- 190	+ 202	+ 220	60	30	90	0

Table 5.4. Electronic transition bands and backbone dihedral angles of random coil and ideal left-handed PPII helix (Adzubei *et al.*, **1993**; Hutchinson *et al.*, **1994**; Rucker *et al.*, **2002**).

In spite of the intensity differences, the curve shapes at concentrations of 20 and 30 µM displayed the same maxima at 198 nm and a negative shoulder at 230 nm, suggesting that rytvela adopted disordered structure at those concentrations. At 50 and 100 µM, the positive maximum shifted from 198 to 202 and to 205 nm, respectively. Moreover, at these higher concentrations, a negative maximum at 230 nm and a positive shoulder at 220 nm were observed, suggesting a PPII helical conformation. The changes in curve shape and increase in ellipticity at 50 and 100 µM may thus be due to aggregation of the peptide in solution (Sahin *et al.*, **2011**). This hypothesis was supported by the predicted aggregation propensity of rytvela, which was performed using the widespread software AGGRESCAN (Sánchez *et al.*, **2005**; Conchillo-Sole *et al.*, **2007**) and Tango (Fernandez-Escamilla *et al.*, **2004**). In a first instance, the computational analysis from AGGRESCAN identified

the portion Thr-Val-Glu-Leu as the aggregation hot spot in 101.10, and estimated the aggregation potential at 12% (data not shown). The Tango algorithm has predicted that the cross-β aggregation tendency of the sequence rytvela, in conditions ressembling that of the recording of the CD spectrum (pH = 7.0, T = 298.15 K, I (ionic strength) = 0 M), was 64.96.

Raman and IR spectroscopy could provide additional information about aggregation of the peptide (Barth *et al.*, **2007**) by probing the amide I vibrational bands; however, due to overlap of this band with that of water and to the clustering of various substrucures absorption bands in the spectral region of 1620-1680 cm^{-1}, only qualitative information can be collected from such studies (Byler *et al.*, **1986**). Alternatively, ^{1}H-NMR methods, which compares the differences in chemical shifts of the amino protons at different concentrations, have been used, but necessitate significant amount of material. Nuclear Overhauser effect spectroscopy (NOESY) experiments have equally been employed to study aggregation by surveying the change in secondary structures adopted by peptides in organic solvents; however, such NMR technique may be complicated because of the existence of in-solution conformational averaging (Jardetzky, **1980**) and the need to use a model structure to resolve the diagnostic NOE crosspeaks (Blanco *et al.*, **1993**). Nonetheless, issues regarding the insufficient quantities available to do the spectroscopic studies, the dryness of the peptide and the lack of model molecules precluded the prompt use of Raman, IR, or NMR techniques to examine more deeply the aggregation of rytvela.

The CD spectra of rytvela in water and trifluoroethanol are distinct (Figure 5.4b): the former suggests a disordered structure, whereas the later indicates a turn motif, with two positive maxima at 202 and 225 nm (Table 5.4). TFE is considered to exhibit helix- and turn-stabilizing effects by a general solvation effect and by destabilization of the coil state, due to less effective hydrogen bonding with the peptide amide bonds. Consequently, in TFE, rytvela may solvate better, and adopt different low-energy conformation. The change in conformation in a more lipophilic solvent may also reflect what may happen to the peptide in a biological environment.

5.3.2 Conformational analysis

Although salts have been shown to affect the free energy and conformation of peptides (Nandi *et al.*, **1972**), the CD curves did not differ significantly for the different salt forms of rytvela (**5.1.1**-**5.1.3**; data not shown), suggesting that the counter-anion had no detectable effect on the conformation of the peptide in a 20 µM solution. Studies have demonstrated that counter-ions may induce greater conformation stabilization effects at higher concentrations (Dempsey *et al.*, **2011**); however, such influence of concentration could not be tested on rytvela due to insufficient quantity of the TFA and acetate salts (**5.1.2** and **5.1.3**, respectively).

Far-UV-CD spectroscopy was used to compare the different aqueous conformations of rytvela analogues (**5.1**-**5.8**; Figure 5.5). The CD spectra of all the analogues relating to contaminating entities of crude 101.10 (**5.2**-**5.5**; Figure 5.5a) all closely ressemble that of rytvela, indicating that addition of a *C*-terminal alanine, removal of the arginine and alanine residues, respectively, had no profound effect on conformation. Divergent bioactivity of such analogues would thus not be due to the difference in aqueous conformations. The CD spectra of the enantiomer RYTVELA (**5.6**), and the retro-enantio analogue ALEVTYR (**5.8**), both exhibited curves of opposite ellipticity and equal magnitude as rytvela (**5.1.1**) and the retromer alevtyr (**5.7**).

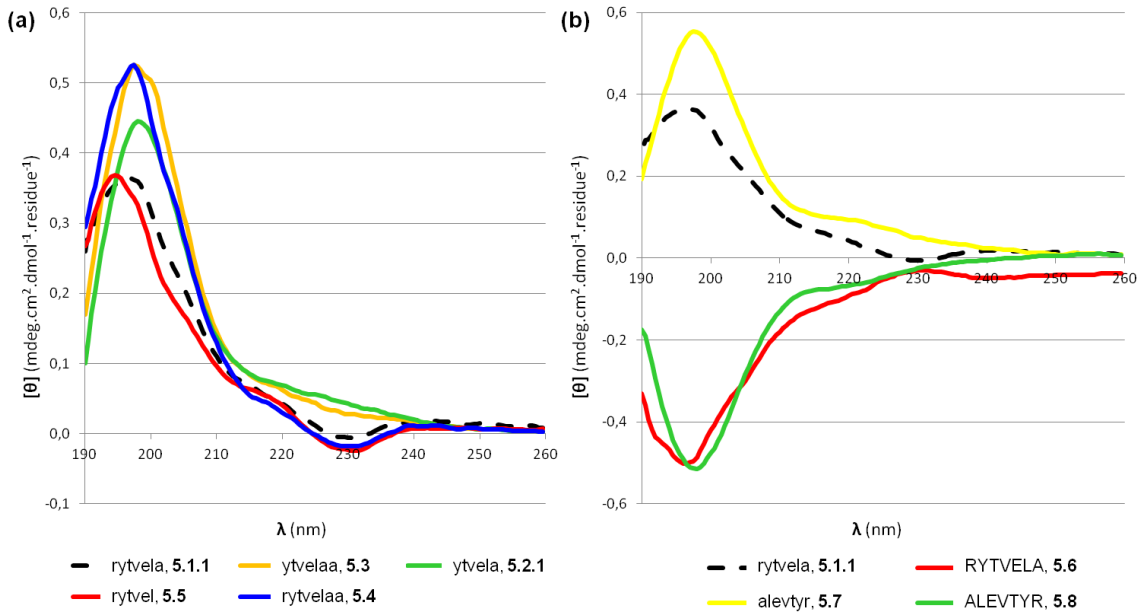

Figure 5.5. CD spectra of rytvela (**5.1.1**), co-synthesized contaminating peptides (**5.2**-**5.5**; a) and retro-enantio analogues (**5.6**-**5.8**; b).

5.3.3 Biological activity

Biological activity of the different rytvela salts and analogues (**5.1**-**5.8**) was determined using the HEK Blue reporter gene and fluodye intercalation assays, measuring the inhibition of IL-1β-induced NF-κB/MAPK activation and thymocytes proliferation, respectively (Figure 5.6). In these assays, kineret, the competitive IL-1R antagonist, blocked completely the induction of NF-κB/MAPK pathways by both exogenous and endogenous IL-1β, and reduced stimulated proliferation by about two thirds. In both assays, the formate (**5.1.1**) and trifluoroacetate (**5.1.2**) forms of rytvela exhibited comparable, relatively poor inhibitory activity, which was later corroborated by *in vivo* studies in which both salts failed to significantly diminish the IL-1β-induced hyperthermia in rats (data not shown) *. On the contrary, the 101.10 sample originating from Elim Biopharmaceuticals (**5.9**) displayed one of the strongest IL-1β blockades of proliferation and pathway induction, albeit with a large SEM that may originate from inhomogeneity of the material. A similar strong effect was reproduced in the NF-κB/MAPK test using a crude sample of rytvela (**5.10**) synthesized in our laboratories. The trifluoroacetate salts of ytvela, ytvelaa and rytvela (**5.2.2**, **5.3**-**5.4**), the three most common contaminating peptides found in crude rytvela, all demonstrated relatively high levels of IL-1β inhibition. Truncating rytvela at its *N*-terminus produced an hexapeptide (**5.2**) that displayed improved activity for both salts in the HEK Blue assay, and for the TFA salt **5.2.2** in the CyQUANT test, compared to rytvela. Removing the *C*-terminal residue (**5.5**) had a profound influence on the anti-inflammatory effect of the peptide, where it lost 80% of its inhibitory efficacy. However, the same deletion had only a modest effect (loss of 23% activity relative to **5.1.1**) in thymocyte proliferation, as previously reported for this analogue (Chemtob *et al.*, **2005**). These results underline the relative importance of both terminal residues (D-Arg^{1} and D-Ala^{7}) to impart the desired bioactivities.

* These *in vivo* IL-1β-induced hyperthermia experiments were performed by Dr. Xin Hou, according to procedures described in the literature (Quiniou *et al.*, **2008**).

Interleukin-33 (IL-33), a related IL-1 family member, shares the same accessory protein (IL-1RAcP) as IL-1, and binds to a receptor, termed IL-1 receptor-like 1 (IL-1RL1, or ST2), that possesses considerable resemblances to IL-1R. The HEK Blue cells used in the reporter gene assay also express the IL-1RL1 at their surface, such that using exogenous amounts of IL-33 to trigger the NF-κB/MAPK cascade in peptide-treated HEK Blue cells, the IL-1/IL-33 selectivity of rytvela and analogues may be tested. For most analogues (data not shown), no influence on the IL-33 stimulation was detected, except for all TFA salts (**5.1.2**, **5.2.2**, **5.3** and **5.4**) that induced an average of 7-10% inhibition of the IL-33 effect compared to kineret and rytvela formate (no effect). Thus, this inhibition of trifluoroacetate on IL-33-mediated activation of inflammatory cascades may account for the differences observed between various salts in the IL-1β-dependent assay. In other words, it may be hypothesized that trifluoroacetates are less specific than their formate counterparts; but a deeper examination of the pharmacological profiles of ytvela, ytvelaa and rytvelaa (**5.2**-**5.4**) is in order to itemize their specificity and efficacy and that of their various salts.

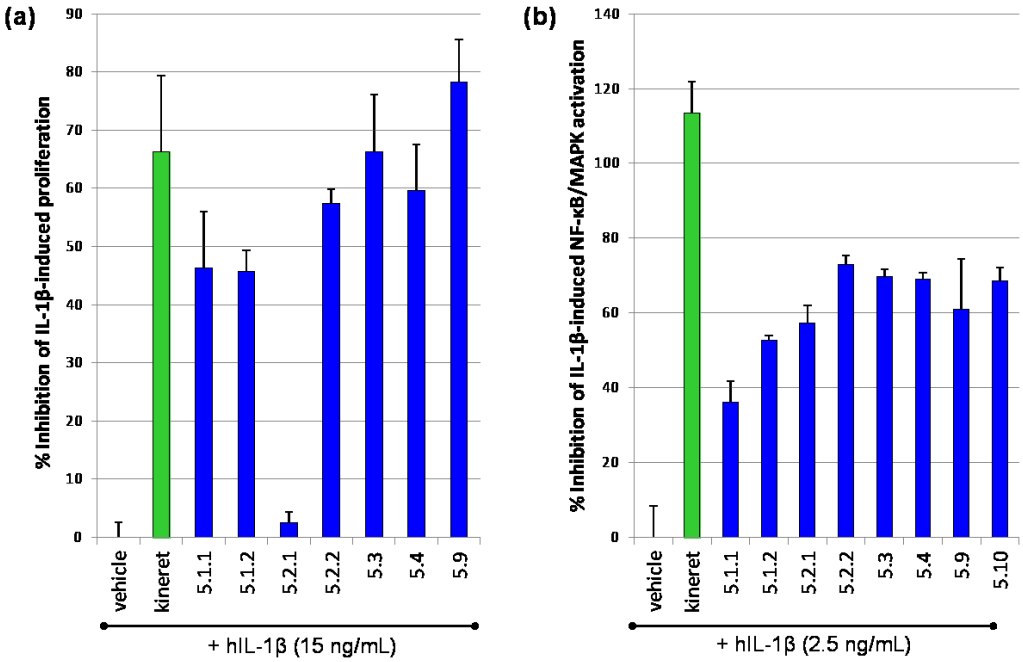

Figure 5.6. Inhibition of IL-1β-induced thymocyte proliferation (a) and NF-κB/MAPK activation (b) by rytvela, salts (**5.1.1** and **5.1.2**) and analogues (**5.2**-**5.4**, **5.9**-**5.10**), as assessed by fluodye intercalation and HEK Blue reporter gene assays, respectively. Sample bars correspond to cells that were stimulated by an exogenous amount of hIL-1β. Data are plotted as percentage of inhibition of IL-1β-induced effect and reported as mean value ± SEM.

In the same *in vitro* assays, the formate salts of the Ret analogues (**5.6**-**5.8**; Figure 5.7) produced significantly weaker inhibitory activity than rytvela (**5.1.1**). The Ret derivatives unanimously inhibited 61% of the NF-κB/MAPK activation, and exacerberated the IL-1β-stimulated proliferation of immune cells. The retro and retro-enantio derivatives exhibited the stronger (40% and 32%, respectively) increase in proliferation, suggesting that sequence has a profound effect on anti-proliferative activity.

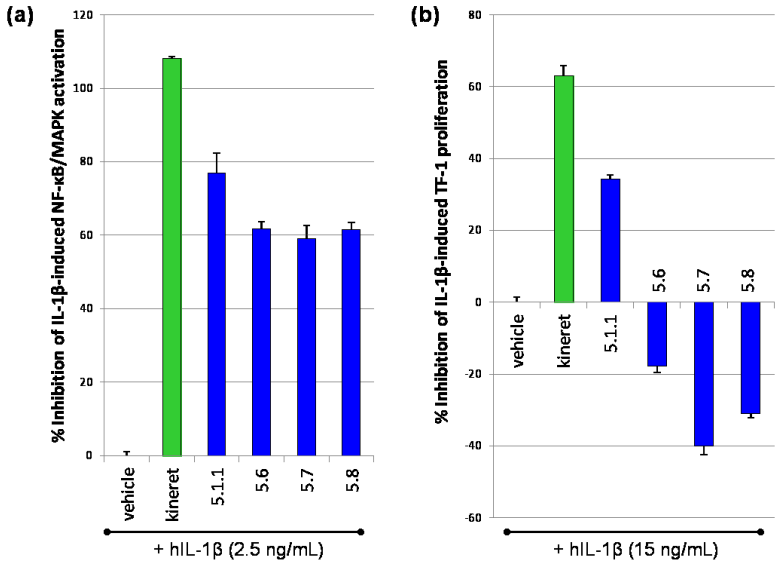

Figure 5.7. Inhibitory activity of rytvela and Ret analogues (**5.6**-**5.8**) on IL-1β-induced NF-κB/MAPK activation (a) and thymocyte proliferation (b). Data are plotted as percentage of inhibition of IL-1β-induced effect and reported as mean value ± SEM.

5.4 Concluding remarks

Employing CD and biological analyses provided additional information on the importance of counter-ion, purity, and sequence for rytvela activity. Although the counter-ion had no pronounced effect on conformation as observed by the similarities in the CD curves of the different rytvela salts, trifluoroacetates (**5.1.2** and **5.2.2**) exhibited somewhat better anti-IL-1β activity than formate salts in the *in vitro* biological assays of rytvela and ytvela. These results were also corroborated by *in vivo* hyperthermia experiments conducted with pure salts. Crude samples of 101.10 (**5.9**-**5.10**) consistently presented higher inhibitory effects than purified rytvela (**5.1**). Trifluoroacetate salts of co-synthesized contaminating peptides (i.e., ytvela, rytvela, ytvelaa, **5.2**-**5.4**) detected in crude 101.10 samples exhibited improved anti-IL-1β activity relative to pure rytvela, yet produced analogous CD spectra. Ret analogues **5.6**-**5.8** engendered CD curves indicative of a disordered structure, and diminished bioactivity compared to rytvela, especially in the thymocyte proliferation assay, in which they augmented IL-1β stimulation by 18 to 40%.

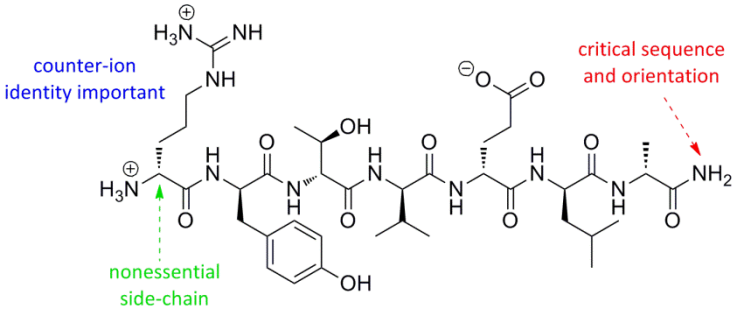

Figure 5.8. Structure-activity relationships observed for the Ret analogues, co-synthesized contaminating peptides and salts of 101.10.

More experiments should be conducted before speculating on the effects of the counter-ion on rytvela behaviour. Various screening techniques may be needed to select the ideal salt for the desired pharmacological profile (Berge *et al.*, **1977**), taking into consideration practical details such as the cost of raw materials, and the ease of preparation and purification. For example, trifluoroacetates generally facilitate HPLC purification by notably suppressing ion-exchange side effect with uncapped silanol groups on the RP-HPLC packing (Bennett, **1991**), are volatile, stick more firmly to the peptide as classified in the Hofmeister series, and are FDA-approved pharmaceutical salts (Gould ,**1986**); yet their environmental impact (Boutonnet *et al.*, **1999**) and toxicity to aquatic organisms (Berends *et al.*, **1999**) limit their use as counter-ion. Salt selection guidelines (Berge *et al.*, **1977**; Kerns *et al.*, **2008**) advocate the use of counter-ions that have a pK_a differing from the drug by only 2-3 units, which is not the case for TFA. In this perspective, the formate (pK_a = 3.75) and acetate (pK_a = 4.75) salt forms may be preferred.

5.5 Experimental section

5.5.1 General

See experimental section of chapter 2.

5.5.2 Solid-phase peptide synthesis

See experimental section of chapter 2.

5.5.3 SPPS according to Good Manufacturing Practices

Optical purity of Fmoc-D-amino acids was assessed by measurement of their specific rotation at the sodium D line (as previously described, chapter 2), at a concentration of 1.0 g/100 mL in either DMF or EtOAc. *Iso*-propanol and di-*iso*-propylether were used in the washing and precipitation steps, instead of their shorter alkyl equivalents, methanol and ethyl ether, due to their lower volatility and hygroscopicity. New or argon-sealed bottles of reagents and solvents were employed. Weight measurements were conducted on a manually calibrated analytical balance (Denver PI-225D; Denver Instruments, Bohemia, USA), and volumes were measured with Becton-Dickinson seringes (BD Biosciences, Mississauga, Canada) or recently calibrated variable volume Eppendorf Research® pipettes (Eppendorf, Mississauga, CA). HPLC-MS purity analyses and preparative RP-HPLC purification of the peptide samples were conducted using a Synergi® RP-Polar column and an optimized elution gradient (0-5 min. at 5% solvent B, 5-20 min. at 5-22% solvent B, 20-25 min. at 20% solvent B, 25-27 min. 20-95% solvent B, followed by column washing and reconditioning; solvent A: H_2O + 0.1% FA or TFA; solvent B: MeCN + 0.1% FA or TFA) which efficiently resolved the desired product peak from the secondary peaks. Crude and purified peptide samples were lyophilized in separate instruments, at 101 mTorr and -86°C.

The GMP procedure for SPPS of rytvela is in essence the same as that reported for standard SPPS protocol, except of the following changes: the loading of the resin was determined twice with parallel methodologies; the peptidic scale used was 0.3 mmol; Kaiser tests were performed after each step and repeated in case of intermediate outcome; all amino acid couplings were carried for 1 hour with 2.5 equiv. of each DIEA,

HBTU and Fmoc-D-amino acid before being tested for completion, and in the negative, restarted for 1 hour with fresh coupling medium.

5.5.4 Characterization and purification

Refer to experimental section of chapter 2.

5.5.5 Ion-exchange chromatography

Oasis® MCX 3cc cartridges (1 meq/g, 60 µm, 80 Å; Waters Corp., Milford, USA) were conditioned with anhydrous MeOH (1 mL) and equilibrated with Milli-Q H_2O (1 mL) before the peptide solutions (ranging from 5 to 10 mM) were loaded. Solvents and samples were passed through the cartridges dropwise. The cartridges were washed with water containing 2% formic acid (2 mL). Then, the adsorbed compounds were ion-exchanged and eluted from the MCX cartridges with 2 x 1 mL H_2O containing 5% NH_4TFA or NH_4OAc followed by 2 x 1 mL MeOH. Eluates were recovered in 10 mL glass test tubes and lyophilized for subsequent analysis.

5.5.6 Reverse-phase chromatography

The counter-anions of peptide samples were exchanged using solid-phase extraction (SPE) C18 column, which is analogous to that used for reverse-phase HPLC chromatography. Essentially, SPE-driven ion-exchange was carried out using 1 mL cartridges packed with 100 mg of AccuBOND^{II} octadecylsilane (ODS)-C18 sorbent (Agilent Technologies, Mississauga, CA). The cartridges were conditioned by passing 1 mL of anhydrous MeOH, and equilibrated with 2 portions of 1 mL of H_2O:ACN 95:5 containing 0.1% TFA. Peptide solutions (100 µL, concentrated at 20 mM) were loaded on the cartridges at a flow rate of one drop per second (3-5 mL/min.) using controlled argon flow. The cartridges were washed with 1 mL of H_2O:MeCN 95:5 containing 0.1% TFA, then eluted with 2 portions of 1 mL of H_2O:MeCN 20:80 containing 0.1% TFA followed by 1 mL of dry MeCN. Eluates were collected in 10 mL glass tubes and freeze-dried for further analysis.

5.5.7 Capillary zone electrophoresis

Relative quantities of the different counter-anions contained in peptide samples were determined, as previously described (Little *et al.*, **2007**) by capillary zone electrophoresis (CZE) using a G1600AX system (Agilent Technologies, Mississauga, Canada) equipped with a diode array UV-detector monitoring at 350 nm, with background signal set at 254 nm. All separations were performed at 25°C in a bare fused silica capillary (Polymicro Technologies, Phoenix, USA) of 54 cm total length and 44 cm effective length (to the detector), with dimensions of 75 µm I.D. x 360 µm O.D. The applied voltage was -20 kV and the background electrolyte (BGE) was 5 mM potassium hydrogen phthalate, 50 mM methylester sulfonate (MES), 0.5 mM tetradecyltrimethylammonium bromide (TTAB), adjusted to pH 5.0 with 0.1 M HCl. Between each injections and separations, the capillary was rinsed at 34.5 mbar with 1.0 M NaOH for 2 min., Milli-Q H_2O for 2 min., 1.0 M HCl for 2 min, 0.1 M HCl for 2 min., and finally with BGE for 2 min. Injection of 20 nL of sample solution (ranging from 0.1 to 10 mM in 100% H_2O) was accomplished by application of 34.5 mbar for 16 s and then BGE for 2 s at the inlet end of the capillary. Relative amounts of counter-ions were determined by calculating the area under the

curve (AUC) of corresponding peaks, relative to signal-to-noise of the background signal. Each separation was repeated three times, and elution times are reported in min.

5.5.8 Ultraviolet-circular dichroism

Similar to the experimental section of chapter 2, except that different aqueous concentrations of rytvela formate salt were used (20, 30, 50, and 100 μM). The CD spectrum of 20 μM of rytvela formate was recorded in TFE, after TFE blank signal was subtracted.

5.5.9 Biological activity screening via fluodye intercalation and HEK Blue reporter gene assays

Same as experimental section of chapter 2.

5.6 References

Adjei, A.; Rao, S.; Garren, J.; Menon, G.; Vadnere, M. *Int. J. Pharm.* **1993**, *90* (2), 141-149.

Adzhubei, A. A.; Sternberg, M. J. E. *J. Mol. Biol.* **1993**, *229*, 472-493.

Altria, K. D.; Assi, K. H.; Bryant, S. M.; Clark, B. J. *Chromatographia* **1997**, *44* (7/8), 367-371.

Avdeef, A. *Curr. Topics Med. Chem.* **2001**, *1*, 277-351.

Avdeef, A. In *Absorption and Drug Development : Solubility, Permeability, and Charge State*; Avdeef, A.; Ed.; John Wiley & Sons, New Jersey, USA, **2003**, 312 pages.

Baciu, M.; Sebai, S. C.; Ces, O.; Mulet, X.; Clarke, J. A.; Shearman, G.C. *Phil. Trans. R. Soc. A.* **2006**, *364*, 2597-2614.

Barth, A.; Zscherp, C. *Q. Rev. Biophys.* **2002**, *35* (4), 369-430.

Bennett, H. P. J. In *High-Performance Liquid Chromatography of Peptides and Proteins:Separation, Analysis and Conformation*; Mant, C.T.; Hodges, R.S., Eds.; CRC Press; Boca Raton, USA; **1991**, 938 pages.

Berends, A. G.; Boutonnet, J. C.; De Rooji, C. G.; Thompson, R. S. *Envir. Toxicol. Chem.* **1999**, *18* (5), 1053-1059.

Berge, S. M.; Bighley, L. D.; Monkhouse, D. C. *J. Pharm. Sci.* **1977**, *66* (1), 1-19.

Blanco, F. J.; Jimbnez, M. A.; Herranz, J.; Rim, M.; Santoro, J.; Nieto, J. L. *J. Am. Chem. Soc.* **1993**,*115,* 5887-5888.

Boutonnet, J. C.; Bingham, P.; Calamari, D.; De Rooji, C.; Franklin, J.; Kawano, T.; Libre, J.-M.; McCulloch, A.; Malinverno, G.; Odom, M.; Rusch, G. M.; Smythe, K.; Sobolev, I.; Thompson, R. S.; Tiedje, J. M. *Human Ecol. Risk Assess.: An Int. J.* **1999**, *5* (1), 59-124.

Cummings, W.G.; Torrance, K. In *Instrumentation Reference Book*, Boyes, W.; Ed.; Butterworth-Heinemann, Burlington, USA, *24*, **2009**, p.365

Byler, D. M.; Susi, H. *Biopolymers* **1986**, *25*, 469-487.

Conchillo-Sole, O.; de Groot, N. S.; Aviles, F. X.; Vendrell, J.; Daura, X.; Ventura, S. *BMC Bioinf.* **2007**, *8*, 65-81.

Collins, K. D.; Washabaugh, M. W. *Quart. Rev. Biophys.* **1985**, ***18*,** 323-422.

Dai, J.; Mendonsa, S. D.; Bowser, M. T.; Lucy, C. A.; Carr, P. W. *J. Chromatogr. A* **2005**, *1069* (2), 225-234.

Dempsey, C. E.; Mason, P. E.; Jungwirth, P. *J. Am. Chem. Soc.* **2011**, *133* (19), 7300–7303.

Esbjorner, E. K.; Lincoln, P.; Borden, B. *Biochim. Biophys. Acta* **2007**, *1768*, 1550-1558.

Fernandez-Escamilla, A.-M.; Rousseau, F.; Schymkowitz, J.; Serrano, L. *Nat. Biotechnol.* **2004**, *22* (10), 1302-1306.

Gould, P. L. *Int. J. Pharm.* **1986**, *33* (1-3), 201-217.

Haynes, D. A.; Jones, W.; Motherwell, W. D. S. *J. Pharm. Sci.* **2005**, *94* (10), 2111-2120.

Hofmeister, F. *Arch. Exp. Path.* **1890**, *27*, 395-413.

Horowicz, P. *Pharm. Rev.* **1964**, *16* (2), 193-221.

Hutchinson, E. G.; Thornton, J. M. *Protein Sci.* **1994**, *3*, 2207-2216.

Jardetzky, O. *Biophys. Biochim. Acta* **1980**, *621* (2), 227-232.

Kasicka, V. *Electrophoresis* **2001**, *22*, 4139-4162.

Kerns, E. H.; Di, L. In *Drug-like Properties: Concepts, Structure Design and Methods*; 1st ed. Elsevier, California, USA, **2008**, 526 pages.

Kunz, W. In *Specific Ion Effects*, Kunz. W., Ed.; World Scientific, Singapore, Indonesia, **2010**, 325 pages.

Little, M. J.; Aubry, N.; Beaudoin, M.-E.; Goudreau, N.; Laplante, S. R. *J. Pharm. Biomed. Anal.* **2007**, *43*, 1324-1330.

Merrifield, R. B.; Juvvadi, P.; Andreu, D.; Ubach, J.; Bomani, A.; Boman, H. G. *Proc. Natl. Acad. Sci. USA* **1995**, *92*, 3449-3453.

Messana, I.; Rossetti, D. V.; Cassiano, L.; Misiti, F.; Giardina, B.; Castagnola M. *J. Chromatogr. B*. **1997**, *699*, 149-171.

Miller, L. C.; Holland, A. H. *Mod. Med.* **1960**, *28*, 312-318.

Miyauchi, Y.; Hojo, M.; Moriyama, H.; Imai, Y. *J. Chem. Soc. Faraday Trans.* **1992**, *88* (21), 3175-3182.

Nandi, P. K.; Robinson, D. R. *J. Am. Chem. Soc.* **1972**, *94* (4), 1299-1308.

Roux, S.; Zékri, E.; Rousseau, B.; Paternostre, M.; Cintrat, J.-C.; Fay, N. *J. Pept. Sci.* **2008**, *14*, 354-359.

Rucker, A. L.; Creamer, T. P. *Prot. Sci.* **2002**, *11*, 980-985.

Sahin, E.; Jordan, J. L.; Spatara, M. L.; Naranjo, A.; Costanzo, J. A.; Weiss, W. F.; Robinson, A. S.; Fernandez, E. J. *Biochemistry* **2011**, *50*, 628-639.

Sánchez De Groot, N.; Pallarés, I.; Avilés, F. X.; Vendrell, J.; Ventura, S. *BMC Struct. Biol.* **2005**, *5*, 18-32.

Sazelova, P.; Kasicka, V.; Solinova, V.; Koval, D. *J. Chromatogr. B* **2006**, *841*, 145-151.

Schwartz, M. A.; Buckwalter, F. H. *J. Pharm. Sci.* **1960**, *51*, 1119-1128.

Scibra, G. K. E.; Psurek, A. In *Methods in Molecular Biology*, Schmidt-Kopplin, P., Ed.; Humana Press Inc., New Jersey, USA; *384* (19); **2008**, 483-506.

Shai, Y.; Flashner, M.; Chaiken, I. M. *Biochemistry* **1987**, *26* (3), 669-675.

Shozo, M.; Midori, O.; Tanekazu, N. *Int. J. Pharm.* **1980**, *6* (1), 77-85.

Sonnichsen, F. D.; Van Eyk, J. E.; Hodges, R. S.; Sykes, B. D. *Biochemistry* **1992**, *31* (37), 8790-8798.

Stahl, P. H.; Wermuth, C. G. In *Handbook of pharmaceutical salts : properties, selection, and use*; Verlag -VCH, Zürich, Switzerland, **2002**, 374 pages.

Takacs-Novak, K.; Szasz, G. *Pharm. Res.* **1999**, *16* (10), 1633-1638.

Terabe, S.; Otsuka, K.; Ichikawa, K.; Tsuchiya, A.; Ando, T. *Anal. Chem.* **1984**, *56* (1), 111-113.

Wermuth, J.; Goodman, S. L.; Jonczyk, A.; Kessler, H. *J. Am. Chem. Soc.* **1997**, *119* (6), 1328-1335.

Woody, R. W. *Chirality* **2010**, *22*, E22-E29.

CHAPTER 6

Conclusion and Perspectives

6.1 Conclusion

As one of the major pro-inflammatory mediators in humans, IL-1β participates in numerous intracellular pathways upon binding to its receptor (IL-1RI), which leads to severe immune disorders and acute bouts of inflammation (Dinarello, **2011**). Current anti-IL-1β approaches under development involve recombinant natural antagonists, monoclonal antibodies, fusion proteins and small organic molecules (Dumont, **2006**). Kineret® (IL-1Ra) is the only product fully approved so far that selectively targets IL-1β by competing with the latter for receptor binding. Inconveniences of this daily administered compound include poor bioavailability, immunogenicity, increased susceptibility to infection, short half-life and high costs. Small molecule inhibitors of IL-1RI would offer a prolonged duration of action, a good enteral bioavailability, and be hopefully more affordable. Such a major breakthrough for IL-1R antagonists remains a clear and unmet medical need. The D-heptapeptide 101.10 (rytvela) has demonstrated features of a negative allosteric modulator and exhibited high potency and efficacy in blockade of various IL-1β-mediated effects both *in vitro* and *in vivo*. However, considering that peptides do not generally possess sufficient "drug-like" properties which allow them to efficiently cross physiological barriers, one of the objectives of the present studies was to develop peptidomimetics of 101.10 which display improved anti-IL-1β efficacy and optimal physicochemical properties.

In order to explore the relationships between peptide composition, conformation and biological activity, different series of analogues were synthesized and examined to understand the factors influencing the inhibitory actions of the peptide 101.10 on IL-1β. Common peptidomimetism strategies were employed to probe the pharmacophores of 101.10, which include: rigid scaffold such as amino-γ-lactams, indolizidinone amino acids and proline; *N*- and *C*-terminal truncations; substitution by analogous amino acids; and sequence and chirality inversions.

The synthesis and evaluation of a library of α- and β-amino-γ-lactam analogues of 101.10 (Jamieson *et al.*, **2009**; Boutard *et al.*, **2011**) showed that higher bioactivity was generally exhibited by the (*R*)-Agl and (*S*)-Bgl series, relative to their enantiomeric counterparts, suggesting that these complementary lactams may adopt similar conformational space. Position-dependent bioactivity was also observed in scanning the sequence with the different amino-γ-lactams. For example, replacement of D-Arg^{1} for (*R*)-Agl^{1} produced an analogue exhibiting the best anti-proliferative effect, whereas substitution of D-Thr^{3} and D-Val^{4} for Agl and Bgl residues showed that although IL-1β inhibition was maintained, lower efficacy was observed in the 3-position relative to the 4-position.

Results from the applications of amino-γ-lactams raised questions concerning the trade-off or the loss of side-chain function for the gain in conformational restriction. When the chirality was exchanged at Thr^{3}-Val^{4}, divergent behaviours were observed relative to inhibition of IL-1β-mediated thymocyte proliferation and NF-κB/MAPK pathways activation; suggesting that these peptidomimetics exhibited functional selectivity towards the IL-1RI. Using α-amino-β-hydroxy-γ-lactams as constrained Thr^{3} mimetics, the importance of side-chain versus stereochemistry versus conformation was probed. For example, peptides containing a L-Thr^{3} or a (3*S*)-Hgl^{3} demonstrated improved inhibition of immune cell proliferation over rytvela (**5.1**) and (*R*)-Agl^{3} (**2.8**); and derivatives including a L-Val^{4} or a (3*R*)-Hgl^{3} exhibited retained blockade of NF-κB/MAPK compared to rytvela, but lower relative to [(*R*)-Agl^{3}]-101.10. Moreover, substitution of D-Thr for either L- or D-Val resulted in reduced activity, supporting the importance of the hydroxyl group for blockade of IL-1β.

The D-Thr^3-D-Val^4 residues were then replaced by indolizidin-2-one amino acids of different stereochemistry. Although [(3*R*,6*R*,9*R*)-I^{2}aa^{3,4}]- and [(3*S*,6*S*,9*S*)-I^{2}aa^{3,4}]-101.10 (**4.20** and **4.24**) had respectively little influence on IL-1β effects, [(3*R*, 6*R*, 9*R*)-I^{2}aa$^{3\text{-}4}$, ΔAla^7]-101.10 (**4.19**) exhibited the strongest inhibitory efficacy of the examined series in both assays. In comparison, [D-Pro^4]-101.10 presented high anti-IL-1β activity, contrary to its *C*-truncated counterpart. The biological data of the mimetics bearing respectively lactam residues (Agl/Bgl and I^{2}aa) and proline supported the importance of D-amino acid stereochemistry in the Thr^3-Val^4 region for imparting activity.

Retro-, enantio- and retro-enantio isomers were then prepared as to probe the influence of sequence directionality and side-chain configurations on the global conformation and bioactivity of 101.10. Relative to rytvela, all retro-enantio analogues respectively exacerbated and slightly inhibited IL-1β-induced immune cell proliferation and inflammatory pathways induction, confirming the appropriate sequence direction and global side-chain chirality of the D-sense heptapeptide rytvela.

Exchanging counter-anion had limited influence on the CD spectrum of rytvela, but influenced the capacity to block IL-1β *in vitro*: trifluoroacetates consistently displayed stronger inhibition of cell proliferation and downstream signaling activation than acetates and formates. This effect may be due to the weaker selectivity of the trifluoroacetate salts towards the homologous cytokine IL-33. The purity of the 101.10 samples was demonstrated to be of high impact. Commercial samples (**5.9** and **5.10**) were shown to contain significant contaminants and exhibited stronger inhibition of IL-1β effects relative to purified rytvela, raising interest in the inividual activity of contaminants. For example, the truncated sequences ytvela and rytvel demonstrated respectively a significant loss in potency and retained activity, comparable to that of other commonly found impurities such as rytvelaa and ytvelaa.

Attempts to restrict the parent peptide resulted in changes from random coil to ordered structure as observed by CD spectroscopy. For example, the majority of Agl and Bgl analogues displayed CD curves suggestive of type I and II' β-turns, which possess similar torsional angles. The most active (3*S*,4*R*)-Hgl analogue exhibited a spectrum characteristic of a type I β-turn. Indolizidin-2-one analogues showed indications of polyproline-like helical structure and the proline-containing peptides exhibited CD data characteristic of a type I β-turn. In addition, certain Thr^3-Val^4 diastereomeric analogues exhibited β-fold CD spectra, which corresponded to turn types of comparable configurations in Hgl^3 mimetics. Alternatively, the different salts of 101.10, the retro, retro-enantiomeric and enantiomeric isomers, as well as the truncated peptides, all demonstrated unanimously curves similar to that of rytvela. Taken all together, the spectroscopic and biological data highlights the importance of peptide folding to elicit improved activity at the IL-1R complex.

In brief, guidance has been gained from the clustering of analogues that exhibited CD curves characteristic of folding motifs and improved activity towards optimization of the lead peptide. For example, peptidomimetics that displayed improved anti-proliferative activity relative to rytvela possessed CD curves indicative of either a type I or II' β-turn. Analogues that exhibited stronger blockade of IL-1β-mediated inflammation compared to rytvela produced CD spectra suggestive of type I and type II' β-folds. Finally, the few compounds that superiorly inhibited both IL-1β effects demonstrated absorption bands characteristic of type I β-turn and polyproline type II helical structures. As ideal ϕ and ψ dihedral angles for β-turns of type I and II' and that of poly-D-proline of type II are similar to each other (Tables 3.3 and 4.1), all these conformers exist in a dynamic

equilibrium, in which a slight change in rigidification or configuration may favour one conformer over the others. It is the relative amounts of these conformers that emerge in aqueous CD spectoscopy.

To conclude, the compilation of SARs has served to elaborate four main aspects of the project: 1) crude samples are more active than purified rytvela both in *in vitro* and *in vivo* tests, suggesting there may be an effect of counter-anion or an unidentified contaminant; 2) several peptidomimetics exhibited functional selectivity towards IL-1β-mediated immune and inflammatory responses, an important features of IL-1RI allosteric modulators; 3) identification of some pharmacophore elements in the parent peptide, highlighted the importance of the hydroxyl in Thr^3 side-chain, and of the D-stereochemistry at 3- and 4-positions; and 4) discovery of a new lead (**4.19**), which displayed improved efficacy in both cellular assays relative to rytvela.

6.2 Perspectives

Peptidomimetics discussed in the present studies possessed notable advantages over 101.10: they have been produced in high purity and bound to a known counter-anion; they may display improved selectivity and efficacy due to their reduced flexibility; and they can be accessed through straightforward and stereoselective synthetic approaches. In an effort to better understand how 101.10 exerts its biological effect upon binding to IL-1RI, the new lead mimetic [(3*R*,6*R*,9*R*)-$I^2aa^{3,4}$, ΔAla^7]-101.10 (**4.19**) could be further characterized and developed. Assessment of the *in vivo* efficacy of this analogue could be performed in murine models of IL-1β-induced hyperthermia and PMA-mediated contact dermatitis, which would validate the *in vitro* activities observed. Subsequently, the new lead could be further optimized towards improving bioavailability and efficacy versus toxicology, by: alkylating the 4-position of the I^2aa bicycle to probe the need of hydroxyl group with this particular scaffold; choosing amino acids that have been shown to be unimportant for antagonistic activity, and use their side-chain to construct cyclic structures and lock a portion of the mimetic into a fold of a pre-defined size; or replace these superfluous residues by constrained derivatives, such as trimethyltyrosine (TMT) and cyclovaline (c_3Val); performing amide bond isosteric replacement (see chapter 1); substituting an internal residue for glycine or a constraining moiety such as α,α-dialkyl amino acids (see chapter 1). Additionally, permeability of the lead could be enhanced by the addition of hydrophobic entities or alteration of polar groups, such as substitution of D-Tyr for D-cyclohexylalanine (Cha) or of D-Glu for D-2-amino-4-phosphonobutanoic acid (AP4), or by choosing a lipophilic counter-anion such as phosphate or nitrate (Takacs-Novak *et al.*, **1999**; Sarveiya *et al.*, **2005**).

In addition, although the agonistic analogues (IL-1β stimulatory agents) of 101.10 have not been widely discussed due to the opposite nature of their effects, they may be potentially used as bacterial adjuvants to achieve immunostimulation against host infection (Dumont, **2006**) or as study tools for extended IL-1-related diseases such as brain ischemia (Boutin *et al.*, **2001**), cardiovascular inflammatory conditions (Bujak *et al.*, **2009**; Fearon *et al.*, **2008**), and type 2 diabetes (Donath *et al.*, **2011**).

In a more distant instance, future efforts toward the advancement of this project may englobe a deeper examination of: the aggregation pattern of rytvela using deconvoluted FT-IR, Raman and NMR with a model peptide (Blanco *et al.*, **1993**); the effect of different salts on the *in vitro* and *in vivo* biology of rytvela, as well as the stability, crystallinity, morphology and hygroscopicity of the salt form, allowing to choose the proper counter-ion for subsequent librairies of analogues; the dynamic conformation, as well as the extent of PPII/random

coil/turn equilibrium, for rytvela and selected analogues by high-resolution magic angle spinning (Sarkar *et al.*, **1996**; Furrer *et al.*, **2001**) or 2D-NMR techniques (Ferentz *et al.*, **2000**); and computational docking and virtual screening using improved homology models of IL-1RI/IL-1RAcP complex.

Such computational avenues have already been undertaken for a long time, but have been drastically complicated by the lack of crystal data on the whole receptor complex and by the relatively poor fit of the homology models for transmembrane receptors (Wong *et al.*, **2011**). Because the "RYTVELA" (all L-amino acids) sequence lays in the juxtamembranal portion of IL-1RAcP, more precisely at 1 residue from the membrane, the interface peptide 101.10 is not expected to bind at the crystallisable extracellular portion of IL-1RI (316 amino acids; commercially available), since the section that usually interacts with IL-1RAcP is not included in the ectodomain. However, considering that mimics may interact at a distinct site on the receptor than the parent 101.10, surface plasmon resonance (SPR) binding studies could be conducted with the cytosolic portion of the IL-1RI and IL-1RAcP, using a method previously described in the literature (Wang *et al.*, **2010**).

Although some efforts have been made to crystallize enantiomerically pure and racemic mixtures of rytvela, no X-ray diffraction-suitable crystals have been obtained at this time. However, attempts to crystallize rytvela either alone or bound to the IL-1R may be more successful by employing crystallization screening techniques (some are even automatized HTS method; Rupp, **2007**), such as Grid Screen® (McPherson, **1999**), Footprint screening (Stura *et al.*, **1992**) and stochastic CRYSTOOL® sampling (Segelke, **2001**), in which a collection of different solvents, buffers and pH are used to find the optimal crystallization conditions for your sample. Such high-resolution crystal structures of the heptapeptide may unveil novel information regarding the prevalent conformers (e.g. among type I and II' β-turns, random coil and PPII) when free and receptor-bound, which in turn could contribute to the future rational-based design of mimics.

6.3 References

Blanco, F. J.; Jimbnez, M. A.; Herranz, J.; Rim, M.; Santoro, J.; Nieto, J. L. *J. Am. Chem. Soc.* **1993**,*115,* 5887-5888.

Boutin, H.; LeFeuvre, R. A.; Horai, R.; Asano, M.; Iwakura, Y.; Rothwell, N. J. *J. Neurosci.* **2001**, *21* (15), 5528-5534.

Bujak, M.; Frangogiannis, N. G. *Arch. Immunol. Ther. Exp.* **2009**, *57*, 165-176.

Dinarello, C. A. *Blood* **2011**, *117* (14), 3720-32.

Donath, M. Y.; Shoelson, S. E. *Nat. Rev. Immunol*. **2011**, *11*, 98-107.

Dumont, F. J. *Expert Opin. Ther. Patents* **2006**, *16* (7), 879-912.

Fearon, W. F.; Fearon, D. T. *Circulation* **2008**, *117*, 2577-2579.

Ferentz, A. E.; Wagner, G. *Q. Rev. Biophys.* **2000**, *33* (1), 29-65.

Furrer, J.; Piotto, M.; Bourdonneau, M.; Limal, D.; Guichard, G.; Elbayed, K.; Raya, J.; Briand, J.-P.; Bianco, A. *J. Am. Chem. Soc.* **2001**, *123,* 4130-4138.

McPherson, A. In *Crystallization of Biological Macromolecules*; McPherson, A.; Ed.; Cold Spring Harbor Laboratory Press, Long Island, USA, **1999**, 586 pages.

Rupp, B. In *Protein crystallization strategies for structural genomics*, Chapter 2; Chayen, N. E.; Ed.; International University Line, La Jolla, USA, **2007**, 260 pages.

Sarkar, S. K.; Garigipati, R. S.; Adams, J. L.; Keifer, P. A. *J. Am. Chem. Soc.* **1996**, *118,* 2305-2306.

Sarveiya, V.; Templeton, J. F.; Benson, H. A. *Eur. J. Pharm. Sci.* **2005**, *26* (1), 39-46.

Segelke, B. W. *J. Cryst. Growth* **2001**, *232*, 553-562.

Stura, E. A.; Nemerow, G. R.; Wilson, I. A. *J. Crystal Growth* **1992**, *122*, 273-285.

Takacs-Novak, K.; Szasz, G. *Pharm. Res.* **1999**, *16* (10), 1633-1638.

Wong, W.-C.; Maurer-Stroh, S.; Eisenhaber, F. *Biol. Direct* **2011**, *6*, 57-86.